Experimental and Numerical Analysis of Mechanical Behavior of Fiber–Reinforced Sands based on Critical State Soil Mechanics

by

Jakhongirbek Ganiev

Nagoya University

A dissertation submitted to Nagoya University in accordance with the requirements of the degree of Doctor of Philosophy in the Faculty of Engineering, Department of Civil and Environmental Engineering

September, 2022

限界状態理論に基づく繊維補強砂の力学挙動の実験および数値解析的解釈

ガニエフ　ジャホンギルベク

令和 4 年 9 月

ABSTRACT

Reinforcing soils with tension resisting elements are alternative soils improvement technique confirmed by a series of experimental studies. Several types of ground improvement methods that employ fiber-reinforcement have been developed in recent years. However, despite numerous studies performed in the past few decades there is still a gap between theoretical understanding and practical implementation of fiber-reinforcement on a production scale. For this purpose, this study is aimed to comprehensively investigate the mechanical behaviour of fiber-reinforcement through experimental and numerical analysis with the particular attention to the reinforcing effect and interaction mechanism between soil particles and fibers. This study is divided into two main parts: experimental study and simulation of experimental results by utilizing an existing constitutive model super/subloading yield surface Cam-clay model (SYS Cam-clay model).

Experimental work firstly considered a sample preparation issue, including mixing fibers with sand and placement, where the optimum way of sample preparation was proposed. After that, isotropic compression and consolidated triaxial compression and extension experiments in both drained and undrained conditions were performed on both unreinforced and fiber-reinforced sand specimens.

First, a series of consolidated drained triaxial compression and extenstion tests were conducted here to examine the effect of short fibers on the mechanical properties of sand. As for the fiber, discrete polyvinyl alcohol fibers with the length of l_f=12mm and vinylon filament fibers were utilized with the proportion of 0.0%, 0.2%, 0.4%, and 1% of the dry weight of sand. Specimens were sheared under five different confining pressures of p'_0=50kPa, 100kPa, 200kPa, 400kPa and 600kPa and prepared in three different initial relative densities of D_r=30%, 60% and 80%. The test results showed that the maximum and residual deviator stresses increased, whereas the volumetric expansion decreased with an increase in fiber content in compression. Although the stress ratio η ($=q/p'$) and specific volume changed depending on the fiber content and confining pressure with shear progression, they each reached the same values for a definite fiber content at the end of shearing, independently of initial relative density. In other words, the unique critical state line can be found for a definite fiber content. Moreover, the greater the fiber content, the larger the slope of the critical state line at the end of shear.

Next, a series of undrained triaxial compression and extenstion experiments were conducted. Specimens were prepared with initial relative density of D_r=40% to fully investigate the pore water pressure generation at higher strains and all specimens were sheared under three different confining pressures of p'_0=50kPa, 100kPa, 200kPa. Both unreinforced and fiber-reinforced sand specimens showed similar tendency of mechanical behavior as in drained compression tests. Particularly, despite being sheared under different confining pressures, both unreinforced and fiber-reinforced sands prepared with the same initial relative densities reached to the same deviator stress at around 20% axial strain. Furthermore, residual stress ratio η_r values (critical state parameter M) were similar as were obtained in drained tests. The pore water pressure generation in undrained tests were similar to the volumetric change behavior in drained condition, where fiber-reinforced specimens initially had a higher positive pore-water pressure and had a smaller generation of negative pore water pressure at the end of shearing. Also, fibers were also effective in enhancement of the tensile strength in undrained triaxial extension experiments. With the increase of fiber contents, the tensile strength increased, and there were no transferred shear band as in drained condition.

Finally, numerical analysis of compressive behavior of unreinforced and fiber-reinforced sand were performed. Based on the experimental studies, where even fiber-reinforced sand had a similar mechanical behavior as unreinforced sand and the possibility of describing their mechanical behavior through critical state soil mechanics was revealed, the super/subloading yield surface Cam-clay model (SYS Cam-clay) was used to reproduce the experimental results. The reproduced results were in good agreement with experimental results. Both simulated and experimental results showed that an increase in fiber content led to decrease in initial stiffness and increase in initial volumetric compression. This was attributed to the lower initial anisotropy of reinforced sand due to the fiber inclusions. Furthermore, the simulation results indicated that the fiber inclusions inhibited the development of anisotropy compared to unreinforced sand. Consequently, a higher peak and post-peak stresses with increased critical state parameter M, and less volumetric expansion at higher strain rates observed in fiber-reinforced sand.

ACKNOWLEDGMENT

I am extremely grateful to my academic supervisor Professor Masaki Nakano for his continuous and patient instructions during the entire research work. The professor's door was always open whenever I had questions about the experiments, thesis writing or even personal questions on a daily life. I received great support to study at the doctoral program, from the basic knowledge to solving the real geotechnical problems. Without Professor Nakano's support this research would never have been accomplished. Also, I would like to express my thankful gratitude to Assistant Professor Takayuki Sakai for his endless patience and helpful advices. I learned a lot of things including laboratory experimentation and simulation/modelling using SYS Cam-clay model and GEOASIA step by step.

I would like thank Professor Shotaro Yamada from Tohoku University for his kind guidance and constructive advice on organizing the research work. I have learned a lot from his extensive professional experience.

I would like to sincerely appreciate Professor Toshihiro Noda and Associate Professor Kentaro Nakai for their encouragement and enlightening experience during my laboratory life. I can always receive valuable suggestions and detailed explanation from them whenever I am confused and they always find time to clarify the problem despite their tight schedule. I really appreciate their continuous support during my doctoral course study.

Also, I wish to thank Professor Feng Zhang from Nagoya Institute of Technology for his kind and useful advice in preparing a doctoral dissertation.

I would also like to thank Assistant Professor Takahiro Yoshikawa and Assistant Professor Toyoda for their patience and helpful guidance during my stay in the laboratory. With their support my stay at Nagoya University was very smooth without any major issues.

In addition, I want to express my thanks to the staff of the geotechnical engineering laboratory, Mr. Takaine and Ms. Hitomi Yamada for their advice and support not only in laboratory life, but also out of it.

All staff of Nagoya University and student of geotechnical engineering laboratory are also recognized and appreciated.

I would also like to express my gratitude to the Ministry of Education, Sports and Cultural Activities of Japan for the Monbukagakusho Scholarship.

Finally, the biggest thanks to my family and my wife Violetta for providing me with unfailing support and continuous encouragement throughout my years of study and through the process of researching and writing this thesis. This accomplishment would not have been possible without them.

AUTHOR'S DECLARATION

I declare that the work in this dissertation was carried out in accordance with the requirements of the rules, regulations and procedures for the Doctoral Course Program in Civil and Environmental Engineering of Nagoya University and that it has now been submitted for any other academic award. Except where indicated by specific reference in the text, the work is the candidate's own work. Any views expressed in the dissertation are those of the author.

September 2022

Jakhongirbek Ganiev

TABLE OF CONTENTS

LIST OF TABLES

LIST OF FIGURES

CHAPTER 1

INTRODUCTION

1.1 Research background

In the third decade of the 21st century while our planet is suffering from consequences of unregulated and still expanding construction and urbanization issues, there is a vital need in considering the impact of construction on the environment and following a sustainable development to preserve the nature and inhibit globalization of the environmental issues. At the same time, general civil engineering problems and specific geotechnical issues related to earth work including soil improvement methods and increasing its strength and stability are still the actual problems, that complicates with the current requirements for sustainable construction and an essential of economically beneficial methods and techniques of soil improvement. Some traditional ways of soil stabilization and improvement including mechanical compaction, usage of additives as cement, lime, fly ash and etc., have been successfully used over several centuries. However, both ways of traditional methods of soil improvement have their impact on environment: 1) mechanical compaction needs huge machines with proper space to make it possible to efficiently use them, which requires a lot of energy, time and expenses; 2) structures and ground improved by traditional additives as cement, chemical, lime affect the environment, and moreover, they cause additional severe problems with the disposal of fatigued and damaged reinforced structures. Regarding the need in more ecofriendly techniques of soil improvement, alternative methods of reinforcing soils with tension resisting elements have been considered, which is also considered as a cost-effective technique.

Fiber-reinforcement is similar to the plant roots (Fig. 1.1) and gives the possibility to increase and stabilize near surface layers which was already known from the ancient times. Fiber-reinforcement technique compared to other traditional soil improvement techniques is more ecofriendly in terms of both sustainability in construction with the possibility of using natural fibers (plant fibers (bamboo, jute, coir, hemp, etc.), animal parts containing protein (silk, hair, wool, etc.) and easy utilization/recycling of fatigue structures. Therefore, recently, over the past 30 years, fiber-reinforcement has raised a high interest in both researchers and practicing engineers. However, despite numerous studies and validation of the effectiveness of fiber-reinforcement both experimentally and numerically, there is still a gap between undisclosed potential of fibers for

practical implementation and the mechanism of fiber-reinforcement through theoretical investigations (see Chapter 2 for details). Additionally, laboratory investigations on the mechanical behavior of reinforced soils have brought some discrepancies on the results and understanding of the mechanism of fiber-reinforcement considering interaction between fiber and soil particles still has not been fully studied. Therefore, having studied the above-mentioned shortages of understanding the potentials of this promising technique and a need in further research, a comprehensive experimental and numerical study has been performed to complement the existing data. Furthermore, it is believed that the results of this study will make a contribution to further understanding the mechanism, potential benefits and limitations of this technique and will bring closer the practical application to various geotechnical structures.

Fig. 1.1 Photograph of tree roots

1.2 Research Objectives

The two main parts of the present research were to experimentally investigate the mechanical behavior of unreinforced and fiber-reinforced sand and propose a possible mechanism of the reinforcing effect of fibers and to numerically simulate the mechanical response by an existing constitutive model developed within critical state soil mechanics theory (Roscoe et al., 1958; Schofield and Wroth, 1968; Atkinson and Bransby, 1978) and further modify it if necessary. Experimental work has been conducted on the conventional triaxial apparatus which allows testing of specimens under various condition as drainage characteristics, applied stress range and

investigation of compressive or extensive response. The detailed objectives for each part of the current research are given below:

(1) Experimental study was performed:

- To investigate sample preparation issues including mixing fibers with soils and placement into the triaxial mold, and to determine the optimum method for the specimen preparation with high reproducibility.
- To obtain compression/swelling parameters of both unreinforced and fiber-reinforced sand in isotropic compression, and to study the influence of the fiber contents on the compressibility characteristics, which is assumed to be a part of mechanism for fiber-reinforcement.
- To investigate comprehensively the influence of fibers on drained and undrained shear characteristics of sand in compression and extension, where wide range of confining pressures were applied, with particular attention on volumetric change and pore water pressure generation characteristics. For this purpose, mainly three fiber contents of 0.0%, 0.2% and 0.4% were used with further investigation of the impact of fiber length.
- To explore the possible description of the mechanical behavior of fiber-reinforced sand through critical state soil mechanics and to obtain elasto-plastic parameters needed for the proper usage of the constitutive models. In particular, the present study addressed deviator stress q, mean effective stress p' and specific volume v through the shearing process and up to the end of the test, and focused on the effect of fiber contents on the critical state line of fiber-reinforced sand.
- To investigate the anisotropic behavior of unreinforced sandy specimens depending on the sample preparation methods and the influence of fibers on the initial anisotropy and development of anisotropy with the shear progression.

(2) Numerical study was performed:

- To efficiently use and apply the existing constitutive model (SYS Cam-clay model), developed by the geotechnical group of Nagoya University based on soil skeleton structure concept within critical state soil mechanics, to a wide range of experimental results obtained in this research;
- To investigate the influence of fibers on the mechanical behavior of sand through the analysis of the effect of fibers on elasto-plastic and evolution rule parameters, and to propose the mechanism of fiber-reinforcement based on both experimental and numerical simulation. Particularly, the

effect of fiber inclusions on the initial degree of anisotropy and the subsequent development of anisotropy in unreinforced and fiber-reinforced sand;

- To determine the necessary physical and mechanical parameters for further implementation on the modeling issues.

1.3 Research outline

The present study or research consists of six chapters. Following this chapter, Chapter 2 presents previously published works with experimental and theoretical/numerical findings on fiber-reinforced soils from laboratory investigations and trial field scale applications of this technique. In Chapter 2, main outcomes regarding the impact of fibers on the mechanical behavior of soils and a possible interaction mechanism of fibers and soils particles, along with the effect of fibers on the enhancement of soil stability and strength from previous studies will be presented.

Chapter 3 consists the information on the experimental apparatus, the materials for both host soil and the fiber, and the methods for the sample preparation with choosing the optimum way with a high reproducibility. Also, information on the host soil including grain size distribution and physical properties, and properties of the reinforcing materials presented by the manufacturer will be presented. Triaxial testing apparatus that allows to conduct both drained and undrained experiments with possibility of pore water pressure measurement have been used for all the experiments.

Chapter 4 presents the results of the experimental work including isotropic compression, consolidated drained triaxial compression and extension, consolidated undrained triaxial compression and extension tests performed on unreinforced and fiber-reinforced sands. Experimentations have been conducted under various confining pressure on the specimens with different initial relative densities. Particularly, effectiveness of fibers as a reinforcing material have been investigated for different density condition including loose, medium loose, medium dense and dense conditions. As for the consolidation pressure the range of confining pressure have been applied from 50kPa to 600kPa. Also, effect of fibers on the small-strain characteristics as well as its effect on the residual stress behavior with particular attention to the critical state have been thoroughly investigated. Possible interpretation of unreinforced and fiber-reinforced sand through the critical state soil mechanics have been also discussed. Additionally, this chapter reports some assumptions regarding

the impact of fiber inclusion on the failure modes, which is supposed to have an influence on the shearing behavior.

Chapter 5 reports numerical analysis of both isotropic compression and triaxial shearing behavior of unreinforced and fiber-reinforced sand through the elasto-plastic model that is called a super/subloading yield surface Cam-clay model (SYS Cam-clay) (Asaoka et al., 2002; Asaoka, 2003). SYS Cam-clay is a constitutive model based on the critical state soil mechanics theory, which considers the evolution of soil skeleton structure associated with the development of plastic deformation. By utilizing material parameters of unreinforced and fiber-reinforced sand obtained in the experimental work, sensitivity analysis and the effect of definite parameters of the model has been considered. Additionally, the possibility of reproduction of undrained mechanical behavior of unreinforced and fiber-reinforced sand has also been studied using input parameters of the model from a single simulated drained experimentation. Moreover, effect of fibers on the initial degree of anisotropy of sand and on consecutive shearing behavior has been numerically analyzed by emphasizing the fiber-sand particles interaction. Finally, a possible mechanism for the fiber-reinforcement has been proposed based on both experimental and numerical analysis.

Chapter 6 presents discussions on the anisotropic behavior of sand according to the obtained results from experimental and simulation work. Also, the mechanism of fiber-reinforcement and the effect of fibers on the initial anisotropy of sandy soil and the further progression of anisotropy with the shearing progression have been discussed. Two types of the host soil with different degree of roundness and two types of fibers with different properties as tensile strength and Young's modulus have been considered.

Chapter 7 draws main conclusion from conducted experimental work and considered constitutive model, SYS Cam-clay, briefly summarizing main results and findings and limitations of this research, and proposing suggestions for the future studies.

Appendices consist the information about the determination of the void ratio of fiber-reinforced sand through different approaches, where the effect of consideration of fibers as a part of solid or void on initial relative density is given. Also, the sensitivity analysis of the SYS Cam-clay model and the effect of each evolution rule parameters and initial state parameters has been shown.

CHAPTER 2

LITERATURE REVIEW

2.1 Introduction

Soil stabilization and soil strength improvement issues have been actively investigating through many years. From the ancient times it is well-known that the strengthening soils by mixing with other additives are efficient ways that were observed in the nature due to the external actions caused by animals and plants impact. From year to year the soil stabilization and improvement techniques have been gradually improved and have been successfully applied to a variety range of geo-structures. Especially, for the last 30 years more and more attention has been payed to fully understand the mechanism of reinforcement by different additives as cement, lime, fly ash, and etc., and to obtain a deeper view on the benefits of soil strengthening by adding various inclusions. At the same time, the consequences of using different methods of soil improvement was not counting the impact on the environment, and issues related to the recycling the unusable and fatigued structures.

The use of alternative technique of soil improvement by adding different types of fibers, both natural and synthetic, rises more and more interest among practicing engineers and researches, considering the fiber-reinforcement more cost effective and relatively less harmful to the nature. The idea of using tension resisting elements was created based on the plant roots effect in improving near surface soil layers, especially attractive is the increased stability of soils with plant roots at the slope stability near mountainous area. Recently, more and more attempts have been applied to practically implement the fiber-reinforcement on various geo-structures, including thin soil layers, footings and pavement, earth retaining structures and repairmen of failed slopes. However, further studied are required to fill the existing gap between theoretical understanding of the potentials of fiber-reinforcement and its mechanism on enhancing the soil strength and application of this technique on a production scales including soil mixing issues. Moreover, comprehensive analysis of the potentials and limitations of fiber-reinforcement should be performed to allow the application of this technique to more complex geo-structure as dams, foundation and embankments, excavated slope stability, where stronger and liquefaction resistant earth fills are needed.

2.2 Experimental work

The effectiveness of tension resisting elements has been studied for many years. Fiber inclusions have similarities with root reinforcement in soil (Wu et al., 1979; Muir Wood et al., 2016), which has raised great interest as an alternative soil stabilization technique. Several types of geotechnical structure might be improved by fiber-reinforcement, such as retaining structures, embankments, and slopes, as well as subgrade strengthening beneath footings and pavement. The influence of flexible fibers on the shear-strength and volumetric change behavior of soils has been investigated through different type of experimentations: direct shear (Gray and Ohashi, 1983; Gray and Al-Refeai, 1986; Jewell and Wroth, 1987; Yetimoglu and Salbas, 2003; Ibraim and Fourmont, 2007; Sadek et al., 2010; Falorca and Pinto, 2011; Eldesouky et al., 2016; Muir Wood et al., 2016); conventional triaxial compression and extension under both drained and undrained conditions (Maher and Gray, 1990; Michalowski and Ĉermak, 2003; Consoli et al., 2007a; Consoli et al., 2009; Chen, 2010; Diambra et al., 2010; Dos Santos et al., 2010; Lirer et al., 2011; Ibraim et al., 2012); and bender element and ring shear tests (Heineck et al., 2005; Consoli et al., 2007b; Liu et al., 2011).

2.2.1 Materials

Previous studies have been experimentally investigated the effectiveness of several type of fibers on the different soils including both cohesion and cohesionless types. For example, low plasticity clay, soft clay, quartz beach sand, non-plastic uniform fine and coarse sands, silty sand, borucatu clayey sand, sandy gravel, poorly graded sand and full-size, 1/3 and 1/5 scaled railway ballast and etc.

As for the fibers, both natural fibers – reed, palmyra a tough fiber obtained from the African palmyra palm, jute and coir fibers, and synthetic fibers – plastic (PVC), copper wire, polyamide monofilaments, steel galvanized wire, fibrillated and monofilament extensible polypropylene fibers, crimped Locsand fibers, tape-like polyethylene fibers and so on. Along with the type of fibers, geometric effect of fibers has also been investigated. For instance: the different length, different size of cross sections (diameter) and aspect ratios of fibers to check the effect and contribution to the strength enhancement and find out the limit to the maximum effective length.

2.2.2 Sample preparation

Sample preparation is one of the most important issues that needs a careful attention to reach the satisfactorily good distribution of fibers throughout the whole soils with high homogeneity. In previous studies different methods of mixing fibers with soils and different placement techniques for

specimen formation have been used (Michalowski and Ĉermak, 2003; Ibraim and Fourmont, 2007; Gao and Huang, 2021). Generally, the sample preparation includes two stages: mixing fibers with soil and placement/compaction into desired sample size.

Primary attempts were performed to mix fibers manually with scoop in dry condition similarly to one for the powder additives as cement and fly ash. However, once the fiber content increased to more than 0.5% by dry weight of soils, the segregation of fibers and soil were noticed, and the addition of water was required. According to some previous studies (Ibraim and Fourmont, 2007; Eldesouky et al., 2016) the optimum moisture content that was found through the modified Proctor compaction tests was equal to approximately to 10%. Furthermore, Ibraim and Fourmont, (2007) revealed that there is a limit of fiber contents that can be mixed with soil to get a desired density, after which the preparation of reinforced specimen is not possible.

Specimen formation was also performed in different ways. Most of the studies placed samples in several layers through tamping or vibration (side tapping) to put the whole mass to the desired density. At the same time, there are some studies that considered placement of whole mixed mass in one layer to make the orientation of fibers more random. According to some reported researches, placement in one layer leads to high inhomogeneity of fibers' distribution. Considering the mixed mass to be in moisture condition, additional weight was needed to compress to get definite dimensions (Fig. 2.1).

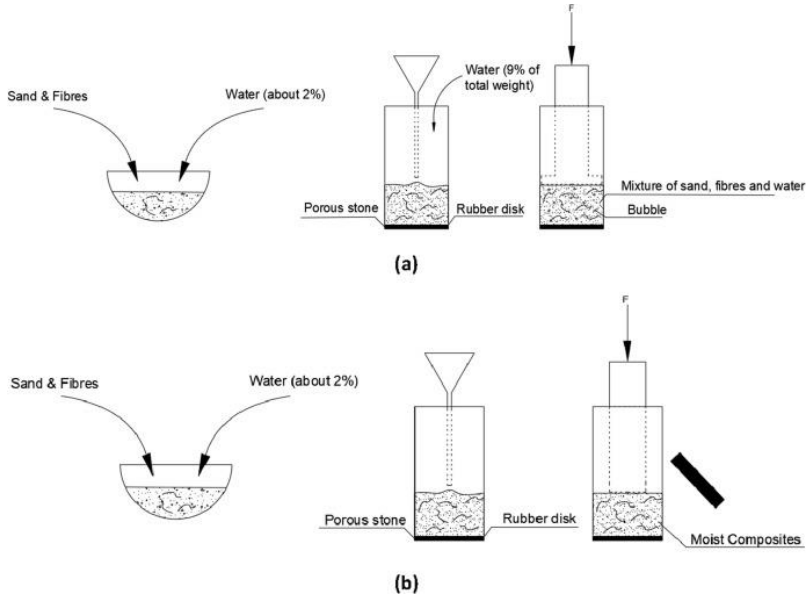

Fig. 2.1 Illustration of the sample preparation methods: (a) Moist tamping and (b) moist vibration (after Gao and Huang, 2021)

Although, most of the studies assumed and investigated the mechanical behavior of fiber-reinforced soil through the random distribution of fibers in the soils, according to some previous studies (Ibraim and Fourmont, 2007; Consoli et al., 2009; Diambra et al., 2010) moist tamping or moist vibration methods of sample formation creates more horizontally preferred orientation of fibers within the specimen. In order to solve this issue and make the specimen with less oriented distribution of fibers and increase the homogeneity of reinforced specimens, Michalowski and Ĉermak, (2003) developed a tool to change the initial orientation of fibers in the samples (Fig. 2.2). Regardless of the way of sample preparation the homogeneity is always in a high priority to avoid an unintended deformation on a specific part of the sample (construction).

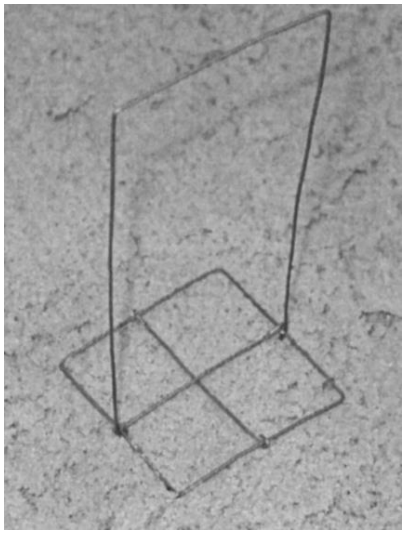

Fig. 2.2 Wire grid tool used to alter orientation of fibers during specimen preparation (after Michalowski and Ĉermak, 2003)

2.2.3 Typical results

Most of the previous studies have been focusing on the shear strength enhancement by adding different type of fibers. Figs. 2.3-2.5 present results of some relatively early experimental works performed on fiber-reinforced sand through direct shear (Gray and Ohashi, 1983; Jewell and Wroth, 1987) and triaxial compression tests (Maher and Gray, 1990). From the results of experimentations, it was concluded that depending on the fiber properties the enhancement of the shear strength of sand will vary. Also, as it can be seen in Fig. 2.3 and Fig. 2.5 one of the major properties of fibers is an aspect ratio, including length and diameter. Furthermore, fiber-reinforced sand specimens had more dilative behavior in the direct shear test (Fig. 2.4). In early studies, there was no particular suspicious

influence of the fiber inclusions on the shear properties. However, in the later studies, some important points and some debatable questions revealed.

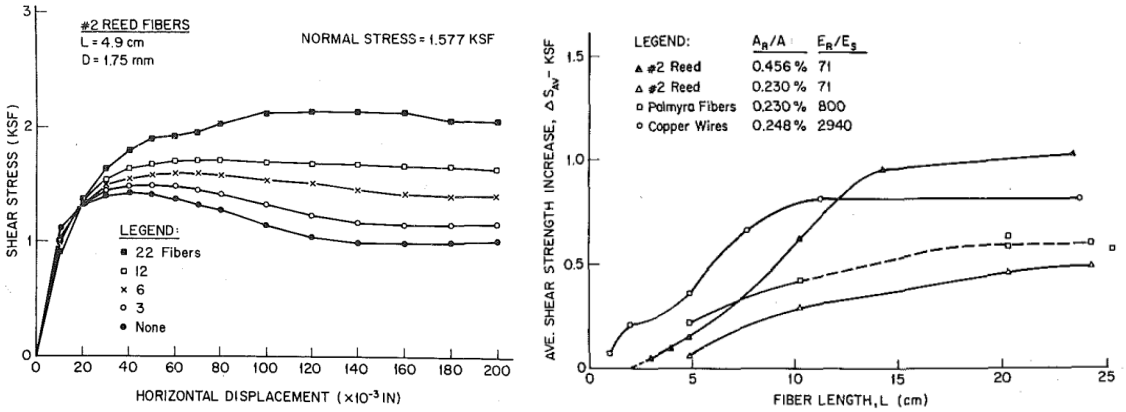

Fig. 2.3 Influence of number of reed fibers and the length of different fibers on stress-deformation behavior of a dense, dry Muskegon dune sand (after Gray and Ohashi, 1983)

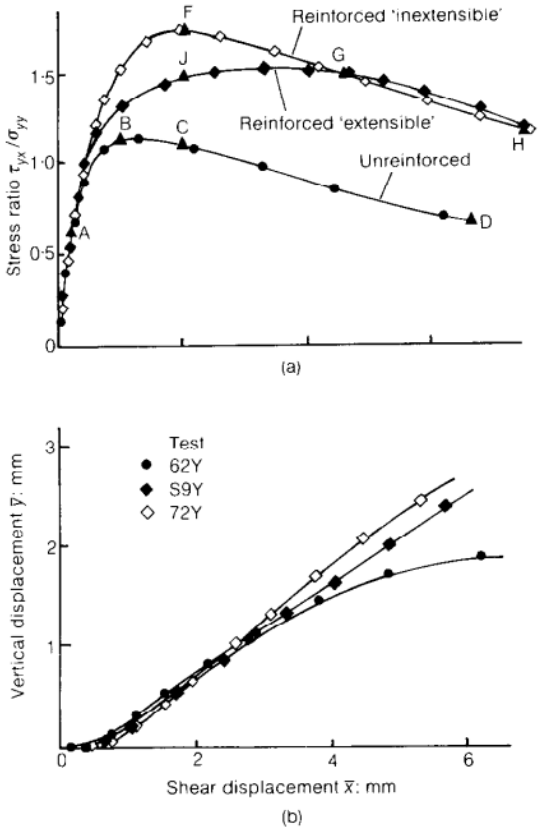

Fig. 2.4 Results of direct shear tests on reinforced sand with extensible and very stiff reinforcement (after Jewell and Wroth, 1987)

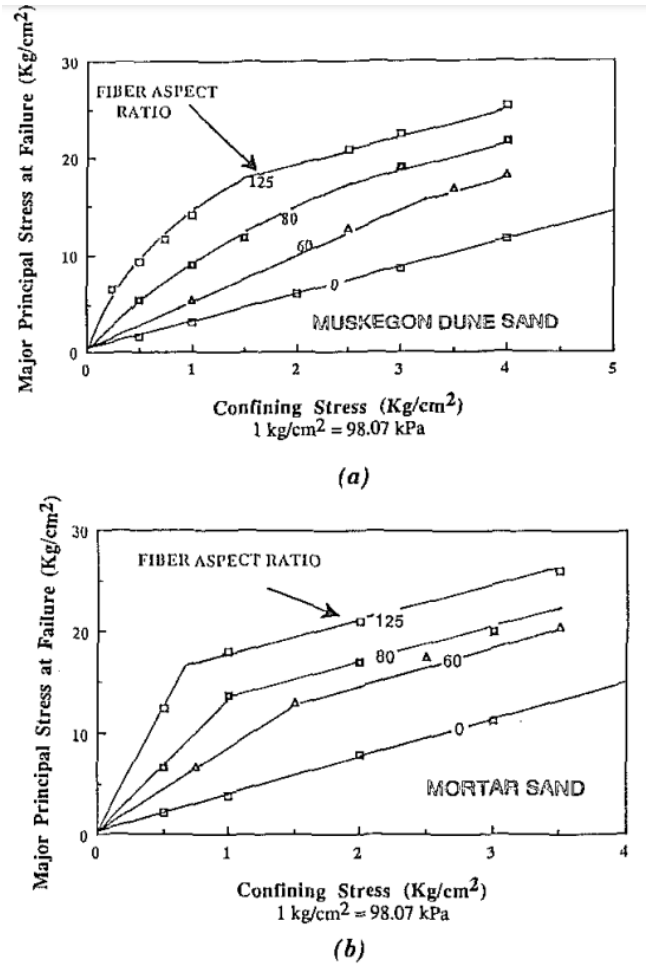

Fig. 2.5 Principal stress envelopes from triaxial compression tests on reinforced sands: (a) Muskegon dune sand; and (b) Mortar sand (glass fibers at 3% by weight, aspect ratio = 60, 80, 125) (after Maher and Gray, 1990)

For example, depending on the fiber type and the size of the host soil, especially depending on the Young's modulus and tensile strength of the fibers, fiber-reinforced sands experienced decreased initial stiffness (Michalowski and Ĉermak, 2002; Michalowski and Ĉermak, 2003; Ajayi et al., 2017; Li and Senetakis, 2017; Li et al., 2019, Mandolini et al, 2019), while most of other studies did not observe. Figs. 2.6-2.7 show some typical results of the triaxial compression tests performed on the reinforced sands, where decreased initial stiffness was shown. From these results, it was revealed that fibers might not be effective on small-strain characteristics of sands, attributed to the fiber sand interaction mechanism. A higher strain and a higher aspect ratio of fibers compared to the host soil (at least one order higher) was needed to efficiently use for the small strain related issues.

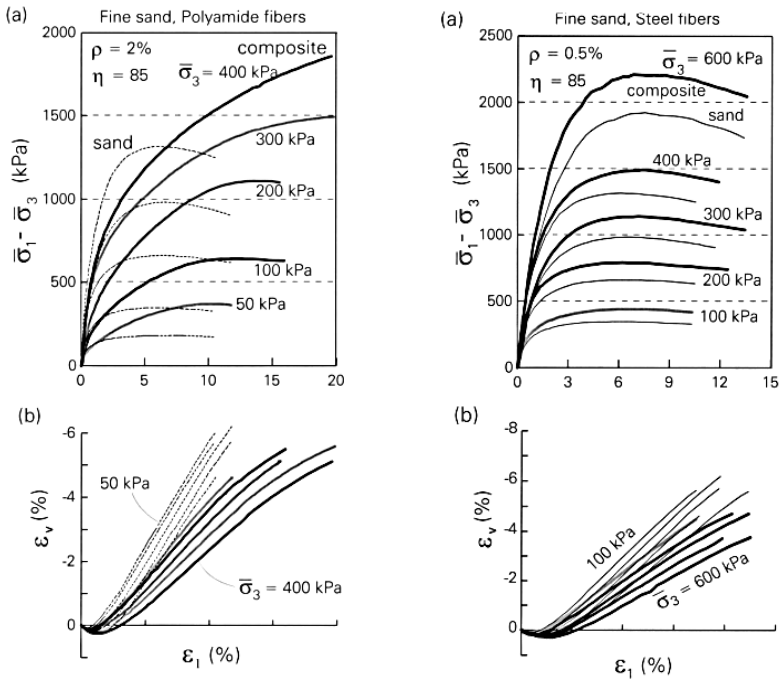

Fig. 2.6 Triaxial compression tests on fine sand with polyamide and steel fibers (after Michalowski and Ĉermak, 2003)

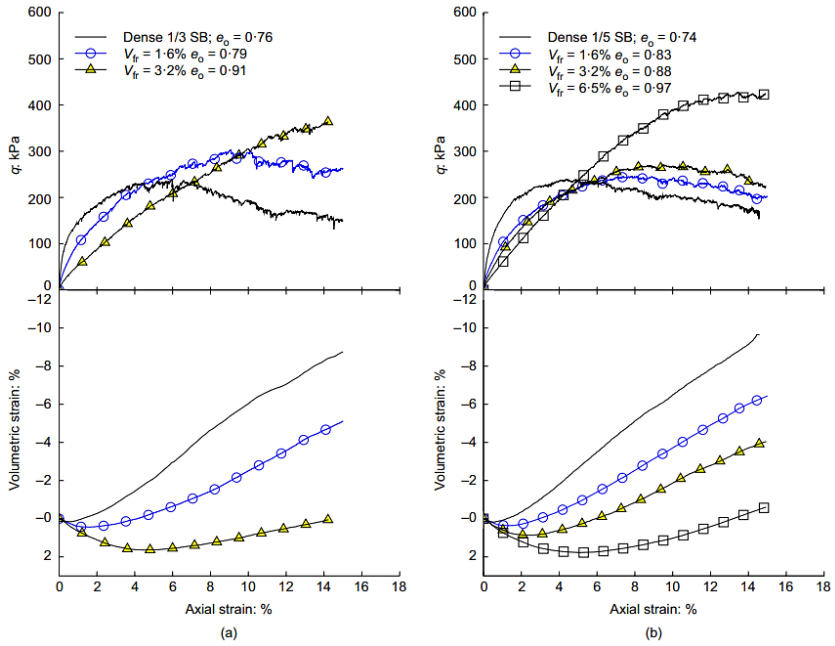

Fig. 2.7 Conventional deviator stress, $q = (\sigma_a - \sigma_r)$, and volumetric strain plotted against axial strain for unreinforced specimens of (a) 1/3 SB and (b) 1/5 reinforced SB with different fiber contents. Cell pressure = 30 kPa (after Ajayi et al., 2017)

Another important point was related to the dilatancy properties of the reinforced soils. Some researchers showed a more dilative behavior of fiber-reinforced specimens, while others presented opposite conclusions. The more dilative behavior in the test results was explained as the effect of fibers on the initial void ratios, where consideration of fibers as a part of solids or voids results in a significant difference of the relative densities. Consequently, when fiber inclusions increased the initial relative density, the mechanical response was more dilative. In contrast, fiber inclusions make a positive contribution on the effective stress with adding up confinement and contracting the specimen with less dilatancy with the shear progress. Moreover, as the shear progresses, the tensile forced is produced more intensively at a higher strain rates than at the initial stage of shearing.

As presented above, early studies reported that the fibers are more effective when the aspect ratio and length of the fibers are longer. Primary understanding of effectiveness of fibers was the longer the fiber the more positive contribution to the strength enhancement. However, according to later studies (Falorca and Pinto, 2011; Mirzababaei et al., 2018), investigation on the effectiveness of the fiber length on the different type of soils (cohesive – clay, and cohesionless – sand) showed that there is a limit of the effective length of fibers, after which the effectiveness of fiber-reinforcement will reduce (Fig. 2.8).

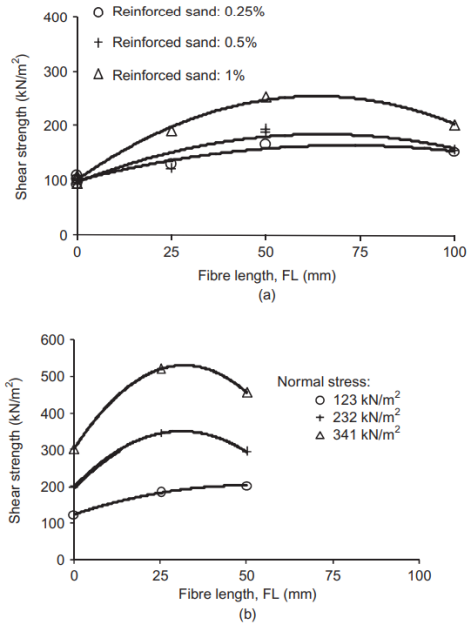

Fig. 2.8 Influence of fiber length on the shear strength for: (a) reinforced sand and (b) reinforced clay (after Falorca and Pinto, 2011)

Last, but not least, the effect of sample preparation of both unreinforced and fiber reinforced specimens should be pointed out. According to some basic investigation of the behavior of unreinforced sand prepared with different methods as moist tamping/tapping and dry deposition through vibration or pluviation (Miura and Toki, 1982; Wood et al., 2008), there were some differences on the mechanical behavior especially regarding the volumetric change behavior in drained condition and stress paths in undrained condition. Similarly, the influence of the sample preparation method on the shear properties of fiber-reinforced sands were investigated in some previous studies through drained triaxial compression tests (Diambra et al., 2010; Ibraim et al., 2010; Ibraim et al., 2012; Diambra et al., 2013). Ibraim et al., (2012) concluded that there was no significant difference between shearing properties of fiber-reinforced specimens prepared by moist tamping and moist vibration (Fig. 2.9). However, some recent studies (Gao and Huang, 2021) reported opposite results regarding the effect of sample preparation on the shearing behavior of fiber-reinforced sand (Fig. 2.10). According to Gao and Huang, (2021) and some previous studies performed to investigate the effect of sample preparation on the mechanical response of sandy soils (Oda, 1972; Miura and Toki, 1982), in fact, the different sample preparation methods do not significantly affect the shearing behavior of unreinforced sand. Particularly, there was only a small effect on the intermediate or small stain characteristics. In contrast, as can be observed in Fig. 2.10, the sample preparation methods for fiber-reinforced sand essentially influenced both stress-strain and volumetric change characteristics. This issue will be further discussed and a possible explanation will be given in Chapter 4.

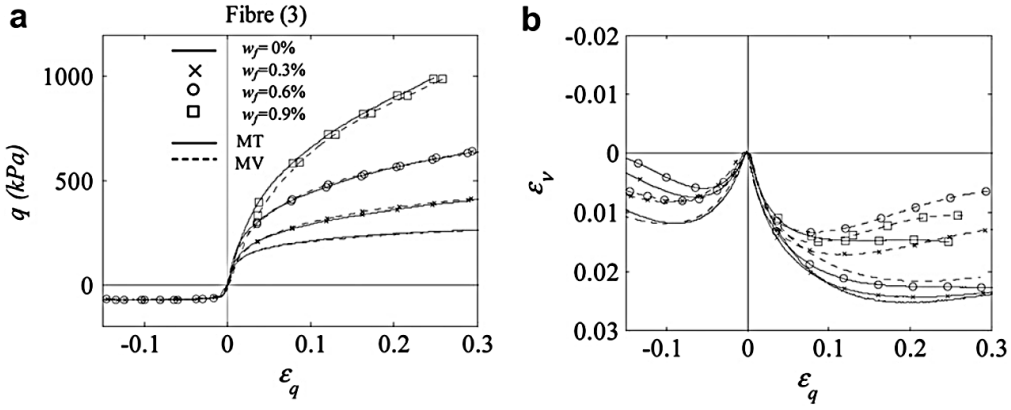

Fig. 2.9 Triaxial compression tests performed on reinforced specimens with moist tamping (MT) and moist vibration (MV) (after Ibraim et al., 2012)

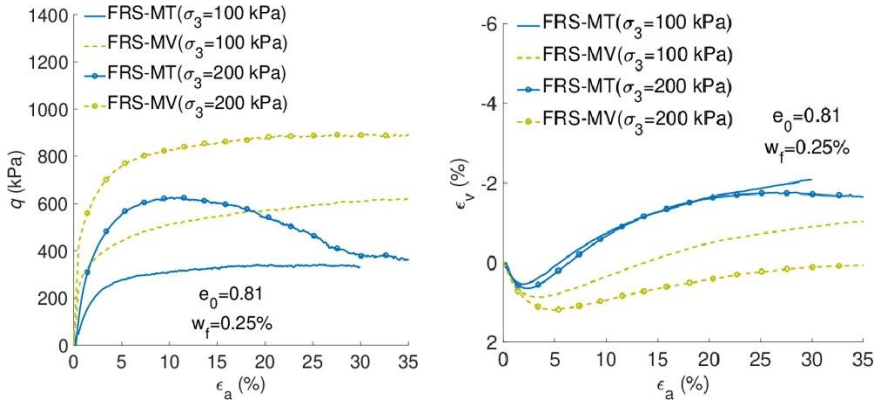

Fig. 2.10 The comparing results of FRS with different preparation methods under the confining pressure of 100 and 200 kPa (e_0 = 0.81) (After Gao and Huang, 2021)

2.2.4 Discussion

According to previous studies (Michalowski and Ĉermak, 2003; Heineck et al., 2005; Sadek et al., 2010; Lirer et al., 2011; Ajayi et al., 2017; Gao and Huang, 2021), some typical outcomes were obtained: fiber-reinforced specimens exhibited an initial stiffness reduction with increase of the peak strength and reduction in the post-peak strength loss related to the nature of the fibers and grain size of the host soil in drained triaxial tests; the investigation on the impact of fibers on the dilatancy behavior of soils was also conducted, where decreased volumetric change with the increase in fiber content was observed. In contrast, in some other studies volumetric change behavior was rendered more dilative by introducing fibers into the soil (Ibraim and Fourmont, 2007; Consoli et al., 2009; Diambra et al., 2010). Most previous experimental studies examined the effects of not only fiber content and length of fibers, but also confining pressure and relative density on the mechanical behavior of fiber-reinforced sand. They have presented valuable results. However, few studies have discussed the simultaneous changes in deviator stress *q*, mean effective stress *p*', and specific volume *v* until the end of shearing in the drained triaxial compression test and, focused on the critical state line of fiber-reinforced sand based on the critical state concept. It should be useful to interpret the shear behavior of fiber-reinforced sand based on the critical state concept to construct a constitutive model for describing fiber-reinforced sand.

The critical state concept (Roscoe et al., 1958; Schofield and Wroth, 1968; Atkinson and Bransby, 1978) is one of the most important and basic concepts for understanding the mechanical behavior of soil. This concept has contributed to the proposal of many constitutive models for describing soils.

An idealized family of critical state lines from high plastic silty clays and clays to almost non-plastic silty sandy soils were shown through the concept (Schofield and Wroth, 1968). The critical state of sandy soil has been presented and discussed in previous studies (Roscoe et al., 1958; Atkinson and Bransby, 1978; Verdugo and Ishihara, 1996). However, studies focused on the interpretation of the mechanical behavior of sand reinforced with fibers through the critical state framework have been limited (Dos Santos et al., 2010). Furthermore, analysis of the experimental work has been limited regarding the influence of various parameters and testing conditions on the composite materials.

2.3 Numerical analysis of mechanical behavior of fiber-reinforced soils

Fiber reinforcement has advantages in increasing the soil strength and improving the stability of geo-structures that was proved by experimental investigations. In order to describe and assess the effect of fiber inclusions in soils a suitable constitutive equation is necessary with considering different testing conditions (drainage characteristics, density, applied stress, etc.). Constitutive models for fiber-reinforced soils have been developed to evaluate the behavior of geotechnical structures improved by fiber-reinforcement. There are different approaches in the existing methods to predict and describe fiber-reinforced soil behavior.

2.3.1 Different approaches

The existing methods to predict and describe fiber-reinforced soil behavior include two main approaches: discrete and composite. The discrete approach implies modeling soil behavior, effect, and interaction of reinforcing material with soil separately (Zornberg, 2002; Lirer et al., 2011; Babu and Chouksey, 2010). In the composite approach, fibers and soils are treated as a composite material (Gray and Ohashi, 1983; di Prisco and Nova, 1993; Maher and Gray, 1990; Michalowski and Ĉermak, 2002; Diambra et al., 2010; Diambra and Ibraim, 2015; Gao and Diambra, 2020; Gao et al., 2020). The composite approach includes different concepts such as force equilibrium models (Gray and Ohashi, 1983; Maher and Gray, 1990; Sadek et al., 2010; Shukla et al., 2010), energy-based homogenization technique (Michalowski and Zhao, 1996; Michalowski and Ĉermak, 2002; Michalowski and Ĉermak, 2003; Michalowski, 2008; Jamie et al., 2013), equivalent additional stress method (Jie et al., 2012; Wang et al., 2019), superimposition of the fiber and sand matrix (Diambra et al., 2010; Diambra et al., 2013; Diambra and Ibraim, 2014; Diambra and Ibraim, 2015), a combination of energy-based homogenization technique and superimposition methods (Wang et al., 2018). Additionally, some studies have applied a curve fitting technique based on finite element

methods (Ibraim and Maeda, 2007; Maeda and Ibraim, 2008; Babu et al., 2008; Babu and Chouksey, 2010; Zhang et al., 2013; Kanchi et al., 2015).

2.3.2 Constitutive models for predicting mechanical behavior of fiber-reinforced soils

Zornberg, (2002) was one of the first researchers who proposed a discrete model to analyze the mechanical behavior of fiber-reinforced soil. In discrete model fibers are treated as discrete elements that contribute to stabilize soils by producing tensile stresses along the shear plane. Later, some other studies have also been conducted to further elaborate on improving and application of discrete model on fiber-reinforced soil (Lirer et al., 2011; Babu and Chouksey, 2010). All of later studies made some contribution in developing the discrete approach. Fig. 2.11 presents comparison of results in terms of friction angle at failure between experimental and analytical work according to the equation proposed by Lirer et al., (2011). In reported analytical results fibers and soil grading effect were simultaneously considered on micromechanical level based on discrete approach. Almost all studies on the proposal of the discrete models on the fiber-reinforcement had closer approach to curve fitting technique by proposing simple equation to account the fibers' existence. In fact, discrete modeling of fiber-reinforcement through the FEM analysis is more time requiring and more complicated in terms of realization of the calculation (Babu and Chouksey, 2010; Zhang et al., 2013; Kanchi et al., 2015). Additionally, consideration of fibers and host soil particle interaction mechanism is less likely to be taken into account.

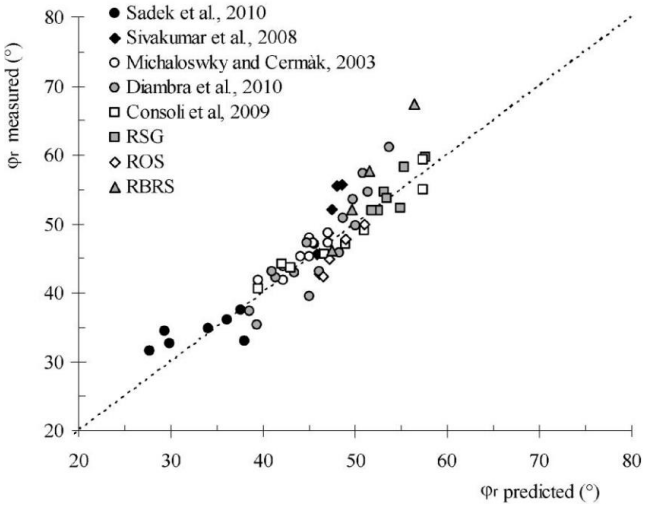

Fig. 2.11 Measured and predicted frictions angles of fiber-reinforced specimens (after Lirer el al., 2011)

In case of composite approaches most of the models were proposed by utilizing and modifying already existing models for unreinforced soils. For example, Severn-Trent sand model proposed by Gajo and Muir Wood, (1999) as a kinematic hardening model which modifies the Mohr-Coulomb frictional model to describe the mechanical behavior of unreinforced sand. Simultaneously, the shear-lag theory with further modification were successfully utilizing for the constitutive relationship of mixture constituents to reproduce shearing behavior of fiber-reinforced soils (Diambra et al., 2010; Diambra et al., 2011; Diambra et al., 2013; Diambra and Ibraim, 2014; Diambra and Ibraim, 2015; Muir Wood et al., 2016). Fig. 2.12 shows the triaxial testing results and model simulation of the fiber-reinforced Hostun sand by modified Severn-Trent sand model with the shear-lag theory. In the studies of the above-mentioned authors, the interaction of fibers with cohesionless and cohesive soils has different mechanism, where fibers brought more dilatancy to the host sand and had a contracting effect on the host clay.

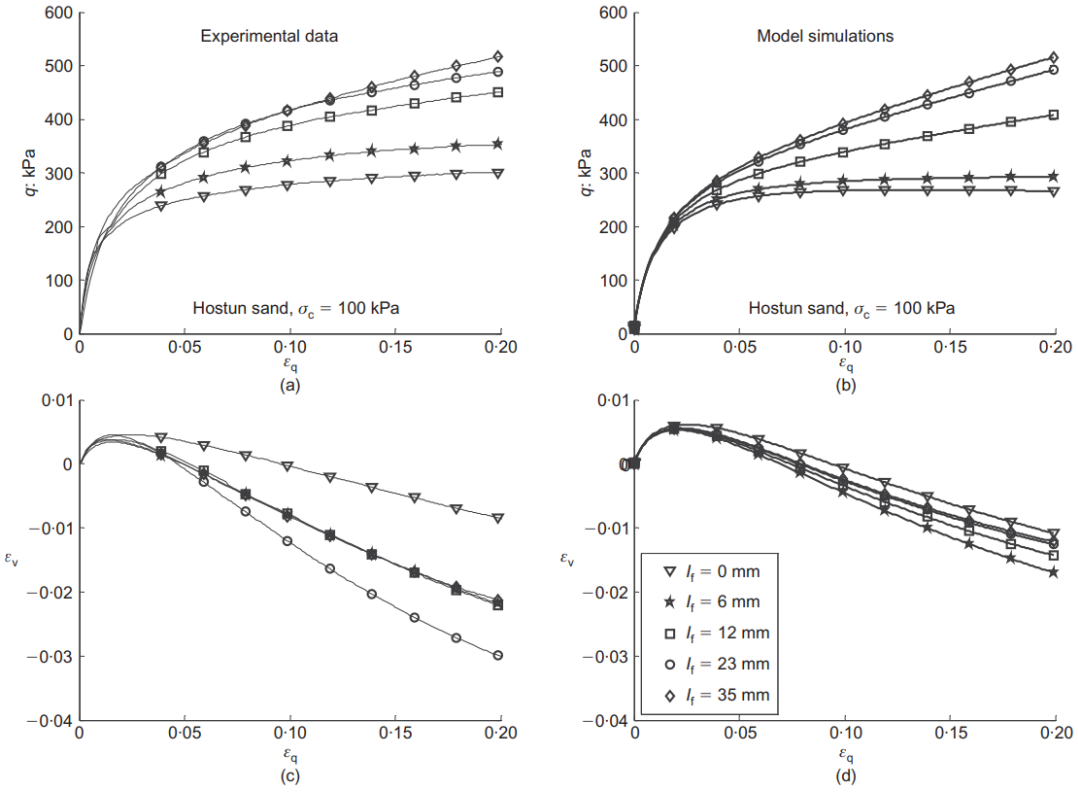

Fig. 2.12 Triaxial test results (a and c) and model simulations (b and d) for Hostun sand unreinforced and reinforced (0.3% fiber content) specimens, tested under 100 cell confining pressures (legend indicates the fiber length) (after Diambra and Ibraim, 2015)

Numerical studies regarding the fiber-reinforced cohesive soils were limited. Recently, some numerical studies concerning on the modeling of fiber-reinforced clay were presented (Wang et al., 2018; Wang et al., 2019). Fig. 2.13 shows the modeling results of Wang et al., 2018 and Wang et al., 2019 performed on fiber-reinforced clay under 200kPa confining pressure. In the first case (Wang et al., 2018), a combination of energy-based homogenization technique (Michalowski and Zhao, 1996; Michalowski and Ĉermak, 2002; Michalowski and Ĉermak, 2003; Michalowski, 2008; Jamie et al., 2013) and superimposition methods (Diambra et al., 2010; Diambra et al., 2013; Diambra and Ibraim, 2014; Diambra and Ibraim, 2015) were used. In the second case (Wang et al., 2019), the analysis was performed based on equivalent additional stress method (Jie et al., 2012). Mechanical behavior of fiber-reinforced clay was fairly captured by both methods, however, both numerical results by both methods look quite similar.

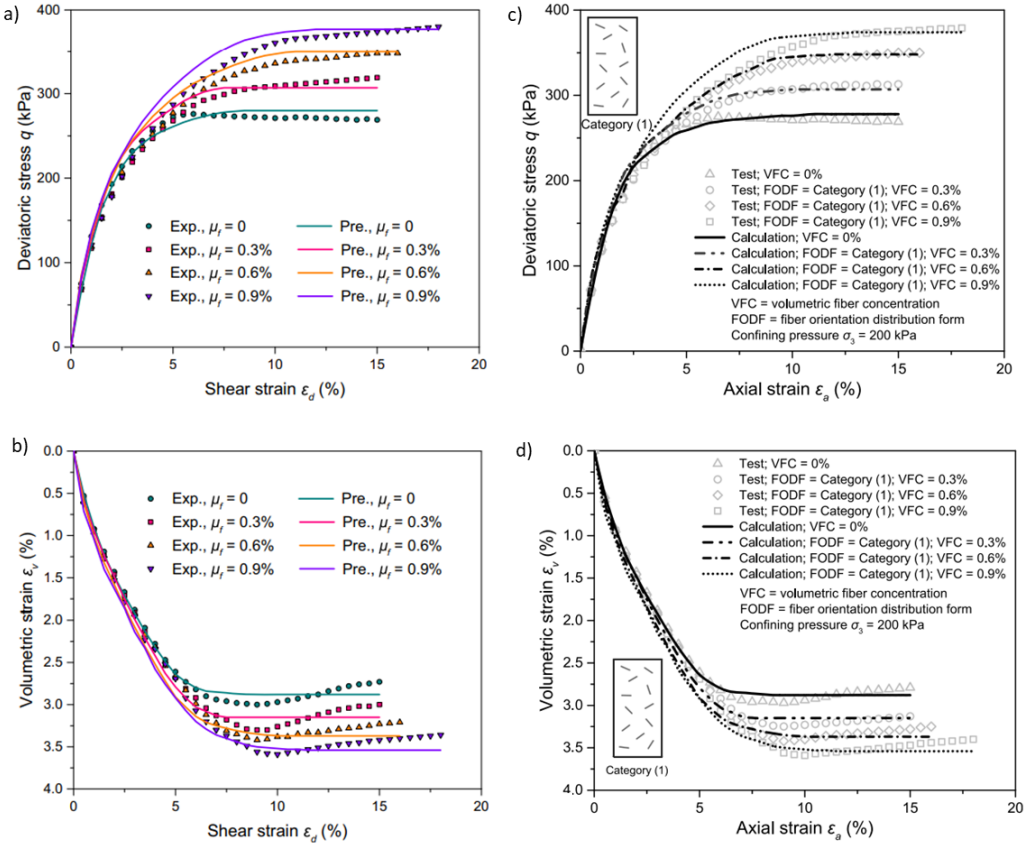

Fig. 2.13 Comparison between experimental (Exp.) and predicted (Pre.) behavior of samples at a 200kPa confining pressure: a, b combination of superimposition and energy-based homogenization technique; and c, d equivalent additional stress concept model (Wang et al., 2018; 2019)

During the last decade there were a lot of attempts to reproduce elasto-plastic behavior of fiber-reinforced soils. In some cases, the anisotropic distribution of fibers was also considered and attempts to take into account the anisotropy of fiber-reinforced composite were performed. However, a full anisotropic model for fiber-reinforced sand was proposed for the first time by Gao and Diambra, (2020). The model was proposed by introducing four new parameters to an existing constitutive model proposed by Li and Dafalias, (2002). Some results of the model simulation on Hostun sand is given in Fig. 2.14. Furthermore, some other studies were successfully developed within the constitutive model of Li and Dafalias, (2002) by implementation effective skeleton stress and void ratio concept considering various testing conditions (Gao et al., 2020; Gao and Huang, 2021).

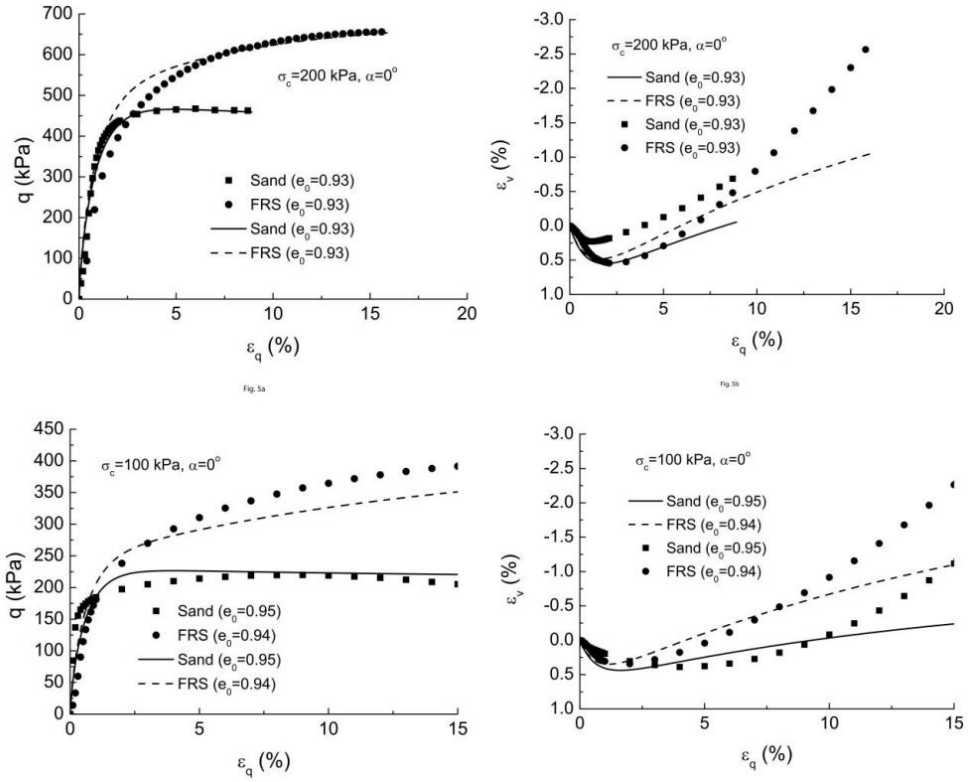

Fig. 2.14 Comparison between the test data and model simulations for the stress-strain relationship of fiber-reinforced Hostun RF (S28) sand at (experimental data from Mandolini et al., 2019) (after Gao and Diambra, 2020)

2.3.3 Discussion

Numerous experimental and numerical studies have proven the value of reinforcing soils for improving strength using different types of tension resisting elements. In addition, some field studies

have investigated fiber reinforcement (Santoni and Webster, 2001; Falorca et al., 2011; Shukla, 2017), revealing issues and challenges for implementation. Despite having a huge number of reported results, there is still a gap between laboratory investigations and practical implementation of this techniques because of big differences in the mechanism of fiber-reinforcement. Moreover, there are still several points that should be further elaborated to compromise on the diverging points.

Purpose of proposal of discrete methodology (Zornberg, 2002; Lirer et al., 2011) to describe the mechanical behavior of fiber-reinforced soils is that there might not be necessity in conducting various experiments on the composite materials, but knowing the properties and shearing behavior of reinforcing materials and the host soil separately might be enough to predict the mechanical behavior of the composite materials. It might be very helpful to save time and expenses on performing different type of experimental investigations. However, despite a lot of numbers of attempts to follow and further develop discrete approach in analyzing the behavior of fiber-reinforced soils, there are still some difficulties in widely utilization of this method, especially regarding the interaction mechanism between the host soil and the reinforcing materials.

Valuable results were presented in previous studies regarding numerical analysis of fiber-reinforced soil by a composite approach. Various testing conditions, including stress ratio, types of host soil and reinforcing material, effect of fibers' distribution were also considered. However, as can be observed from some presented results of numerical simulation, most of the studies considered loose condition of soils, where in most cases only hardening behavior is more likely to occur, with compression on the volumetric change response or very small expansion. Moreover, even considering loose fiber-reinforced samples, these results and the mechanism of fiber-reinforcement vary study to study, which should be also elaborated.

2.4 Brief summary

Despite the existence of a relatively large number of laboratory studies, there are still discrepancies in the test results and challenges in fiber-reinforced sample preparation, which inhibits wide-spread practical application of this alternative soil stabilization technique. Some typical outcomes of previous studies were as follows: in monotonic loading tests fiber-reinforced specimens exhibited an increase in peak and post-peak strength; in dynamic testing of soils there was an increase in composite material damping conditioned with the presence of fibers. The most important factor of the effectiveness of fiber-reinforcement is considered to be the interaction between fibers and a host

soil, specifically regarding the grain size of the host soil and geometry and percentage of fibrous materials.

Two points of contention from previous studies should be noted. Firstly, there is the impact of fibers on the dilatancy behavior of soils. In some cases, decreased volumetric change of the reinforced soil with an increase in fiber content was observed compared to unreinforced soil (Michalowski and Ĉermak, 2003; Heineck et al., 2005; Ajayi et al., 2017; Li et al., 2017); in contrast, in some other studies volumetric change behavior of soil was rendered more dilative by fiber inclusions (Ibraim and Fourmont, 2007; Consoli et al., 2009; Diambra et al., 2010; Ibraim et al., 2012; Mandolini et al., 2019). Secondly, although some previous studies reported a decrease of small-stain/initial stiffness of reinforced soil, other researches did not observe this tendency. According to Michalowski and Ĉermak, (2003), such a reduction in initial stiffness of the composite was due to the characteristics of fibrous materials (stiffness and roughness), the grain size of the host soil, and the content of the reinforcing material. Moreover, it was concluded that the effectiveness of fiber inclusions on the behavior of soils depends on the considered strain magnitude, where fiber-reinforced soils exhibited a decrease in small-strain stiffness and an increase in the linearity of stiffness reduction curves (Li et al., 2017; Li and Senetakis, 2017; Li et al., 2019).

In numerical simulation the two approaches, discrete and composite, were successfully implemented in describing fiber-reinforced soil's behavior. The discrete approach might be useful to reduce the number of required experimental work on the composite materials with the only requirement to parameter for the host soil and reinforcing material. However, at the same time it is difficult to consider the interaction mechanism of fibers with the soil particles on the micro level. Also, modeling of fiber-reinforced sand through FEM analysis utilizing discrete approach makes it more complicated in terms of time and cost. On the other hand, developed composite approaches were also able to fairly reproduce the mechanical behavior of fiber-reinforced sand. Most of the numerical studies on the fiber-reinforced sand composites were based/modified on already existing constitutive equation for the unreinforced soils either by introducing new parameters in the basic model or combining several methods. The existing model and the reproduced results is quite sizeable in terms of the density of composite soils, because in the proposed models mainly loose condition were considered. Moreover, the results of fiber-reinforced sand have discrepancies and the reinforcing mechanism with the effect of fibers on shear-stress-volumetric change behavior are still contentious issues.

CHAPTER 3

EXPERIMENTAL WORK, MATERIALS AND SAMPLE PREPARATION

3.1 Introduction

This chapter describes materials that were used in the experimental work including the host soil and reinforcing agent. Description of the procedures for the experimental work along with the details of the apparatus used in the experimentations including pre-consolidation stage for a saturation is included. Also, detailed description of the sample preparation for unreinforced and fiber-reinforced sand with varying the fibers' content is provided. Moreover, analysis of the fibers' distribution within the specimen through the close investigation of the exhumed sample and checking the reproducibility are given.

3.2 Triaxial testing apparatus

Experimental work has been performed on triaxial apparatus (Fig. 3.1) that allows measurement of volumetric change behavior by recording the volumetric strain in drained condition, and measurement of the generation of pore water pressure in undrained condition. Loading was applied from the upper part of the specimen by the air pressure supplied to the bellofram cylinder with an internal load cell (gage based transducer) of 5 kN capacity. The axial strain was measured using an LVDT placed outside the triaxial cell. The displacement that controls the supplied pressure to the bellofram cylinder and applies load at a constant strain rate was monitored. Volumetric strain was measured by a strain-gage based transducer connected to the drainage burette.

Conventional stress and strain variables were used for axisymmetric triaxial conditions. The deviator stress q and the mean effective stress p' were the stress invariants; volumetric strain ε_v and axial strain ε_a were the strain invariants. These invariants are defined under the triaxial shear condition:

$$p' = \frac{1}{3}(\sigma_1' + 2\sigma_3');\ q = \sigma_1' - \sigma_3';\ \varepsilon_a = \varepsilon_1;\ \varepsilon_s = \frac{2}{3}(\varepsilon_a - \varepsilon_3);\quad \varepsilon_v = \varepsilon_1 + 2\varepsilon_3 \tag{3.1}$$

where σ_1', σ_3' indicate a maximum and minimum principal effective stress, while ε_1, ε_3 are the maximum and minimum principal strain, respectively. Volumetric change was investigated according to the specific volume $v = 1+e_r$, where e_r is the void ratio considering fiber content as defined below.

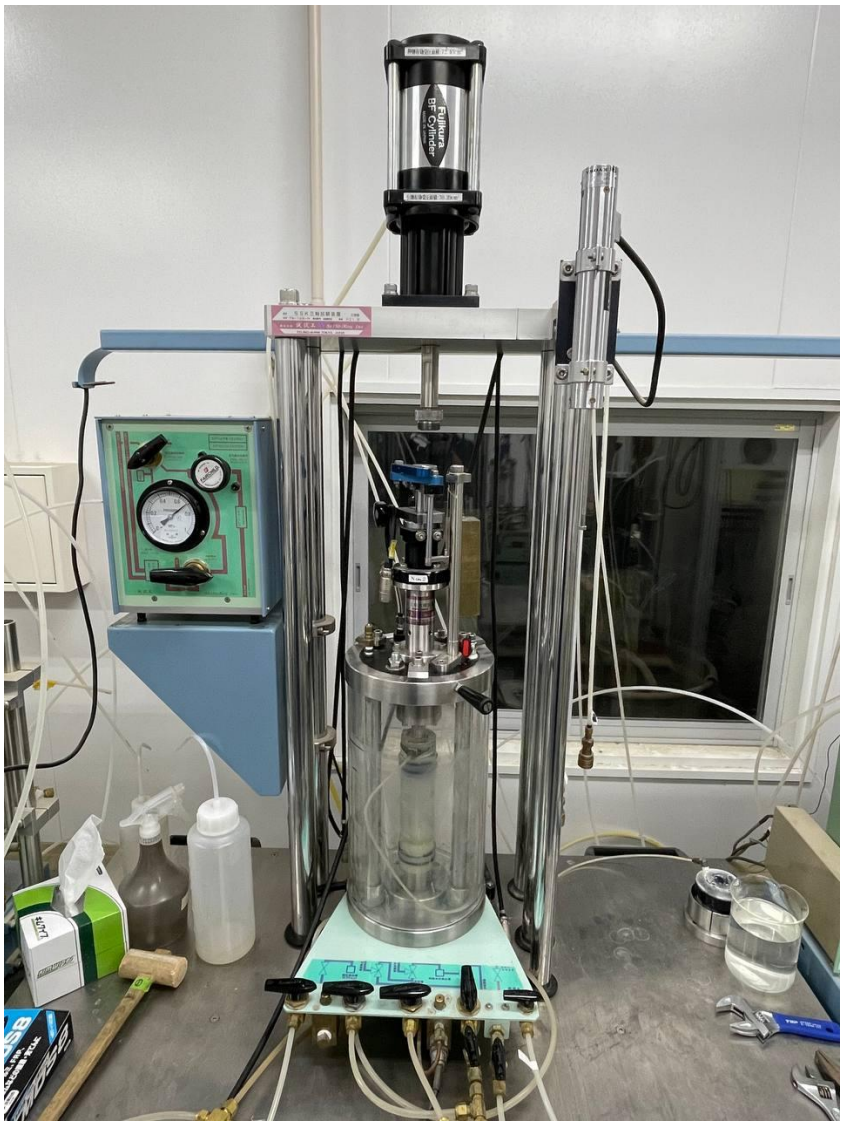

Fig. 3.1 Photograph of triaxial apparatus – triaxial cell and loading frame

3.3 Materials

3.3.1 Sands

Toyoura sand, the standard sand for laboratory testing in Japan, was used for most of the experiments. Toyoura sand is classified as a clean and uniform fine sand (SP) in the Unified Soil Classification System (USCS), with sub-angular and angular shaped particles (Fig. 3.2). Its grain size distribution was obtained following the procedures specified in JGS 0131 (Fig. 3.3). Its physical properties are given in Table 3.1.

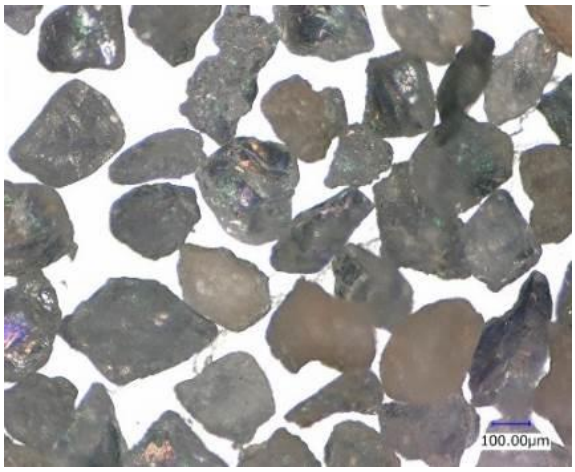

Fig. 3.2 Microscopic image of Toyoura sand

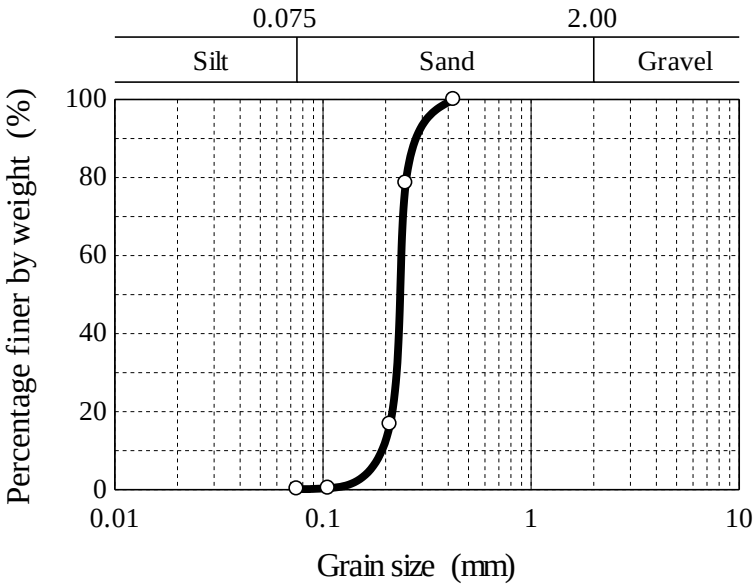

Fig. 3.3 Cumulative grain size distribution of Toyoura sand

Table 3.1 Properties of Toyoura sand

Specific gravity, G_s	Maximum void ratio, e_{max}	Maximum void ratio, e_{min}	Coefficient of uniformity, C_u	Coefficient of curvature, C_c
2.65	0.985	0.639	1560	41

Additionally, a different type of sand with more rounded shape were utilized to investigate the effect of shape of the host soil on the mechanical behavior of fiber-reinforced sand with particular attention on the anisotropic characteristics attributed to the sample preparation methods in Chapter 6. For this reason, Mikawa silica sand #6 with standard and more rounded particles shapes were used

(Fig. 3.4). Comparison of the grain size distribution of rounded Mikawa #6 silica sand with standard Mikawa #6 and Toyoura silty sand is given in Fig. 3.5. Properties of both types of Mikawa sand including maximum and minimum void ratios are given in Table 3.2. Determination of the maximum and minimum dry density of all sands were performed following the standards JGS 0161.

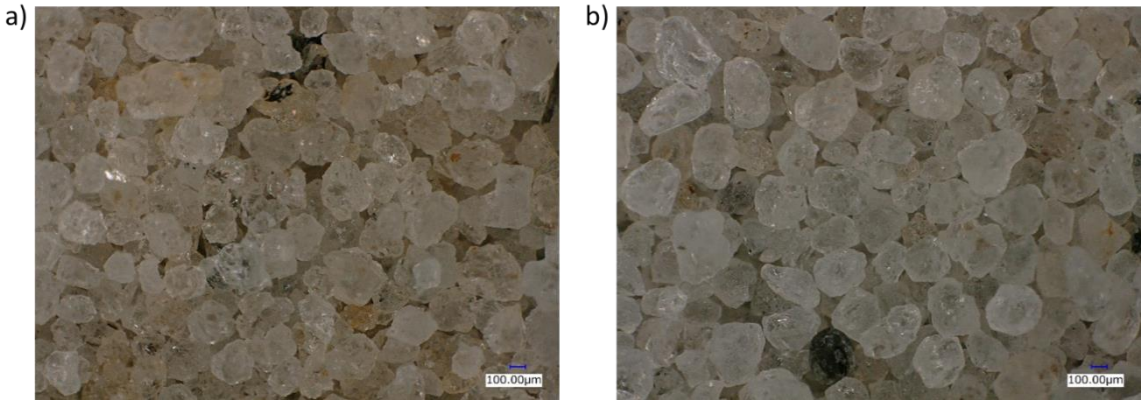

Fig. 3.4 Microscopic image of Mikawa silica sand #6: a) standard and b) rounded

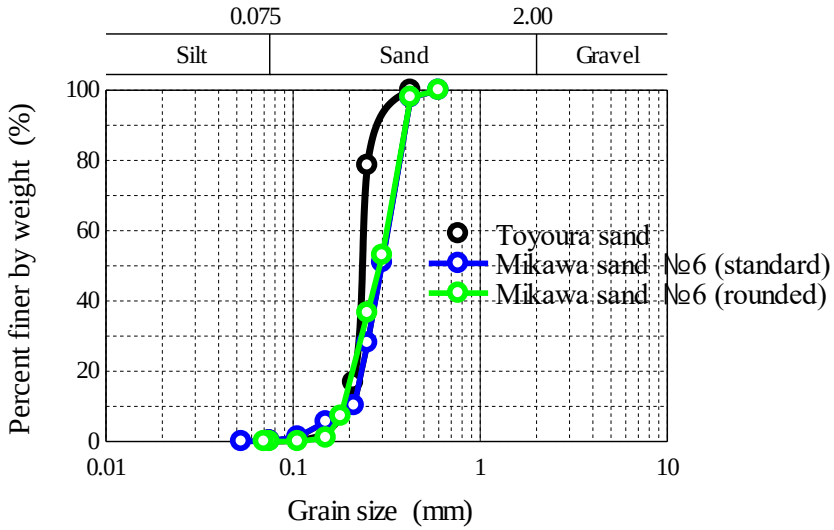

Fig. 3.5 Cumulative grain size distribution of sand used in this study (legends give sand type)

Table 3.2 Properties of Mikawa silica sand #6

	Specific gravity, G_s	Maximum void ratio, e_{max}	Maximum void ratio, e_{min}
Standard	2.65	1.018	0.643
Rounded	2.65	0.901	0.598

3.3.2 Fibers

Two types of synthetic fibers have been used as a reinforcing material. The first type fibers are short discrete fibers - polyvinyl alcohol (PVA) fibers with the length of l_f=12mm and diameter d=0.04mm with circular cross-section. PVA fibers were mainly used in the present study. The second type of fibers are the roll type fibers – vinylon filament (VF) with the diameter of d=0.035mm with circular cross-section. The second type of fibers can be prepared in any desired length. A photograph of the fibers is in Fig. 3.6 and the main properties are summarized in Table 2.

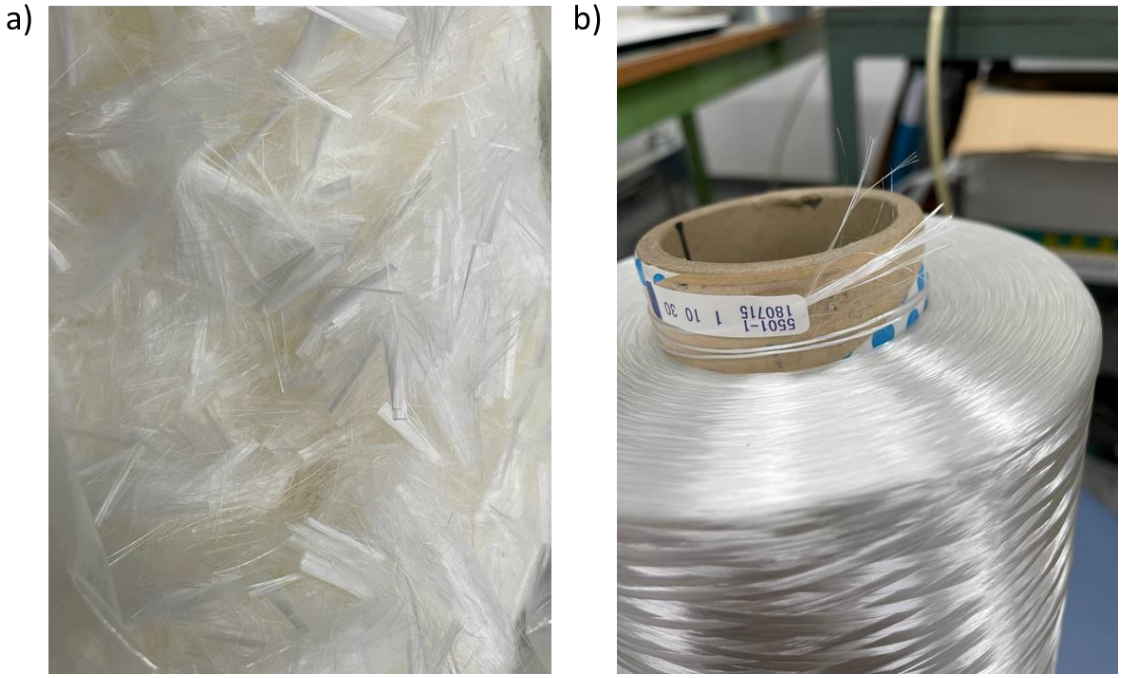

Fig. 3.6 Photograph of a) polyvinyl alcohol and b) vinylon filament fibers used in this study

Table 3.3 Properties of the fibers

	Length (mm)	Diameter (mm)	Specific gravity	Tensile strength (MPa)	Young's modulus (GPa)
PVA	12	0.04	1.3	1560	41
Vinylon filament	-	0.035	1.3	1060	23

3.4 Specimen preparation

Several fiber contents w_f were utilized to determine the correlation between the stress ratio and fiber content, and the evidence of fiber-reinforcement: 0.0%, 0.2%, 0.4% and 1%. The fiber content can be defined as a mass ratio through the following equation:

$$w_f = \frac{m_f}{m_{sp}} \tag{3.2}$$

where m_f and m_{sp} are the mass of the fibers and mass of soil particles, respectively.

The void ratio of fiber-reinforced sand is determined as shown in the following formula, considering fibers as a part of solids (Michalowski and Ĉermak, 2003; Heineck et al., 2005; Dos Santos et al., 2010):

$$e_r = \frac{V_v}{V_s} = \frac{V_a}{V_{sp}+V_f} \tag{3.3}$$

where V_a is the volume of air, V_f is the volume of the fibers and V_{sp} is the volume of soil particles; V_v is the volume of the voids and V_s is the volume of solids. Additional information on the different methods for void ratio determination of fiber-reinforced sand is given in Appendix 1.

An initial relative density D_r can be established according to the following equation:

$$D_r = \frac{e_{max}-e_r}{e_{max}-e_{min}} \tag{3.4}$$

where, e_{max} and e_{min} are the maximum and minimum void ratios of unreinforced sand, respectively.

3.4.1 Mixing and placement

The specimen preparation involved mixing fibers with sand and molding. Firstly, the fibers were weighed to achieve the desired percentage of fiber content. The fibers had to be manually dispersed from their bunched condition before being added to the sand, as seen in Fig. 3.7. Secondly, a small amount of fiber was allocated and placed on the plate and covered with a layer of sand. Thirdly, this procedure was then repeated until all fibers and all of the sand had been added, forming a "sandwich" (Fig. 3.8 mixing). Finally, the mixing was determined through a trial-and-error method to obtain shear behavior with high reproducibility among four considered methods (Fig. 3.9):

a) manual mixing with a scoop in a dry condition, similar to mixing of two different sized granular soils.
b) manual mixing with a scoop, while adding 10% water content.
c) automatic mixing using an electrical mixer in a dry condition.
d) automatic mixing using an electrical mixer, while adding 10% water content.

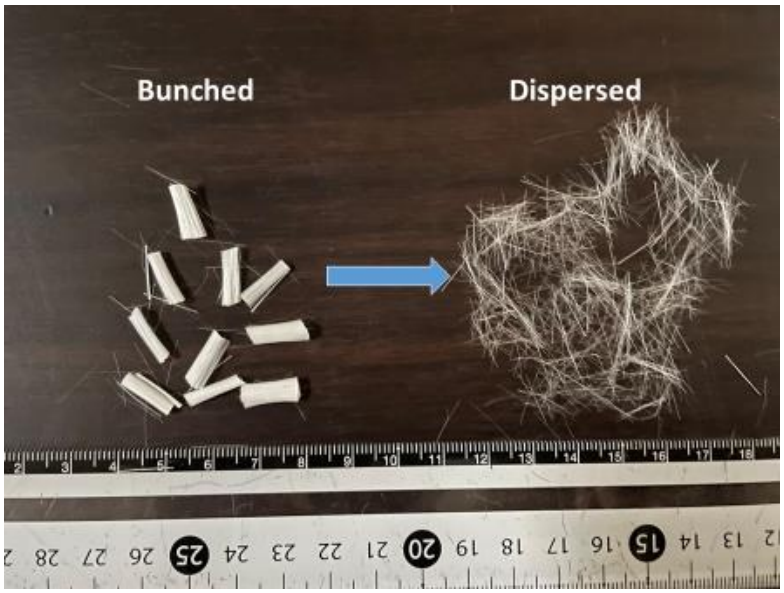

Fig. 3.7 Stage of fibers dispersion from their bunched condition

Fig. 3.8 Sample preparation of fiber-reinforced sand (example of 0.4% fiber content)

Fig. 3.9 Sand – fiber admixture after the mixing process performed in 4 different methods

As can be seen from Fig. 3.9 a), manual mixing in a dry condition was sufficient for homogenization of the admixture (sand + fiber) with low percentages of fiber inclusions (0.2% and 0.4%). Manual mixing of fibers with sand in a moist condition was also uniform enough. However, it was decided to compact the admixture into the mold by dry deposition identically with pure sand specimens. Once the percentage of reinforcing material increased to 1.0%, the segregation of sand and fiber was revealed (Fig. 3.9 c)), which required the addition of water (10% of moisture content) and changing from manual mixing to automatic mixing.

Once the fiber-and-sand mixtures appeared to be visually uniform, these masses were molded. A cylindrical specimen of 100 mm height and 50 mm diameter was used (Fig. 3.8 – placing), and an initial relative density D_r was established. The effect of the fibers on the properties of the sand was investigated based on random orientations. Hence, to ensure a random distribution of fibers through the entire height of the specimen, all samples were molded and compacted in one layer. As with the mixing process, the molding processes for lower (0.2% and 0.4%) and higher (1%) percentages of

fiber inclusions were different. In the case of 0.2% and 0.4% fiber content, the admixture was placed into the mold and compacted through vibration as for a pure sand. As it was mentioned above, different placement of the specimens might lead to a significant difference in shear behavior, the same way of placement as for the pure sand was followed as much as possible. The 1.0% fiber-reinforced sample that was automatically mixed with 10% water content was compacted by tamping, because the vibration method was not appropriate for inputting the entire mass into the determined sample size for a desired relative density.

3.4.2 Confirmation of reproducibility of shear behavior and homogeneity of fiber's distribution

The assessment of the distribution of fibers through the specimen was checked in several stages. The first step of checking the relatively homogeneous distribution was visual observation during the mixing and placement process. Also, the sample preparation was validated by checking the reproducibility of the test results and failure mode analysis, where the deformation shapes of unreinforced sand specimens were also achieved in fiber-reinforced sand specimens. Fig. 3.10 shows a couple of tests of drained triaxial compression of specimens with 60% relative densities under 100kPa confining pressure. As can be observed, the reference test results indicate that the methods of sample preparation determined by the trial-and-error method for fiber-reinforced specimens gives a high reproducibility of both shear stress-strain and volumetric change characteristics.

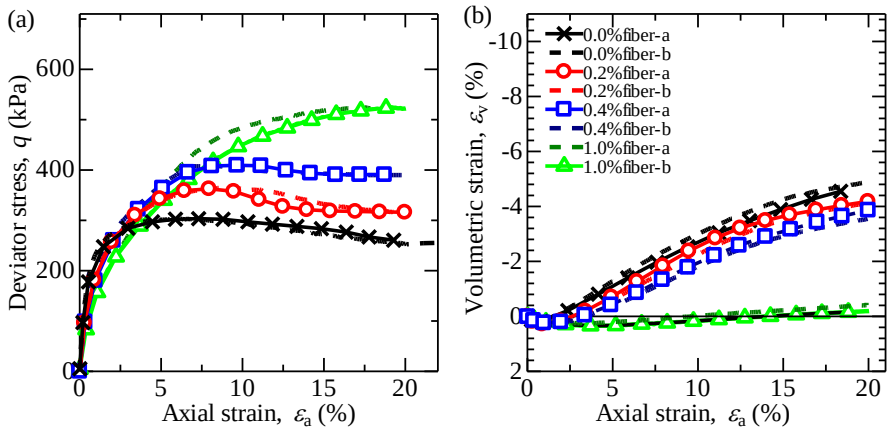

Fig. 3.10 Reference tests to confirm reproducibility of the experiments (D_r=60%, p'_0=100kPa)

Additionally, to check the homogeneity of the samples and the distribution of fibers through the entire height of specimen with avoiding localization in the bottom or top parts, analysis of an exhumed sample has been performed (Fig. 3.11). The exhumed sample was divided into four equal parts and, after drying in oven, the mass of admixture was separated and weighted (example of 0.4% fiber content of reinforced specimen with relative density of D_r=60%). Total initial weight of the fibers was equal to $m_{f1(\text{initial total})}$ = 1.17g. Here, exhumed sample was carefully divided into four equal parts – B1, B2, T1, and T2. Fibers were separated from sand as much as possible (several stages) by using sieve with the size of passage 420 and 360 μm and the weight was measured and the intermediate fibers' weight was equal to m_{f2} = 1.10g. After obtaining the weight of each part, all divided sand particles again were sieved, and additional $m_{f(\text{additional})}$=0.05g of fiber were separated. Total amount of fiber that was able to separate from sand is $m_{ft}=m_{f2}+m_{f(\text{additional})}$=1.10+0.05=1.15g. As can be seen from the weight analysis, approximately equal masses of fibers were distributed in each part. Moreover, despite majority of previous studies reported the relative horizontally preferred orientation of fibers, in the thorough analysis of the exhumed sample the orientation of fibers did not have any relatively high preferred orientation, i.e., the distribution of fibers was random.

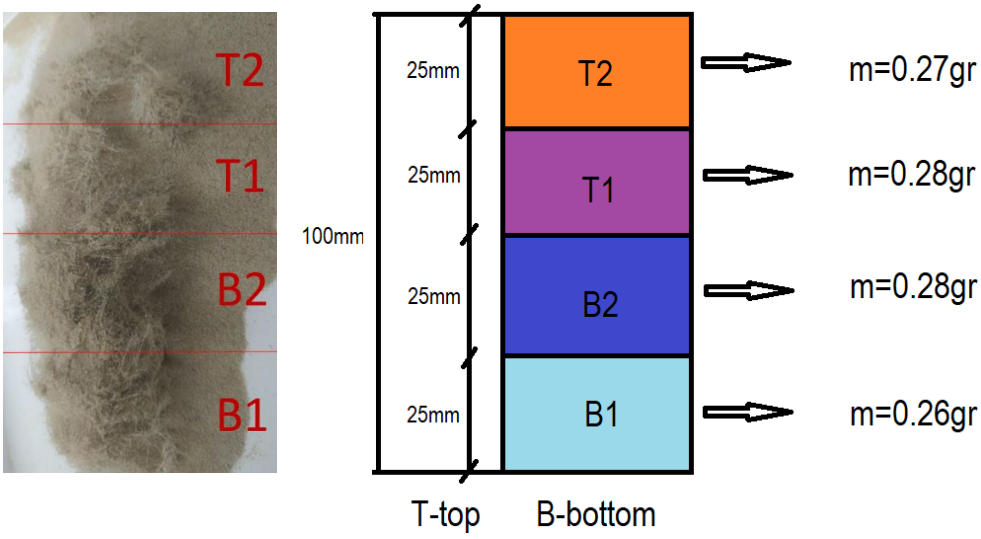

Fig. 3.11 Exhumed and dried sand sample with 0.4% fiber content

3.4 Brief summary

In order to investigate the effect of fibers on the shearing properties of sand two types of fibers with different physical and geometrical properties were used. Also, a more spherical sandy material

Mikawa #6 was also used to compare and comprehensively analyze the effect of anisotropy in unreinforced and fiber-reinforced Toyoura sand due to the geometry of sand particles (prolonged) and sample preparation way which affect the degree of anisotropy. A more suitable sample preparation method for fiber-reinforced sand is proposed. For a lower percentage of fiber inclusions mixing sand with fibers with scoop and placement by side tapping in dry condition in one layer was determined out of four methods. This method of sample preparation for fiber-reinforcement is set to be more fair way of comparison with unreinforced sand and investigation of the effect of fibers on the shearing properties of sand. For considered series of experimentations a high reproducibility of all results was achieved and controlled through the whole experimental work.

CHAPTER 4

EXPERIMENTAL TEST RESULTS

4.1 Introduction

In this Chapter results of experimental work conducted on unreinforced and fiber-reinforced specimens with varying initial testing conditions are presented. In practice, two main characteristics of the soils in terms of the time stages are considered regarding the drainage condition, i.e., short-term characteristics – undrained and long-term – drained. Also, for instance, in the slope stability both compression and extension behavior are necessary depending on the geometry of the structure (compression is mainly in the upper parts of the structure; extension is in the bottom/toe of the structure). Therefore, triaxial compression and extension experiments were conducted under drained and undrained conditions to investigate the effectiveness of fiber-reinforcement in details for the further implementation in different geo-structures.

4.2 Isotropic compression behavior of loose and medium dense specimens

Isotropic compression tests for unreinforced, 0.2% and 0.4% fiber-reinforced sand specimens were performed to obtain isotropic compression and swelling properties and elasto-plastic parameters related to these properties. The isotropic confining pressures were obtained by initial back pressure of 50kPa and cell pressure of 70kPa reaching up to a maximum of 690kPa. Considering the sensitivity of sandy soil to a slight vibration, isotropic compression tests for sands with and without fiber inclusions were conducted in three series.

Figs. 4.1 and 4.2 show the results of the isotropic consolidation test in specific volume v – mean effective stress p' curve for loose and medium dense samples, respectively. Samples were placed in very loose conditions with approximately the same relative densities of about 18%, and medium dense condition with 60% initial relative density. As can be observed in Figs. 4.1 and 4.2, all specimens exhibited similar compressibility with higher confining pressure. The normal consolidation lines (NCL) of all specimens seemed to be parallel, and the NCL of fiber-reinforced sand was situated lower and to the left of that of unreinforced sand.

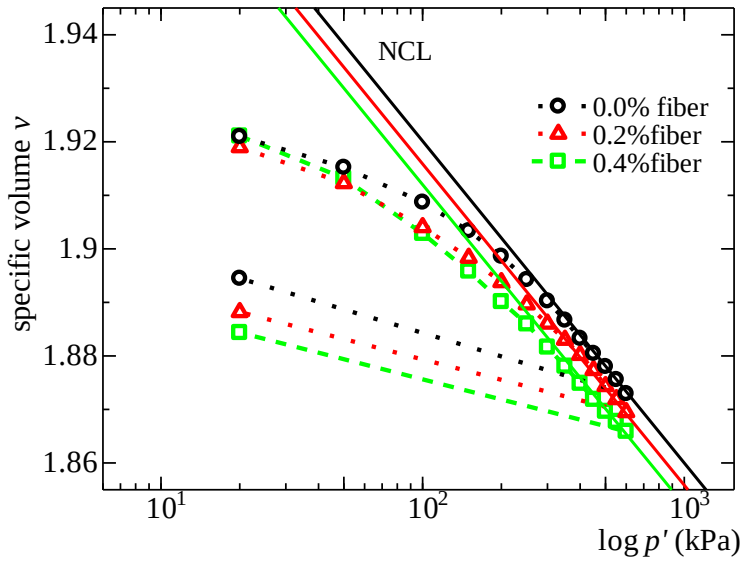

Fig. 4.1 Experimental results of isotropic compression test performed on both unreinforced and fiber-reinforced Toyoura sand prepared in loose condition (initial D_r=18%)

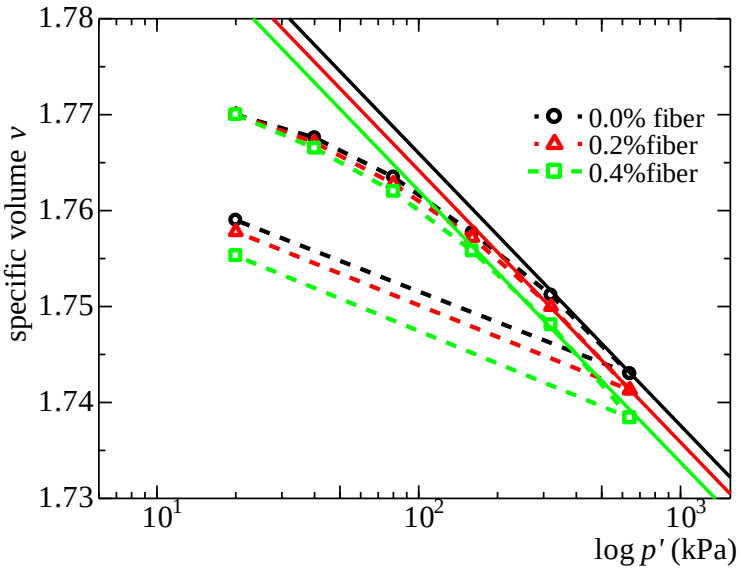

Fig. 4.2 Experimental results of isotropic compression test performed on both unreinforced and fiber-reinforced Toyoura sand prepared in medium dense condition (initial D_r=60%)

Similar test results on the compressibility characteristics with parallel NCLs of both fiber-reinforced and unreinforced sands were obtained in some previous studies (Consoli et al., 2005; Dos Santos et al., 2010), but with higher NCL location of fiber-reinforced sand. A possible mechanism causing the higher loci of NCL of composite material was a lock-in effect of the fibers that allowed

the existence of the composite material with a larger void ratio even at large isotropic compression stresses (≈45000kPa) (Dos Santos et al., 2010), and a development of the tensile stresses in the fibers, even when isotropic stress alone was applied (Consoli et al., 2005). However, according to later studies with both experimental and constitutive modeling of cohesive soil (Kar et al., 2012; Diambra and Ibraim, 2014), a lower location of NCL of a fiber-reinforced specimen was obtained accompanying an increase in fiber content. This observation was attributed to the difference in the global void ratio of unreinforced and fiber-reinforced clay (Appendix 1), where the void ratio of the sample with fiber was smaller than that of the unreinforced clay. Furthermore, Diambra and Ibraim, (2014) concluded that tensile strains cannot develop in the sample during any consolidation loading, thus, tensile stresses in fibers cannot be produced.

Without rejecting the above-mentioned possible mechanisms for characterizing the isotropic behavior of fiber-reinforced soil, the location of NCL of the fiber-reinforced sand below the NCL of the unreinforced sand might be due to the weaker contact forces between sand particles in the fiber-reinforced sand that allows higher compression at the initial stage. Fig. 4.3 is a schematic illustration of the interaction mechanism of the sand particles in unreinforced and fiber-reinforced samples. The sand particles had a stronger and wider area of contact in the unreinforced sample with a possibly more stable structure (Fig. 4.3a), while fiber inclusions weakened these contacts, with intensive further rearrangement of the host soil matrix when isotropic stresses were applied. A similar assumption was declared in previous studies (Li et al., 2017; Li and Senetakis, 2017), where fiber inclusions resulted in a drop of small-strain stiffness of fiber-reinforced sand, which was attributed to the negative contribution of fibers to the transfer of the normal contact forces among soil particles at the initial stage of shearing. Furthermore, the necessity of higher strain levels was proposed to develop the tensile forces in fibers and the effective contribution of fibers to the increase of soil strength. In this study, even experiencing different initial compression curves, the host soil matrix was still the predominant factor for considered percentage of fiber inclusions. Therefore, the subsequent slopes of NCLs became parallel for all specimens. Moreover, such kind of behavior of fiber-reinforced sand in isotropic compression test is also assumed to be due to the effect of initial anisotropy, where the fiber inclusions possibly prevented the preferred orientation of sand particles and created less anisotropic samples.

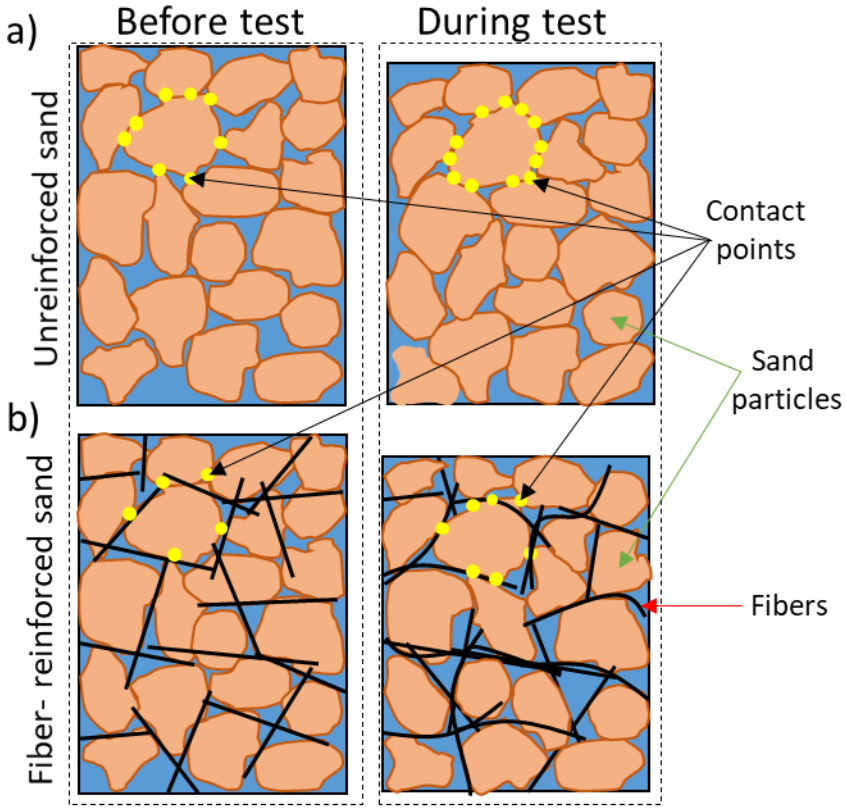

Fig. 4.3 Schematic illustration of the possible interaction mechanism of unreinforced and fiber-reinforced sand before and during isotropic compression

4.3 Drained triaxial compression and extension behavior

The main experimental work was directed to investigate the mechanical behavior of Toyoura sand reinforced with short discrete PVA fibers with the length of 12mm. The consolidated drained triaxial compression and extension experiments were conducted on unreinforced and fiber-reinforced Toyoura sand under several confining pressures with varying the initial density of the specimens.

4.3.1 Testing program

Three types of consolidated drained (CD) triaxial compression tests and an additional series of consolidated drained triaxial extension tests were carried out to investigate the effect and contribution of fibers on the mechanical behavior of sand, including the influence on the critical state line.

(1) **The effect of relative density on unreinforced and fiber-reinforced sand.** The drained triaxial compression was performed under unique confining pressure on samples prepared with different

initial relative densities - 30, 60 and 80%. The experiments were conducted to investigate the effect of initial relative density (loose, medium dense, and heavily compacted sand) on the mechanical behavior of Toyoura sand with different contents of fiber inclusions (0.0, 0.2, 0.4 and 1%) under the confining pressure of p'=100kPa.

(2) **The effect of confining pressure and fiber content on the mechanical behavior of sand.** At first, the drained triaxial compression was performed under three different confining pressures (p'=50kPa, 100kPa, and 200kPa) to compare the effect of the confining pressure on the shear properties for both unreinforced and fiber-reinforced specimens. The range of confining pressures was chosen based on previous studies (Consoli et al. 2009; Diambra et al. 2010; Ibraim et al. 2012). Additionally, experimentation with higher confining pressures of 400kPa and 600kPa were conducted on 0.2% and 0.4% fiber-reinforced specimens to compare the impact of confining pressure on the stress ratio η ($=q/p'$) at the end of shearing.

(3) **The effect of fiber length on the shear stress parameters.** Shearing under 100kPa confining pressure was performed on 0.2% fiber-reinforced samples with different fiber-length. All specimens were prepared with 80% relative density. The experiments were conducted to examine the effect of the fiber length, i.e. aspect ratio, by replacing 12mm-long fibers with fibers of half (l_f=6 mm) and quarter length (l_f=3mm). This investigation was performed to check the effect of fiber length on the stress ratio values and the interaction between sand particles and fibers. Furthermore, consideration of the different fiber lengths offers the possibility of achieving calculation of fiber-reinforced sand's void ratio by counting fibers as a part of solids.

(4) **The effect of fibers on the tensile strength and mechanical behavior of sand in extension.** Drained triaxial extension was performed on densely compacted specimens with 0.0%, 0.2% and 0.4% fiber content. The extension was performed under two different confining pressures of 100kPa and 300kPa. For the broadening the implementation of any technique, both compression and extension characteristics should be considered, especially, for the fiber-reinforcement, as fibers are a tension resisting elements with high tensile strength.

After the sample formation procedure was completed (Fig. 3.8), the saturation process followed. Firstly, CO_2 was infiltrated through the sample to replace the air in the pores. De-aired water then saturated the specimen, expelling CO_2 as completely as possible. After the saturation process was completed, the degree of saturation was checked using Skempton's B value, which is determined as

B= $\Delta u/\Delta\sigma$, where Δu is the increment of pore pressure and $\Delta\sigma$ is the increment in the cell pressure under the undrained condition. For all specimens, the B value reached over 0.95.

Table 4.1 shows a complete list of experiments along with the void ratio at the end of consolidation e_c, and the corresponding relative density D_r, fiber content w_f, fiber length l_f, and confining pressure in the consolidation process, p_0'. The experimental results of reference test are given with index a and b. The confining pressure can be obtained by back pressure of 200kPa and cell pressures of 250, 300, 400 and 500kPa. At higher confining pressures of 400kPa and 600kPa, the back pressure was set at 100kPa due to the safety limitation of the triaxial cell at 700kPa. From the experimental work directed to investigate the effect of initial back pressure, there was no effect on the shearing properties. For all cases the B value was over 0.95. The tests were carried out according to JGS 0524 standard with a strain rate of 0.5%/min until the axial strain reached 20% (capacity of the triaxial apparatus).

Table 4.1 List of CD experiments

Test	Type of experiment	w_f, (%)	l_f, *(mm)*	e_c	D_r, (%)	p'_0, (kPa)	$\eta_r=q_r/p'$
L100-00	C	0.0	-	0.823	30	100	1.34
M100-00-a	C	0.0	-	0.771	60	100	1.34
M100-00-b	C	0.0	-	0.772	60	100	1.34
D-050-00	C	0.0	-	0.721	80	50	1.34
D-100-00	C	0.0	-	0.719	80	100	1.34
D-200-00	C	0.0	-	0.717	80	200	1.34
D-100-02	C	0.2	3	0.717	80	100	1.43
D-100-02	C	0.2	6	0.718	80	100	1.48
L100-02	C	0.2	12	0.829	30	100	1.52
M100-02-a	C	0.2	12	0.77	60	100	1.52
M100-02-b	C	0.2	12	0.773	60	100	1.52
D-050-02	C	0.2	12	0.715	80	50	1.52
D-100-02	C	0.2	12	0.713	80	100	1.53
D-200-02	C	0.2	12	0.709	80	200	1.52
D-400-02	C	0.2	12	0.699	80	400	1.52
L100-04	C	0.4	12	0.821	30	100	1.71
M100-04-a	C	0.4	12	0.772	60	100	1.71
M100-04-b	C	0.4	12	0.774	60	100	1.71
D-050-04	C	0.4	12	0.712	80	50	1.72
D-100-04	C	0.4	12	0.712	80	100	1.71
D-200-04	C	0.4	12	0.705	80	200	1.71
M100-10-a	C	1.0	12	0.775	60	100	1.87
M100-10-b	C	1.0	12	0.772	60	100	1.87
D-050-10	C	1.0	12	0.711	80	50	1.88

D-100-10	C	1.0	12	0.708	80	100	1.85
D-200-10	C	1.0	12	0.705	80	200	1.81
D-100-00-a	E	0.0	12	100	0.707	80	0.81
D-100-00-b	E	0.0	12	100	0.709	80	0.81
D-300-00	E	0.0	12	300	0.704	80	0.69
D-100-02-a	E	0.2	12	100	0.705	80	1.02
D-100-02-b	E	0.2	12	100	0.706	80	0.75
D-300-02	E	0.2	12	300	0.702	80	0.58
D-100-04-a	E	0.4	12	100	0.704	80	0.93
D-100-04-b	E	0.4	12	100	0.703	80	0.93
D-300-04	E	0.4	12	300	0.701	80	0.81

L - loose; M - medium dense; D - dense
C - compression; E - extension

4.3.2 Reproducibility of experimental results

The reproducibility of test results is an important issue for the fairly analyzing the shearing properties of the soils. A couple of tests of drained triaxial compression and extension are presented in Fig. 4.4. As can be observed from Fig. 4.4 the mechanical behavior of both unreinforced and fiber-reinforced sand specimens have a high reproducibility with minor differences in volumetric change curves.

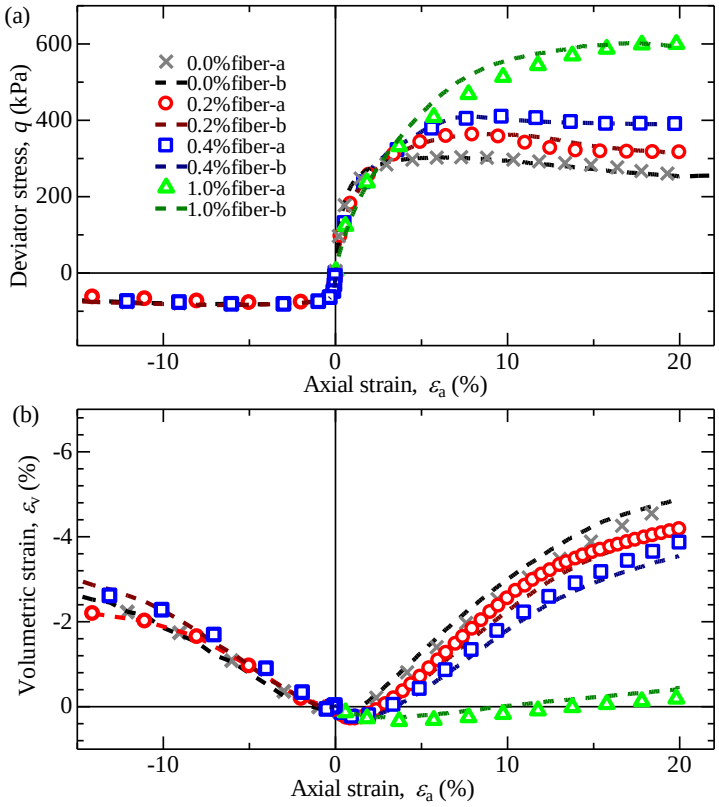

Fig. 4.4 Reference test of drained triaxial compression and extension experiments performed on unreinforced and fiber-reinforced with different fiber contents

4.3.3 Drained triaxial compression test results

4.3.3.1 Shearing of specimens with different initial relative densities

The results of the drained triaxial compression tests under 100kPa confining pressure, performed on both unreinforced and reinforced sands prepared with different initial relative densities, are given in Figs. 4.5 to 4.8. The exhibit includes deviator stress q – axial strain ε_a, deviator stress q – mean effective stress p', specific volume v – axial strain ε_a and specific volume v – mean effective stress p' curves.

Fig. 4.5 shows the typical stress-strain and volumetric change behaviors of unreinforced sand with 30%, 60% and 80% initial relative densities. It is convenient, first, to consider the effect of relative density on sands sheared under unique confining pressure through the existing common framework. Loose specimens in a drained triaxial compression test typically exhibit only strain-

hardening behavior without a marked peak in the stress-strain relationship and reach the flat maximum at the end of the shearing. Loose specimens compress and the volumetric strain increases as the shear proceeds. On the other hand, dense specimens exhibit strain-hardening behavior, reaching a marked peak which turns into strain-softening behavior with decrease of deviator stress towards the ultimate point. Dense specimens contract slightly at lower levels of strain, which is followed by strong expansion until the end of the test.

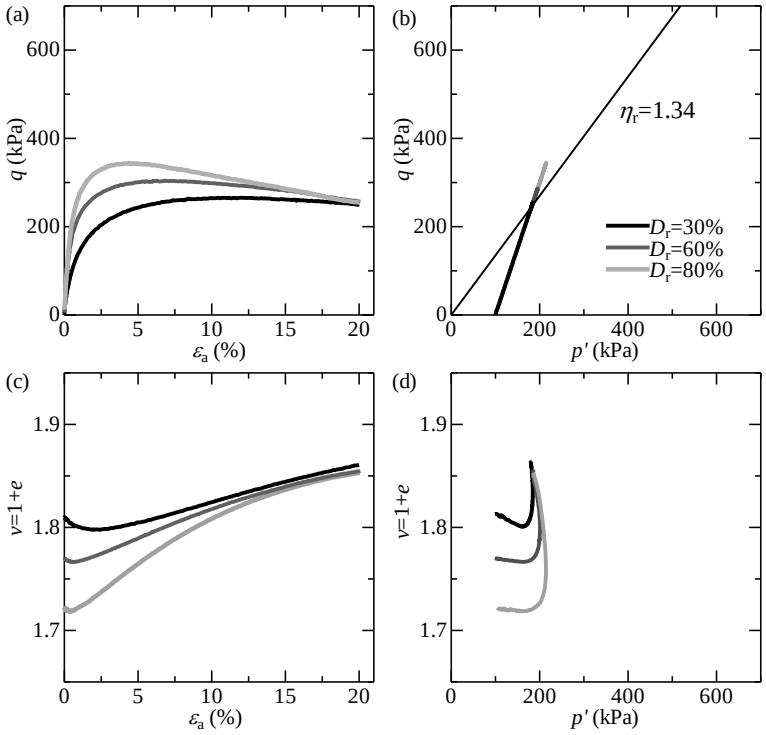

Fig. 4.5 Shear – strain – volumetric response of unreinforced sand for 100kPa confining pressure prepared with different initial relative densities

Similarly, Toyoura sand specimens with 80% and 60% relative density showed strain-hardening behavior until reaching a marked peak deviator stress, which was followed by strain-softening until ultimate residual stresses. Dense specimens showed slight contraction at very low strain levels, which was followed by strong expansion until the end of the test. Specimens with 80% and 60% relative densities were regarded as a dense and medium dense sands, respectively. In contrast, the specimen of Toyoura sand with 30% relative density experienced only strain-hardening behavior and reached a flat maximum at about 20% axial strain. The loose specimen initially showed higher compression

and began expanding slightly at higher strains until the end of the shear. Specimen with 30% relative density was regarded as a medium loose specimen.

Particularly, unreinforced Toyoura sand specimens exhibited different $q - \varepsilon_a$ curves depending on the initial relative densities, whereas the deviator stresses tended to reach the same residual stresses q_r = 250kPa at 20% axial strain. This behavior could also be observed in $v - \varepsilon_a$ and $v - p'$ curves, where all specimens tended to reach the same value of specific volume of 1.86 after shearing, despite the difference in the initial relative densities. It should be noted that the volumetric change is still exist, but with a very small increment. Also, despite small changes, all three specific volumes have the same mean effective stress values of p'=180 kPa at the end of shearing. Regardless of the initial void ratio, the stresses and volumes converged to a common value at the end of the tests. This is a property that is commonly found in the critical state of soils (Schofield and Wroth, 1968; Atkinson and Bransby, 1978), where the existence of the critical state of sand was presented. Therefore, it is assumed that the Toyoura sand at the end of the tests have reached the vicinity of the critical state as in the previous studies.

Fig. 4.6 shows the drained compression test results performed on 0.2% fiber-reinforced specimens with initial relative densities of 30, 60 and 80%. The sand specimens with 0.2% fiber content showed similar mechanical behavior with unreinforced sand. The loose specimen for D_r of 30% in $q - \varepsilon_a$ curve experienced only hardening behavior while reaching a flat maximum deviator stress q_{max} at 20% axial strain. In volumetric change curves ($v - \varepsilon_a$ and $v - p'$), the loose sample initially compressed up to 5% axial strain, which was then followed with expansion towards the maximum value of specific volume. In contrast, the denser specimens exhibited a marked peak in $q - \varepsilon_a$ curve, and deviator stress decreased with the shear progression, i.e., denser specimens underwent both hardening and softening behavior. In $v - \varepsilon_a$ and $v - p'$ curves, denser samples showed smaller initial contraction, then expanded considerably up to the end of shearing. Although each $q - \varepsilon_a$ curves was different and q_{max} increased with initial relative density, the residual stresses q_r for all fiber-reinforced specimen with fiber content of 0.2% were almost the same and equaled approximately to 315 kPa, without depending on the initial relative density (Fig. 4.6(a)). All specific volumes v and the mean effective stresses p' also tended to reach the same values at the end of shearing despite initial differences in specific volumes, as shown in Figs. 4.6(b), (c) and (d). Moreover, the volumetric change behavior in $v - \varepsilon_a$ curves experienced less expansion with v=1.85 than the unreinforced sample at 20% axial strain (Fig. 4.6c and d).

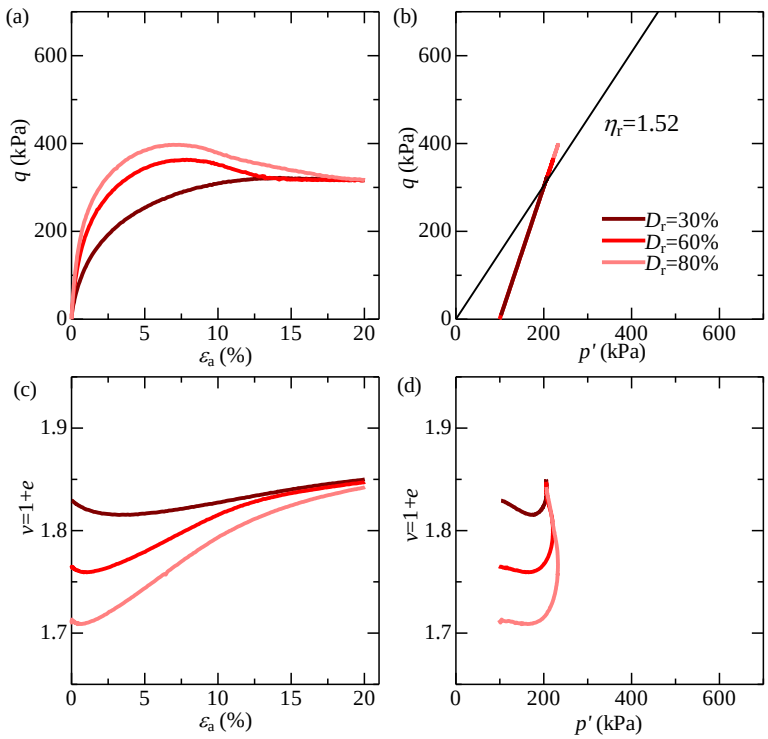

Fig. 4.6 Shear – strain – volumetric response of 0.2% fiber-reinforced sand for 100kPa confining pressure prepared with different initial relative densities

Fig. 4.7 represents results from drained triaxial compression performed on sandy samples with 0.4% fiber content with different initial relative densities. The mechanical behavior of 0.4% fiber-reinforced sand had the same tendency as the unreinforced and reinforced sand with 0.2% fiber content and underwent similar shear behavior. Explicitly, the fiber-reinforced specimens exhibited higher maximum and residual deviator stresses than the unreinforced specimen for all relative densities. The residual stresses q_r, mean effective stresses p' and specific volumes v tended to reach the same value at the end of shearing despite the difference in the initial relative density, *i.e.*, q_r=380kPa, p'=210kPa and v=1.84 at an axial strain of 20%. Compared to the 0% and 0.2% fiber contents, 0.4% fiber-reinforced samples had more pronounced maximum deviator stress and sharper passage to the residual state.

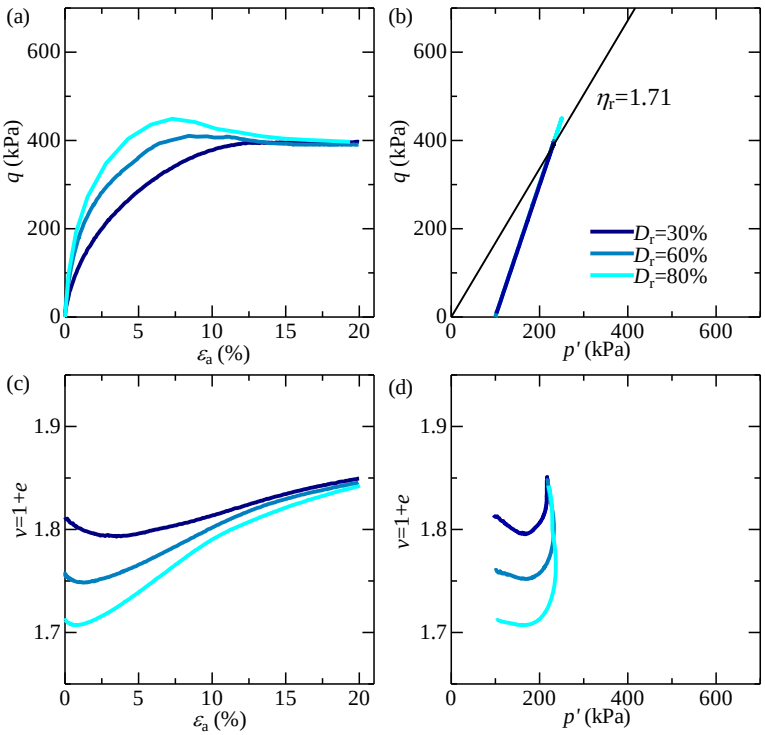

Fig. 4.7 Shear – strain – volumetric response of 0.4% fiber-reinforced sand for 100kPa confining pressure prepared with different initial relative densities

The mechanical properties of the drained shear behavior of 0.2% and 0.4 % fiber-reinforced sand quite resemble those of the typical behavior of unreinforced sand. Overall, the effect of different relative densities on shear-strain-volumetric response of the unreinforced Toyoura sand was also observed in the case of fiber-reinforced Toyoura sand. Since the stress and volume changes converged to a certain value in both cases as in the unreinforced case, despite a very small increment in the specific volumes, it can be considered that the fiber-reinforced sand had also reached the vicinity of the critical state at the end of the tests.

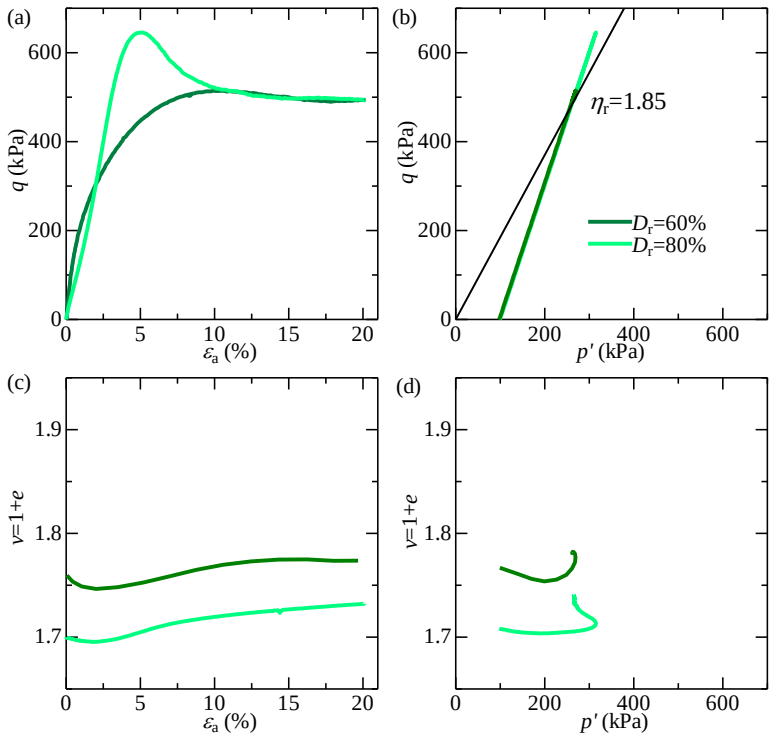

Fig. 4.8 Shear – strain – volumetric response of 1.0% fiber-reinforced sand for 100kPa confining pressure prepared with different initial relative densities

Compared with the lower percentage of reinforcing material, 1.0% fiber-reinforced samples exhibited some differences in their mechanical behavior (Fig. 4.8). The maximum and residual deviator stresses were higher, while volumetric expansion was significantly low. In $v - \varepsilon_a$ and $v - p'$ curves, the specific volumes of 60% and 80% did not reach the same value at the end of shearing. That may be because of the difficulties in specimen preparation compared with specimens having lower percentages of fiber inclusions of 0.2% and 0.4%. Because of the difference in the molding process, the result of 1.0% fiber-reinforced sand prepared in a loose condition (D_r=30%), where molding did not require tamping, was not included in direct comparison with denser samples molded through tamping. Further investigation is needed to understand the behavior of 1.0% fiber-reinforced samples, which have a higher percentage of fiber inclusions.

Fig. 4.9 shows the detailed volumetric change behavior through comparison of the shear behavior of unreinforced sand with the 0.4% fiber-reinforced sand. It should be noted that approximately the same initial void ratio was set to unreinforced and 0.4% fiber-reinforced sand specimens. From v - ε_a curve around the initial stage of shearing, the amount of compression of sand mixed with fibers was

larger than that of unreinforced sand, and the axial strain from compression to expansion was up to 2% (blue bullet), which was also slightly larger than that of the unreinforced sand (black bullet), about 1%. Focusing on the behavior around the maximum deviator stress in v - p' curves, sand with fibers had larger v and p' at maximum deviator stress (point B_1) than unreinforced sand (A_1). Even though the specific volume of reinforced sand was higher (point B_1, v - p' curves) than that of unreinforced sand (point A_1, v - p' curves), the sand with fibers exhibited larger mean effective stress than the unreinforced sand, and therefore larger maximum deviator stress (point A_1 and B_1, q - p' curves, respectively). The fiber insertion effect is in the increase of the amount of compression at the initial stage of shearing and the axial strain from compression to expansion; and even though the expansion due to the shearing is allowed and the specific volume becomes high at around the maximum deviator stress, the residual stress increases with the increase of the confining pressure. Therefore, the sand mixed with fibers showed higher peak and post-peak deviator stresses (shear strength) than that of unreinforced sand, while experiencing less volumetric expansion.

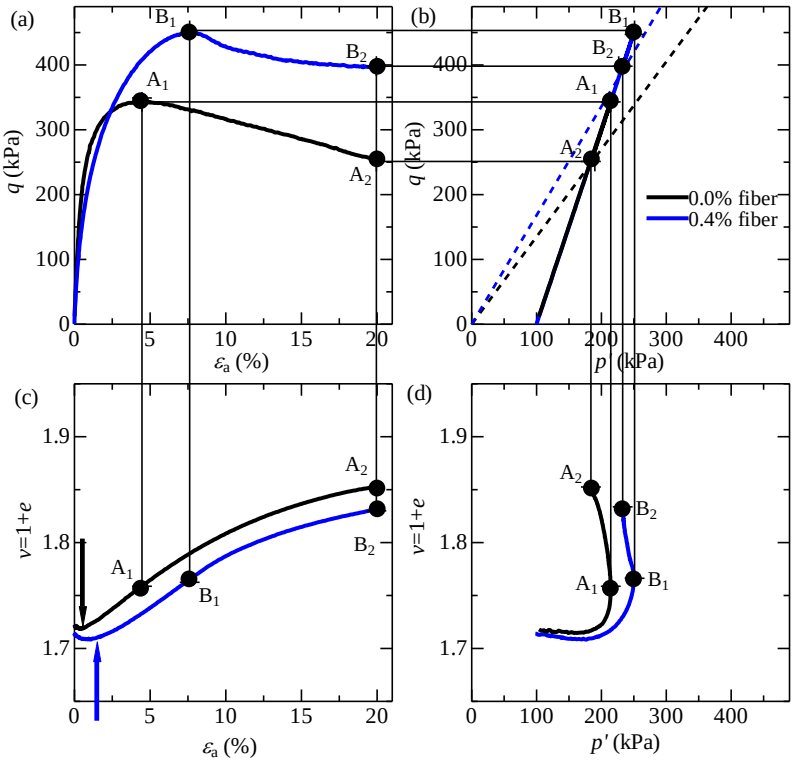

Fig. 4.9 Shear strength and volumetric change behavior of unreinforced sand with 0.4% fiber-reinforced sand

Despite using PVA fibers with a higher Young's modulus and tensile strength than previous studies (Yetimoglu and Salbas, 2003; Diambra et al., 2010; Ibraim et al., 2010), where polypropylene fibers were used, the initial stiffness decreased with the increase in fiber content (Fig. 4.9). The deformation modulus $E_{50} = 0.5 \times q_{max}/\varepsilon_{50}$ was used to express the initial stiffness of both unreinforced and reinforced sand, where ε_{50} is an axial strain at half of maximum deviator stress (Fig. 4.10). The initial stiffness of the fiber-reinforced sand was lower than that of unreinforced sand under all relative densities. Similar outcomes were presented in previous studies (Michalowski and Ĉermak, 2003; Heineck et al., 2005; Li et al., 2017; Li and Senetakis, 2017; Li et al., 2019). As it is known from previous studies (Oda, 1972, Miura and Toki, 1982), even unreinforced sand has a different anisotropy depending on the way of sample preparation, which might mainly affect initial shearing behavior. Similarly, the fiber inclusions probably reduced the initial stiffness of sand as one of the effect of less anisotropy (detailed explanation will be given in Chapter 6). The trend of initial stiffness eventually decreased with the increase in fiber content. Because of the difference in sample preparation methods between lower and higher fiber inclusions, the results cannot be directly compared. Therefore, the results were illustrated by different type of lines representing different sample preparation methods.

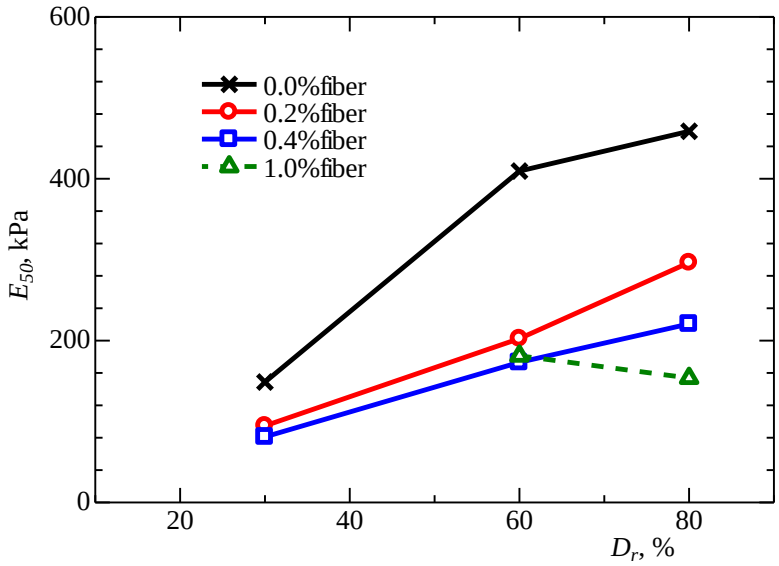

Fig. 4.10 Initial stiffness – relative density dependency, expressed through the deformation modulus E_{50} (solid lines – dry vibration, dashed line – moist tamping)

To compare the trend and effect of fibers on the stress ratio, Fig. 4.11 plotted stress ratio $\eta(=q/p')$ – axial strain ε_a dependency. Fig. 4.11 shows that the adding of fibers increases the stress ratio relative to the fiber content increment. Furthermore, the stress ratios of unreinforced and fiber-reinforced sand specimens reached the same values for a given fiber contents at the end of shearing, independently of the initial relative density.

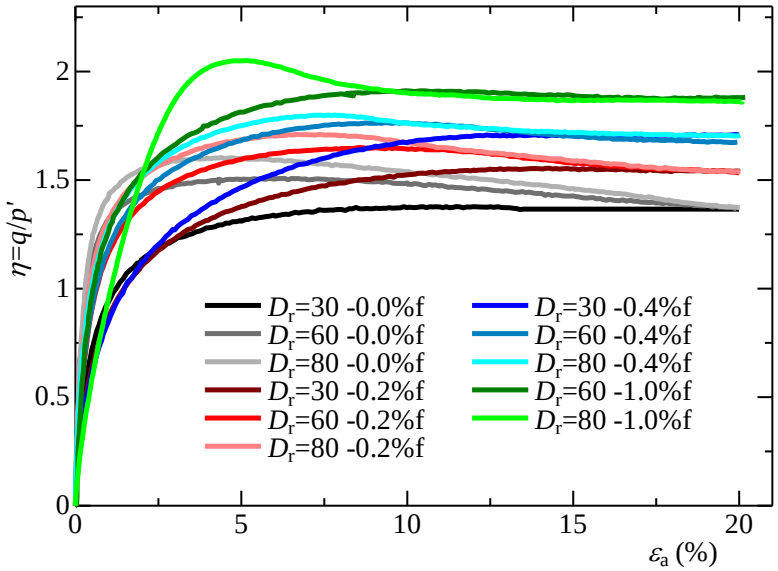

Fig. 4.11 Stress ratio – axial strain dependency for all fiber contents with different initial relative density

Fig. 4.12 represents the phase transformation stress ratio η_{pt} $(=q_{pt}/p')$, at which plastic compression was changed to plastic expansion, the peak stress ratio η_{max} $(=q_{max}/p')$, and the residual stress ratio η_r $(=q_r/p')$ with relative densities. It should be noted that the η_{pt} and η_{max} increase with the increase in relative density (Fig. 4.12 (a), (b)). On the contrary, from Fig. 4.12 (c) it can be confirmed that all η_r was kept constant even with the increase in relative density. The unreinforced sand and sand reinforced with 0.2% and 0.4% fiber contents have η_r of 1.34, 1.52 and 1.71, respectively, at 20% axial strain. In case of 1.0% fiber-reinforced sand, despite reaching the same value of stress ratio, a similar conclusion cannot be made in the same way as for a lower percentage of fiber inclusions. The issue concludes in a perceptible difference in mechanical behavior, especially, in volumetric change characteristics.

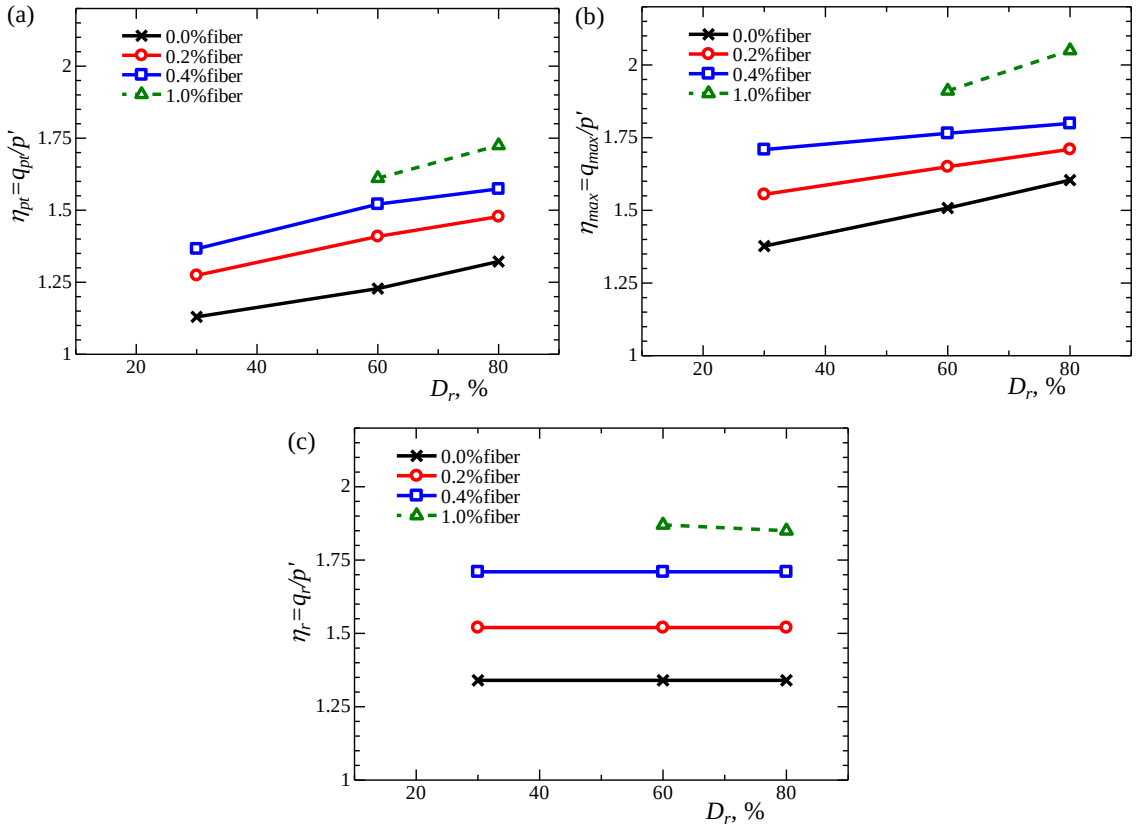

Fig. 4.12 Stress ratio dependency on relative density: a) phase transformation, b) peak, and c) residual stress ratios (solid lines – dry vibration, dashed line – moist tamping)

4.3.3.2 Shearing of specimens under different confining pressures

To convince the existence of a critical state for fiber-reinforced sand as in the case of unreinforced sand, an additional series of experiments was performed to compare the effect of the confining pressure on the shear properties of unreinforced and fiber-reinforced specimens. Figs. 4.13-4.16 represent the shear behaviors of unreinforced and reinforced sand with 0.2%, 0.4% and 1.0% fiber content, respectively, under different confining pressures.

Fig. 4.13 shows the typical shear characteristics of densely packed sand with both hardening and softening behavior. Higher confining pressure produces higher shear stress with the increase in the shear modulus, peak and residual stresses. Additionally, when the relatively high confining pressure is applied to a dense specimen, the shear-strain-volumetric response is quite similar to behavior of a looser specimen, i.e. less marked peak stress and less volumetric expansion.

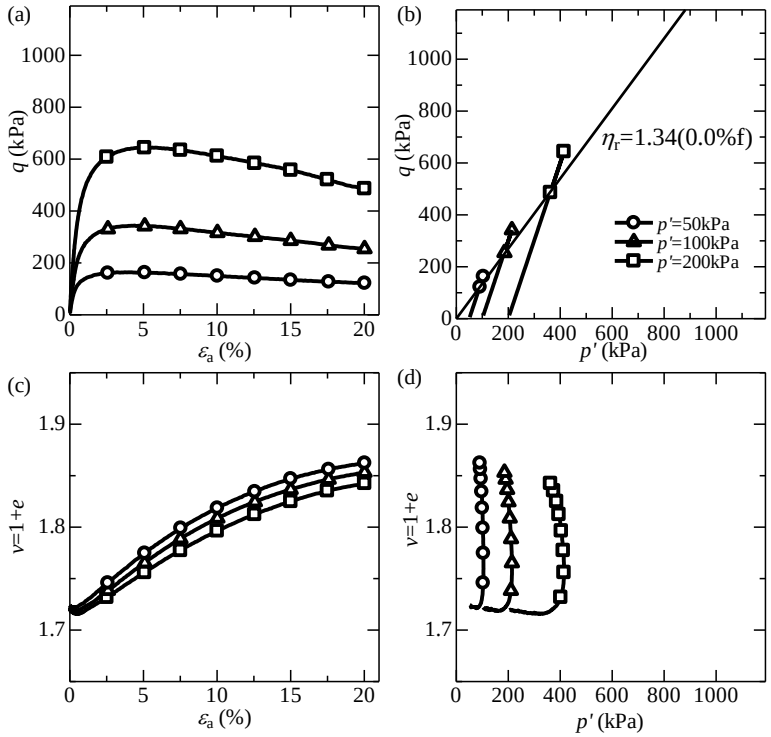

Fig. 4.13 Shear – strain – volumetric response of unreinforced sand for 50, 100, and 200kPa confining pressures prepared with D_r=80%

Toyoura sand specimens sheared under different confining pressures showed identical behavior. Higher confining pressure increased maximum and residual deviator stresses and decreased volumetric expansion, i.e., the greater confining pressure, the less volumetric expansion that can be confirmed on both $v - \varepsilon_a$ and $v - p'$ curves. Connection of all three values of the stress ratios η_r at 20% axial strain in $q - p'$ curve is a straight line through the origin of the stress plane (Fig. 4.13b). Also, despite the difference in stress paths, the values of residual stress ratio were equal to η_r=1.34 for all confining pressures, which was the same value in the case of different initial relative densities (section 4.3.3.1). Therefore, as mentioned in previous studies (Schofield and Wroth, 1968; Atkinson and Bransby, 1978), unreinforced sand can be idealized as having the critical state line.

Fiber-reinforced sand specimens experienced identical mechanical behavior to the unreinforced one: the maximum and residual stresses increased, and volumetric expansion at 20% axial strain decreased, with the increase in confining pressure.

The effect of fiber inclusions was in a higher and more pronounced maximum deviator stress q_{max} and higher residual deviator stress q_r compared to sand specimens without fibers, which can be observed in q - ε_a curves (Figs. 4.14a, 15a and 16a). As shown in Figs. 4.14b and 4.15b, the stress states at the end of shearing were on a straight line through the origin in $q - p$' plane. The tendency was similar to that of unreinforced sand. By idealizing the existence of a critical state (section 4.2.3.1), it can be considered that the critical state line existed in the fiber-reinforced sand depending on the fiber content as well as in the sand. The same conclusion cannot be done for 1% fiber-reinforced sand (Fig. 4.16b), where the stress states at 20% axial strain were on a straight line, but not through the origin in $q - p$' plane.

Initial stiffness E_{50} of fiber-reinforced sand was smaller than that of pure sand under all three considered confining pressures (Fig. 4.17). Furthermore, initial stiffness of both unreinforced and fiber-reinforced sand increased with the increase in confining pressure.

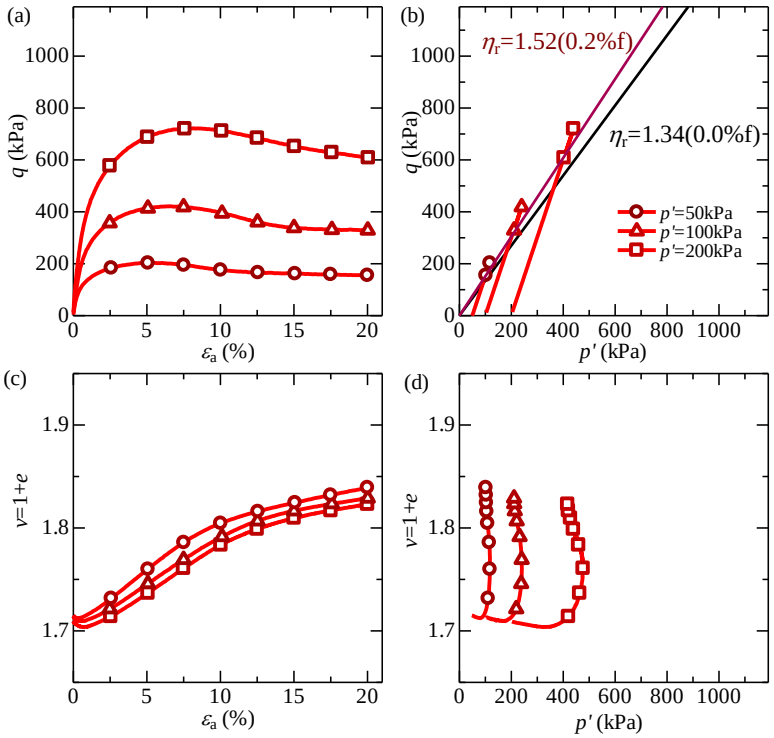

Fig. 4.14 Shear – strain – volumetric response of 0.2% fiber-reinforced sand for 50, 100, and 200kPa confining pressures prepared with D_r=80%

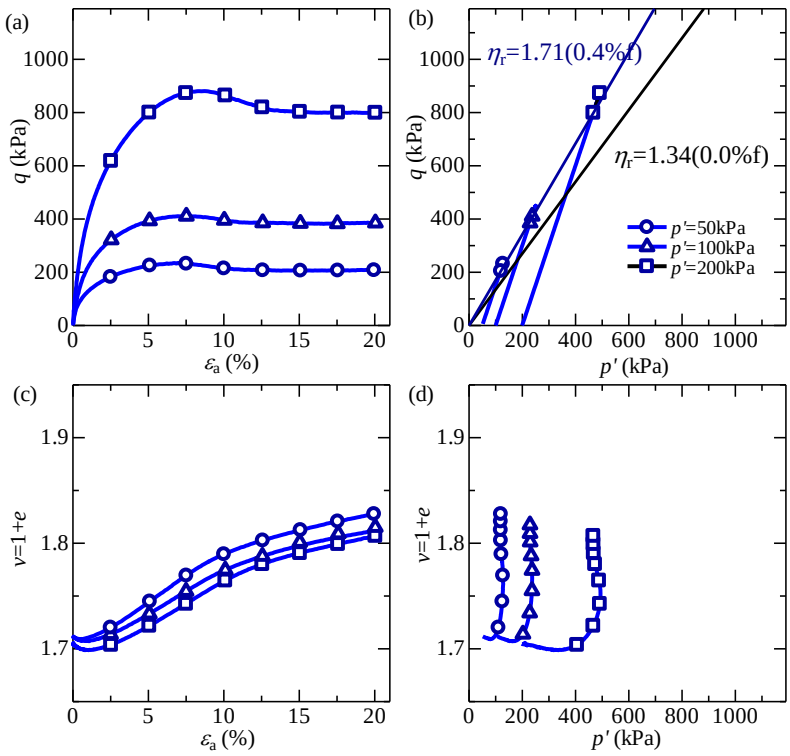

Fig. 4.15 Shear – strain – volumetric response of 0.4% fiber-reinforced sand for 50, 100, and 200kPa confining pressures prepared with D_r=80%

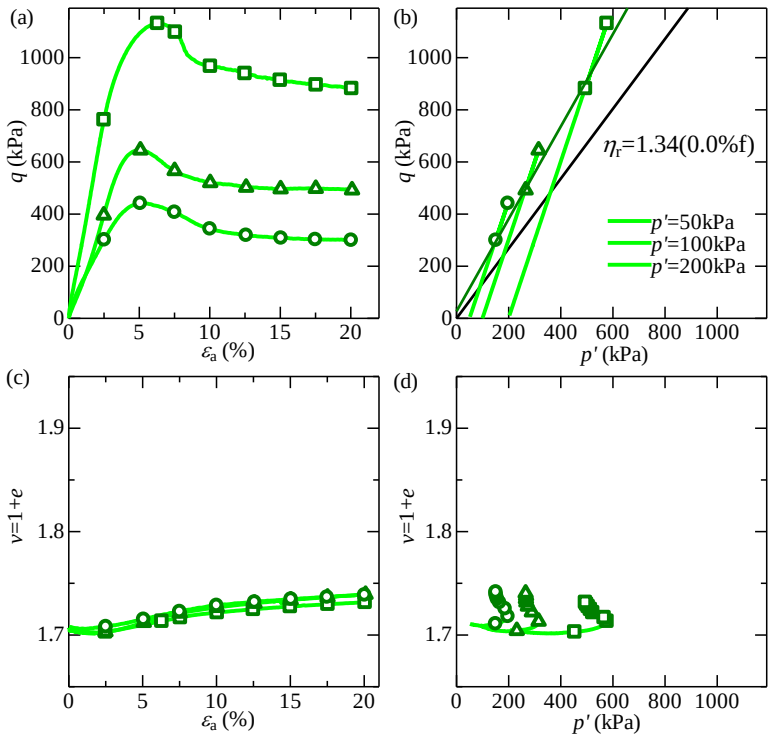

Fig. 4.16 Shear – strain – volumetric response of 1.0% fiber-reinforced sand for 50, 100, and 200kPa confining pressures prepared with D_r=80%

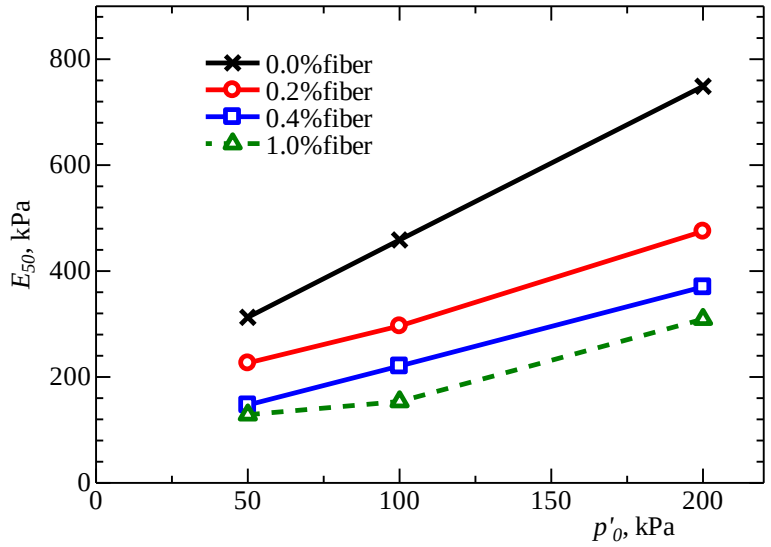

Fig. 4.17 Initial stiffness – confining pressure dependency, expressed through the deformation modulus E_{50} (solid lines – dry vibration, dashed line – moist tamping)

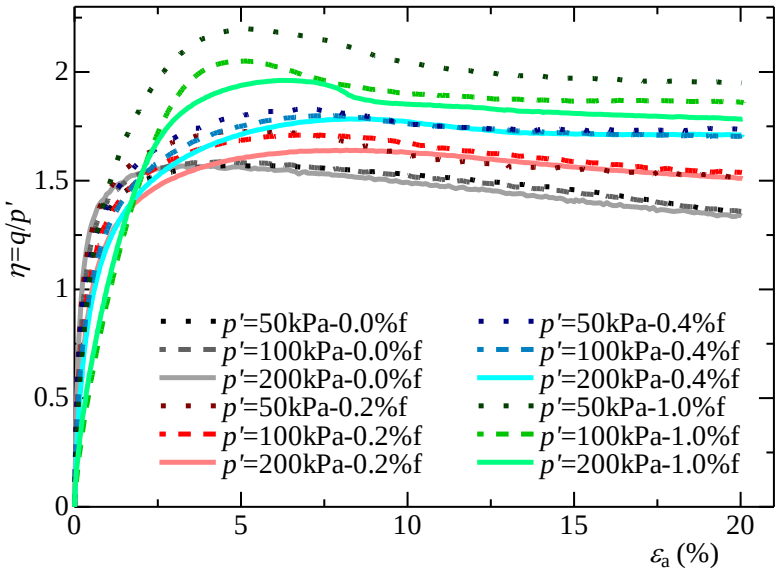

Fig. 4.18 Stress ratio – axial strain dependency for all fiber content sheared under 50, 100, and 200kPa confining pressures

In order to consider the effect of fiber content and confining pressure on the stress ratio, the stress ratio η (=q/p') is plotted against the axial strain ε_a in Fig. 4.18. The trend of increased stress ratio with the fiber content is obvious for all fiber contents and confining pressures. The respective residual stress ratio values η_r (=q_r/p') of 0.0%, 0.2% and 0.4% fiber inclusions reached the same value at 20% axial strain independently of the confining pressure, even though η values at lower axial strain values were different for each confining pressure.

A detailed description of the stress ratios at phase transformation point, maximum shear stress and residual stress is given in Fig. 4.19. The phase transformation and peak stress ratios of fiber-reinforced sand η_{pt}, η_{max} were higher than those of unreinforced sand; stress ratio values increased with the increase in fiber content. It should be noted that the increase in confining pressure led to a slight decrease in phase transformation and peak stress ratios of both unreinforced and fiber-reinforced sand. However, the residual stress ratios η_r (=q_r/p') at 20% axial strain is the same respective values with 1.34 for unreinforced sand, whereas those for reinforced sand with 0.2% and 0.4% of fiber contents are equal to 1.52 and 1.71, respectively (Fig. 4.19c). Nevertheless, compared to a lower percentage of fiber inclusions, 1.0% fiber-reinforced sand experienced a significantly

different trend for a residual stress ratio with the increase in confining pressures; that is, with the increase in confining pressure the residual stress ratio η_r decreased.

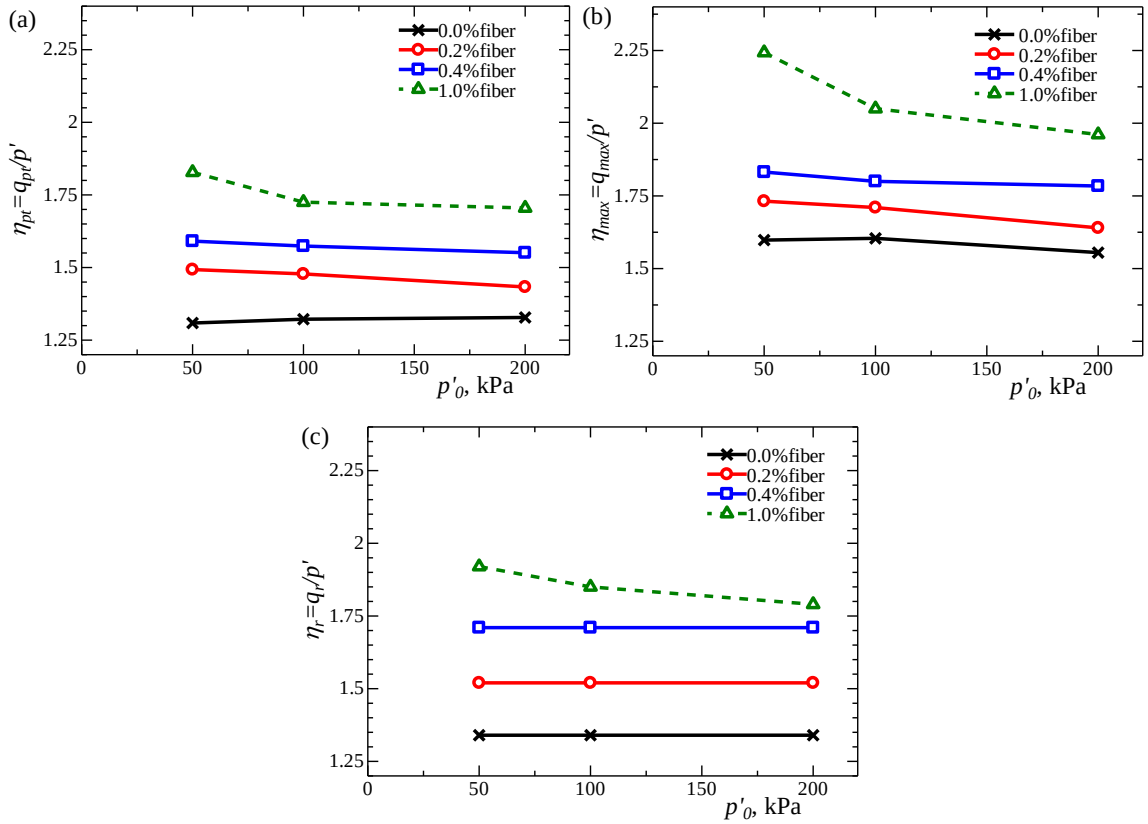

Fig. 4.19 Stress ratio dependency on confining pressure: a) phase transformation, b) peak, and c) residual stress ratios (solid lines – dry vibration, dashed line – moist tamping)

The volumetric change responses of fiber-reinforced sands are presented through the specific volume dependency from an axial strain and mean effective stress in Figs. 4.14c, d, 4.15c, d, and 4.16c, d. The initial volumetric compression increased, and final volumetric expansion decreased with the increase in fiber content. The specific volume of sand with 0.2% and 0.4% fiber content decreased as the confining pressure increased at the end of shearing. It can also be observed in Fig. 4.20a, where the lines that connect values of specific volumes at 20% axial strain depending on the initial confining pressures are compared to the volumetric change of unreinforced sand. The lines are almost parallel and decline with the fiber content. Additionally, specific volume – confining pressure dependency at 20% axial strain is given in v–ln p' curve (Fig. 4.20b). The results of the specific volume change are consistent with the volumetric change tendency in isotropic compression experiments, where fiber-

reinforced sand specimens had a smaller value of NCL parameter N. Here, from Fig. 4.20b considering the dependency of NCL parameter N and CSL parameter Γ through the equation N–Γ= $\bar{\lambda}$–$\bar{\kappa}$, it can be concluded that the value of CSL parameter Γ has a decreasing tendency with the increase in fiber content.

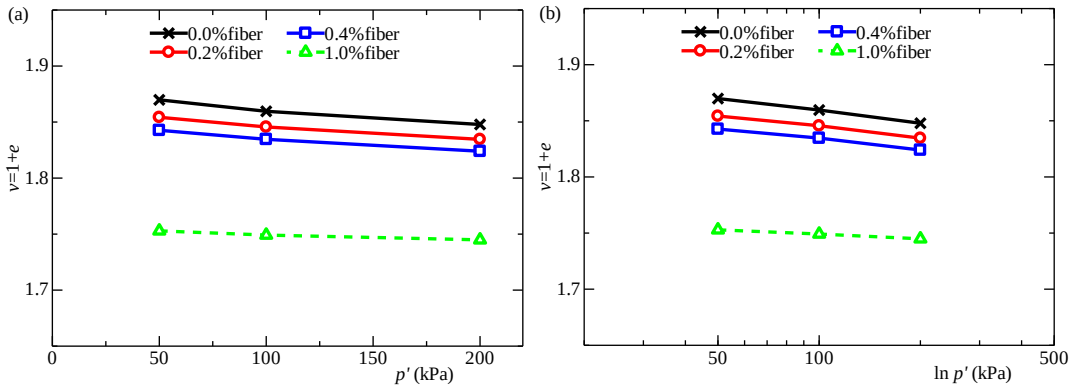

Fig. 4.20 Specific volume *v* at 20% axial strain – confining pressure p'_0 dependency with the fiber content (solid lines – dry vibration, dashed line – moist tamping)

Additional experimentations with higher confining pressures (p'_0=400, 600kPa) were performed on 0.0%, 0.2% and 0.4% fiber-reinforced sand. In case of 0.4% fiber-reinforced sand only 500kPa confining pressure was applied up to a limit stress due to the limitation of load cell. As can be seen from Figs. 4.21-4.23, contribution of fibers increased the deviator stress with the increase in confining pressure, while the stress ratio at the end of shearing was on the critical state line obtained from the shear results under lower confining pressures. This means that once the fiber content was determined, the critical state line corresponding to the fiber content was also determined.

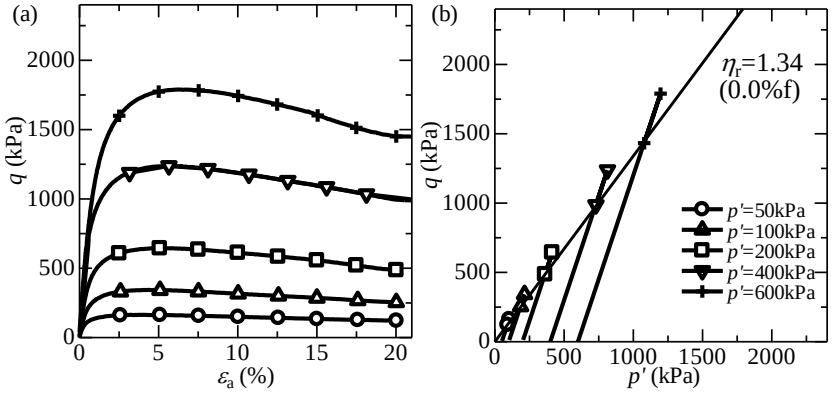

Fig. 4.21 Stress – strain behavior of unreinforced sand sheared under five different confining pressures

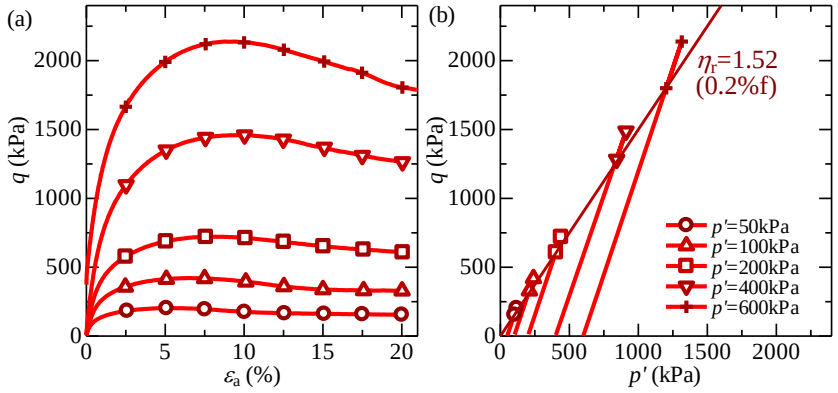

Fig. 4.22 Stress – strain behavior of 0.2% fiber-reinforced sand sheared under five different confining pressures

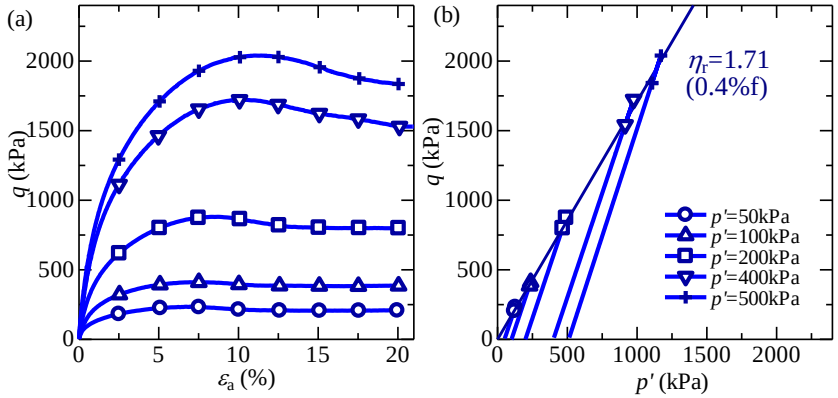

Fig. 4.23 Stress – strain behavior of 0.4% fiber-reinforced sand sheared under five different confining pressures

4.3.3.3 Effect of fiber length on the shearing properties of sand

Fig. 4.24 presents the shear behavior of unreinforced and 0.2% fiber-reinforced sand with the different length fibers: 12 mm, 6 mm and 3mm, respectively. The aspect ratios of 12 mm-long fibers, 6 mm, and 3mm were 300, 150, and 75, respectively. The specimens were prepared in dense condition with the initial relative density of 80% and sheared under 100kPa confining pressure. Sand reinforced with 3-mm and 6-mm-long fibers experienced slightly higher maximum and residual deviator stresses in q–ε_a curves, with lower volumetric expansion than unreinforced sand. The effect of the length of fibers can be concluded as follows: the longer fibers have higher maximum and residual deviator stresses with lower volumetric expansion. Furthermore, shortening the fiber length leads to decrease

in deviator and mean effective stresses and increase in volumetric expansion, i.e. it approaches shear-strain-volumetric change behavior of unreinforced sand.

These observed results are consistent with those of previous studies, where the effect of fibers on shear strength were considered (Gray and Ohashi, 1983; Consoli et al., 2009; Sadek et al., 2010; Falorca and Pinto, 2011; Lirer et al., 2011). Moreover, according to Michalowski and Ĉermak (2003), the reinforcement is effective when the reinforcing material is one order higher than the host soil. As decreasing the length of fiber leads to a decrease in maximum and residual deviator stresses, and mean effective stress, the determination of the void ratio of fiber-reinforced sand should be done by considering the fibers as a part of solids. In the case that the fibers are counted as a part of voids, such varying of the shear behavior would not be observed, i.e. there would be no apparent effect of the fiber's length.

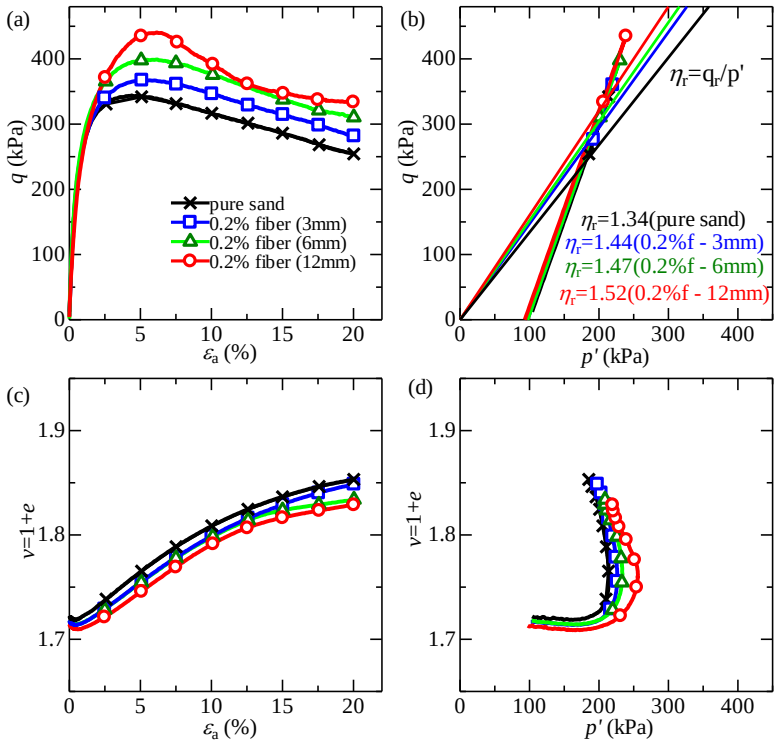

Fig. 4.24 Stress – strain – volumetric change behavior of unreinforced sand and sand reinforced with 0.2% fiber content of different length

Fig. 4.25 represents the stress ratio η – axial strain ε_a dependency. As can be observed, with the decrease in the length of reinforcing material the residual stress ratio values decrease (η_r=1.52 –

0.2% fiber with 12mm length; η_r=1.48 – 0.2% fiber with 6mm length; η_r=1.43 – 0.2% fiber with 3mm length; η_r=1.34 - 0.0% fiber). The full sight of the influence of fiber's length on the different stress ratios is given in Fig. 4.26.

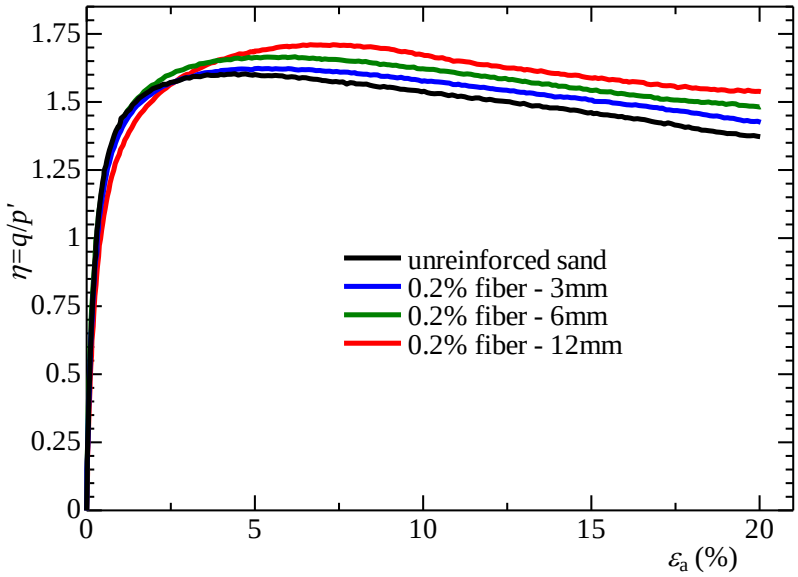

Fig. 4.25 Influence of the length of fiber on the stress ratio (critical state line parameter)

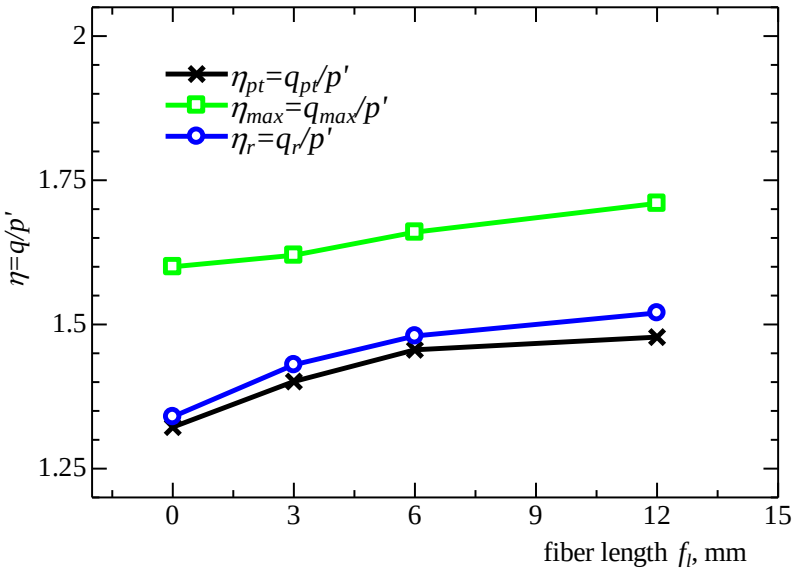

Fig. 4.26 Stress ratios dependency on fiber length with 0.2% fiber inclusions (legends show different stress ratios)

4.3.4 Drained triaxial extension test results

From most previous studies, the effect of fibers on the compressive strength was significantly high. Several attempts of adding fibers to soils as a reinforcing material have also been performed to increase the tensile strength of composite (Chen, 2010; Ibraim et al., 2010; Li et al., 2014; Tang et al., 2016). However, according to the previous studies, the addition of fibers has a negligible effect on the tensile strength enhancement of soils. In drained triaxial extension experiments, some researchers revealed the fiber inclusions as a reinforcing material non-effective with insignificant differences between unreinforced and fiber-reinforced specimens prepared with different relative densities and sheared under various stresses (Chen., 2010; Diambra et al., 2010, Mandolini et al., 2019). Another interesting point has to be clarified: Palacios et al., (2012) represented results of drained triaxial extension tests with a lower tensile strength of fiber-reinforced sand specimens than the unreinforced sand sample. One of the possible reasons for the inefficiency of fiber-reinforcement for increasing the tensile strength is the deformation shape of the specimen, which affects both compressive and extensive strengths. In this section the clarification on the tensile strength of sand reinforced with fiber varying fiber content and confining pressure is presented.

Figs. 4.27-4.28 represent the drained triaxial extension test results, conducted under 100kPa and 300kPa of confining pressures, for both unreinforced and 0.2%, 0.4% fiber-reinforced specimens. Some experimental results are given in a couple of series indicated by a and b (Table 4.2).

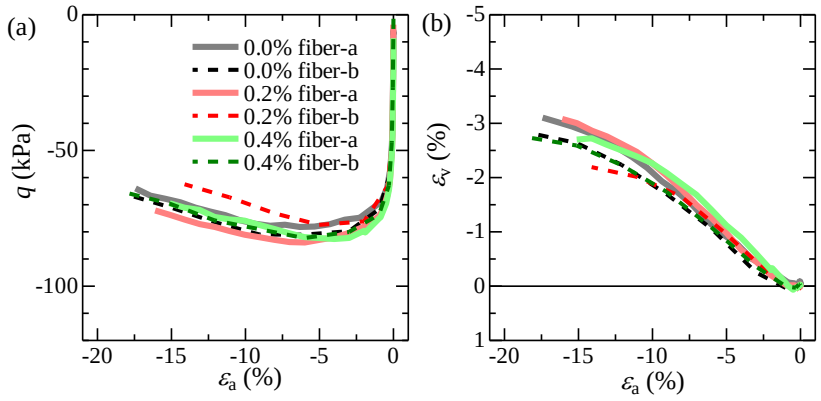

Fig. 4.27 Comparison of drained triaxial extension test performed under 100kPa confining pressures on dense specimens with different fiber contents

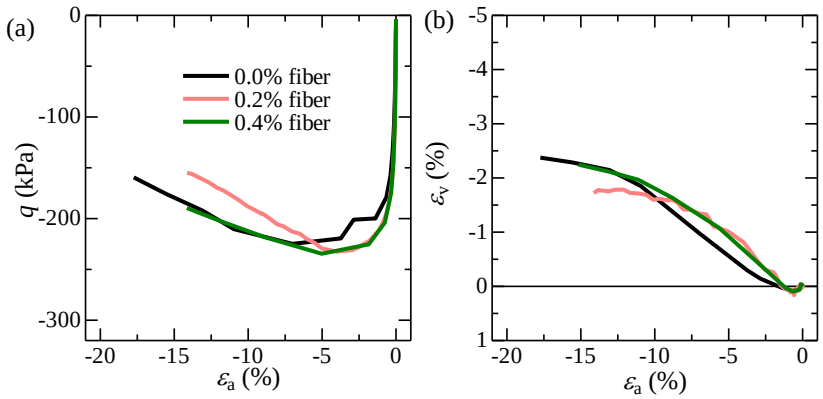

Fig. 4.28 Comparison of drained triaxial extension test performed under 300kPa confining pressures on dense specimens with different fiber contents

Shearing behavior of fiber-reinforced sand obtained from tests performed under 100kPa confining pressure (Fig. 4.27) revealed that fiber inclusions have a negligible effect with the similar path in stress-strain and volumetric change curves with that of unreinforced sand. In particular, deviator stresses of all specimens equaled approximately to q=65kPa at 15% axial strain, whereas all specimens experienced volumetric expansion at the end of shearing. With the increase in the confining pressure up to 300kPa (Fig. 4.28), all specimens' peak and post-peak deviatoric stresses increased. The increase in the tensile strength is only due to the higher confining pressure. However, the contribution of fibers was not observed. Similar to the observed trend in compression experiments, volumetric change decreased with the increase in confining pressure, i.e., the more the confining pressure, the less the volumetric expansion. Another interesting point that must be clarified is that fiber-reinforced sands sheared under higher confining pressure experienced a higher volumetric increase at smaller axial strains (Fig. 4.28b). With the progression of shear when axial strain reached 15% the fiber-reinforced specimens underwent slightly smaller volumetric expansion. In drained triaxial extension test performed under 100kPa confining pressure volumetric change was not affected with the fibers existence. With the increase in confining pressure, fiber-reinforced sand experiences higher expansion in the initial shearing stages. However, at the end of shearing, despite the differences in the intermediate volumetric change behavior, both unreinforced and fiber-reinforced sand reached the exact value of volumetric strain. Compared with the triaxial compression experiments, where the effect of both fiber contents and confining pressure was observed, the tensile strength of fiber-reinforced specimens was not influenced by the existence of fiber inclusions. The possible explanation and further mechanism will be discussed in later sections.

4.4 Undrained triaxial compression and extension behavior

In order to comprehensively analyze the effect of fiber-reinforcement and broaden the applicability of this soil improvement technique not only drained shearing behavior, but also undrained shearing behavior is necessary. For example, undrained behavior refers to the short-term behavior as the impact of earthquake just during the tremor or other similar natural behavior, which can cause the liquefaction problem. Consolidated undrained triaxial compression and extension experiments conducted to check the basic mechanical properties of unreinforced and fiber-reinforced sand specimen, compare with the mechanical properties from drained case and broaden the applicability for the modeling purposes.

4.4.1 Testing program

A series of consolidated undrained triaxial compression and extension experiments were performed on unreinforced and fiber-reinforced sand specimens with varying the confining pressure from 50kPa to 200kPa. In order to consider the higher strain levels and taking into account the susceptibility of Toyoura sand to generate high negative pore water pressures, a medium dense condition of specimens was considered. The sample preparation was identical as in case of drained triaxial compression tests. The reinforced specimens were prepared with fiber of 12mm length and 0.2% and 0.4% content by dry weight. All specimens were placed with approximately 40% relative density which refers to a medium loose condition. In case of undrained triaxial testing back pressure was set at 500kPa, and cell pressure, respectively, at 550kPa, 600kPa and 700kPa to meet the chosen confining pressure values. Triaxial shearing tests were conducted according to JGS 0523 with a strain rate of 0.5 %/min. Table 4.2 shows a complete list of experiments along with the void ratio at the end of consolidation e_c, and the corresponding relative density D_r, fiber content w_f, and confining pressure in the consolidation process, p_0'.

Table 4.2 List of CU experiments

Test	Type of experiment	w_f, (%)	e_c	D_r, (%)	p'_0, (kPa)	$\eta_r=q_r/p'$
CU050-00	C	0.0	0.845	40	50	1.34
CU050-02	C	0.2	0.837	40	50	1.52
CU050-04	C	0.4	0.838	40	50	1.71
CU100-00	C	0.0	0.844	40	100	1.34
CU100-02	C	0.2	0.827	40	100	1.48
CU100-04	C	0.4	0.835	40	100	1.68
CU200-00	C	0.0	0.840	40	200	1.34
CU200-02	C	0.2	0.827	40	200	1.51
CU200-04	C	0.4	0.826	40	200	1.65
CU100-00	E	0.0	0.838	40	100	-0.79
CU100-02	E	0.2	0.837	40	100	-0.92
CU100-04	E	0.4	0.840	40	100	-0.98
CU200-00	E	0.0	0.838	40	200	-0.81
CU200-02	E	0.2	0.837	40	200	-0.88
CU200-04	E	0.4	0.840	40	200	-0.98

C - compression; E - extension

4.4.2 Undrained triaxial compression test results

The results of the undrained triaxial compression tests under 50kPa, 100kPa and 200kPa confining pressures, performed on both unreinforced and fiber reinforced sands prepared with similar initial relative densities, are given in Figs. 4.29-4.31. The exhibit includes deviator stress q – axial strain ε_a, deviator stress q – mean effective stress p', excess pore water pressure (PWP) Δu – axial strain ε_a and specific volume v – mean effective stress p' curves. Fig. 4.29 shows the typical stress-strain and excess PWP behaviors of unreinforced sand with similar initial relative densities sheared under different confining pressures.

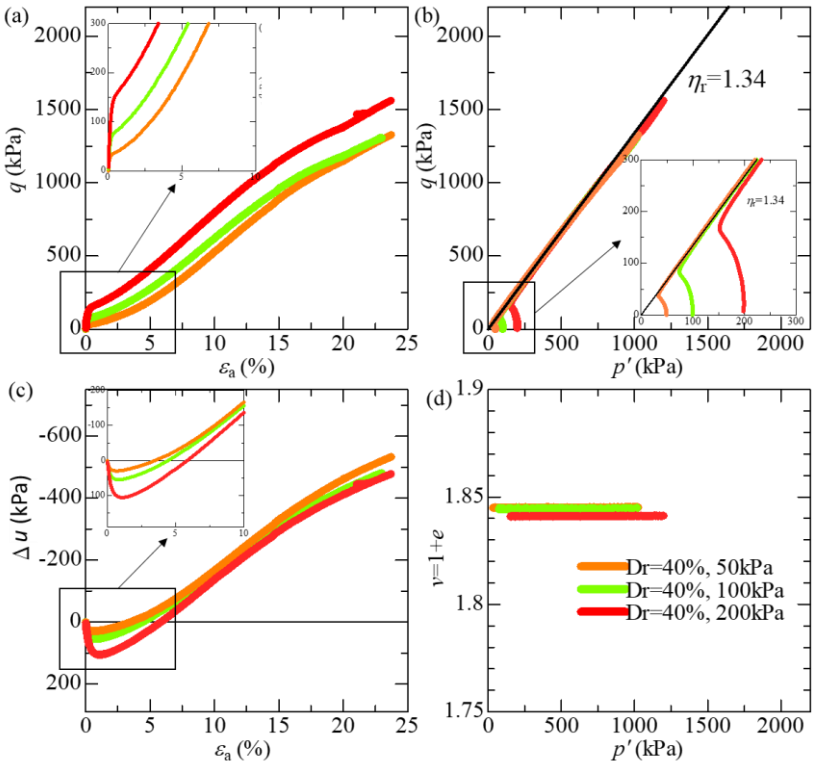

Fig. 4.29 Shear – strain – pore water pressure response of unreinforced sand for 50, 100, and 200kPa confining pressures prepared with D_r=40%

Similarly, unreinforced Toyoura sand specimens exhibited different $q - \varepsilon_a$ curves depending on the initial relative densities, whereas the deviator stresses tended to reach the same residual stresses at 25% axial strain. This behavior could also be observed in effective stress path, where all specimens reached to the stage where further shearing after phase transformation point occurred on the critical state line. Similar results of undrained shearing were presented in previous studies performed on Toyoura sand (Verdugo and Ishihara, 1996). The specimen sheared under 200kPa confining pressure has a slightly higher value of deviatoric stress in $q - \varepsilon_a$ curves compared to specimens sheared under 50kPa and 100kPa confining pressure, which corresponds to the higher change in specific volume during the consolidation process, and eventually the specimen became denser. It should be noted that similarly the volumetric change with a very small increment in drained condition, the PWP is still also changing but with very small increment. The generation of PWP is similar to the volumetric change behavior in drained condition, where the higher confining pressure produced initially higher positive PWP which turned to the negative PWP at higher strain rates, and reached to a smaller value of excess PWP at the end of shearing.

Undrained shearing behavior of fiber-reinforced is quite similar to the undrained sand behavior with identical strain-softening and strain-hardening characteristics. Particularly, 0.2% fiber-reinforced sand specimens prepared with approximately similar initial relative densities sheared under different confining pressures (in Fig. 4.30) initially experienced different stress-strain response, while tented to reach to the same value of residual stress at 25% axial strain. A small difference of the specimen sheared under 50kPa confining pressure is attributed to the smaller compression in consolidation process which led to the specimen to be in more loose condition just before shearing. In the effective stress path, irrespective of the initial state of specimens, all stresses reached to the same stress ratio and was on the same stress ratio at 20% axial stain as in case of drained condition.

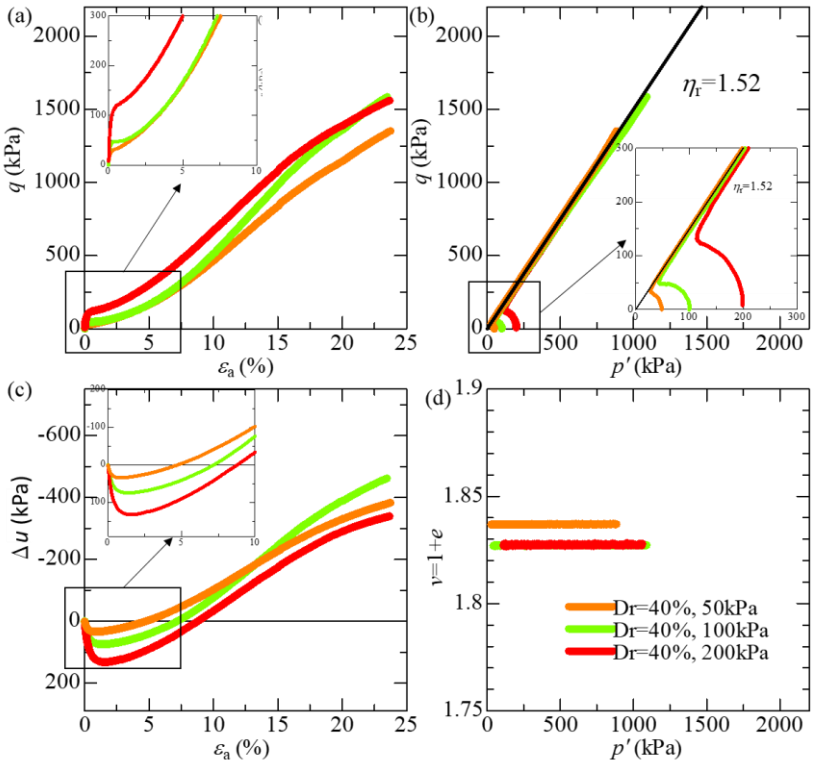

Fig. 4.30 Shear – strain – pore water pressure response of 0.2% fiber-reinforced sand for 50, 100, and 200kPa confining pressures prepared with D_r=40%

There are some differences in the mechanical properties of the undrained shear behavior of 0.4 % fiber-reinforced sand compared to those of a lower fiber content (Fig. 4.31). When the percentage of the reinforcing material increased, the placement of samples with exactly the same initial relative density is quite difficult due to the unstable compressive behavior during the consolidation process. Similarly, even though the specimens were prepared with high accuracy, due to the different

compression during the consolidation attributed to different applied confining pressure, specific volumes as well as initial relative densities of 0.4% fiber-reinforced specimens after consolidation were different. However, the overall tendency of stress-strain-PWP response of 0.4% fiber-reinforced sand was similar to unreinforced and 0.2% fiber-reinforced sand. It should be noted that the stress ratio values of unreinforced and fiber-reinforced sand at the end of shearing is approximately the same to the stress ratios obtained from the drained triaxial compression tests. Taking into account all these features, it can be considered that even fiber-reinforced sand had also reached the vicinity of the critical state at the end of the tests as well as unreinforced sand.

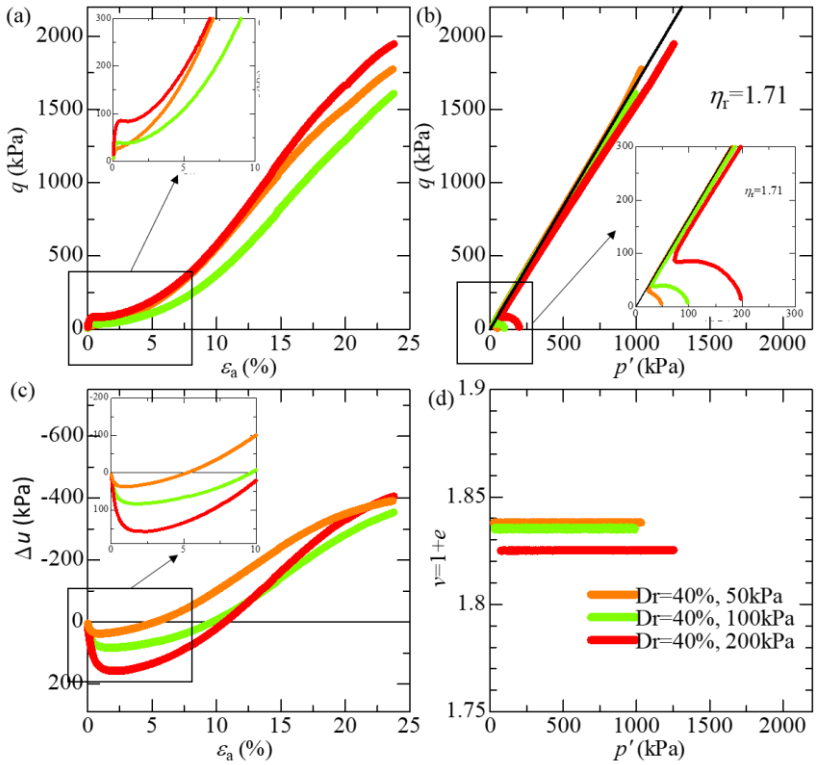

Fig. 4.31 Shear – strain – pore water pressure response of 0.4% fiber-reinforced sand for 50, 100, and 200kPa confining pressures prepared with D_r=40%

In Figs. 4.29-4.31 the similar tendency of the undrained shearing behavior of unreinforced and fiber-reinforced sand was observed. However, the fiber inclusions led to some differences of initial stiffness in deviatoric stress – axial strain curves, effective stress paths, and less generation of negative PWP in excess PWP – axial strain curves.

In order to compare the mechanical behavior of unreinforced and fiber-reinforced sand and to reveal some essentials of fiber-reinforcement, experimental results of undrained triaxial compression test of unreinforced, 0.2% and 0.4% fiber-reinforced sand sheared under 100kPa confining pressure were plotted in Fig. 4.32. As can be seen in Fig. 4.32, the specimen with higher fiber content experienced a higher reduction in initial stiffness ($q - \varepsilon_a$ curves), higher initial decrease of mean effective stress in effective stress path similar to looser unreinforced specimen, and higher positive PWP at smaller strains. However, the intensity of the increase in deviator stress of fiber-reinforced sand increased with the shear progression, where 0.2% and 0.4% fiber-reinforced sand specimen reached higher value of deviatoric stresses at q_{25}=1500kPa and q_{25}=1700kPa, respectively, compared to unreinforced sand with q_{25}=1300kPa. Initial reduction of deviatoric stresses with more obvious softening behavior in fiber-reinforced specimens is assumed to be related to the anisotropic effect that will be discussed later in Chapter 6. Also, after reaching to the phase transformation point with more pronounced strain-softening in the fiber-reinforced sand, 0.2% and 0.4% fiber-reinforced sand specimens reached a higher stress ratio with the shear progression. The phase transformation point is a threshold between plastic volumetric compression and expansion, where fiber-reinforced sand specimens initially experienced higher positive PWP, and turned to negative PWP generation phase at higher axial strains, and, eventually reached to smaller values of negative PWP at the end of test. Such kind of behavior of PWP generation is similar to a volumetric change behavior of unreinforced and fiber-reinforced sand in drained condition, where fiber-reinforced specimens showed more contractive behavior with smaller dilatancy ratio (section 4.3.3.1).

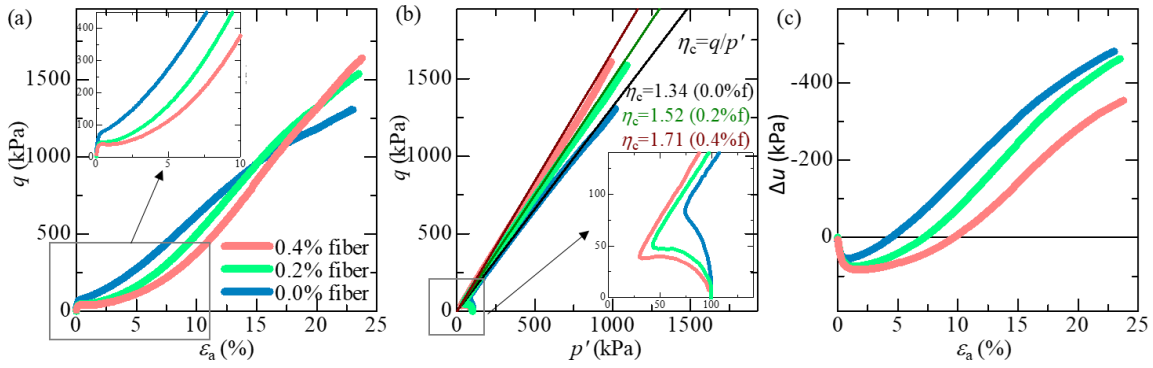

Fig. 4.32 Comparison of undrained triaxial compression tests results of unreinforced, 0.2% and 0.4% fiber-reinforced specimens sheared under p_0'=100kPa

4.4.3 Undrained triaxial extension test results

Figs. 4.33-4.34 present results of consolidated undrained triaxial extension experiments conducted on specimens placed in medium dense condition and sheared 100kPa and 200kPa confining pressures, respectively. Compared to drained behavior of unreinforced and fiber-reinforced sand in extension with no explicit tendency for the shearing behavior, undrained behavior revealed clear effect of fiber inclusion on the undrained tensile strength of sand. Particularly, the tensile strength ($q - \varepsilon_a$ curves) of sand increased with the increase in fiber content under both confining pressures. Furthermore, the deviator stress increased at higher confining pressure. On the effective stress diagram there is an obvious tendency with a smaller decrease of stress path (strain-softening) of fiber-reinforced sand and the higher stress ratio up to a point, after which all specimens experienced reduction in deviator stress, somewhat forming a "hook". Formation of a "hook" is attributed to strain localization with a clear shear band in both unreinforced and fiber-reinforced sand, after with shear behavior cannot be considered as a one element behavior. The information on the effect of strain localization will be presented in next section.

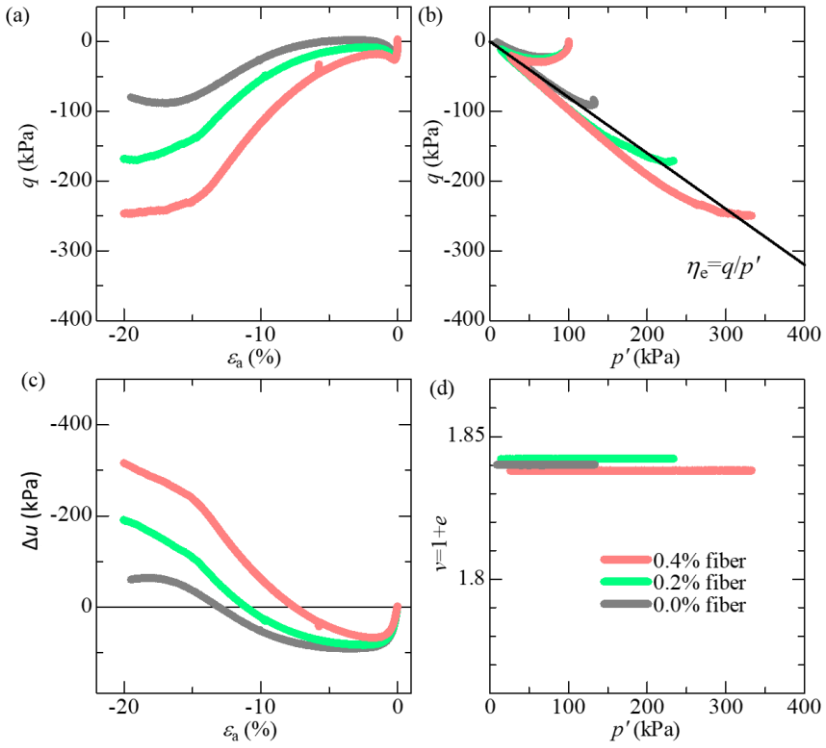

Fig. 4.33 Comparison of undrained triaxial extension test results of unreinforced, 0.2% and 0.4% fiber-reinforced specimens sheared under p_0'=100kPa

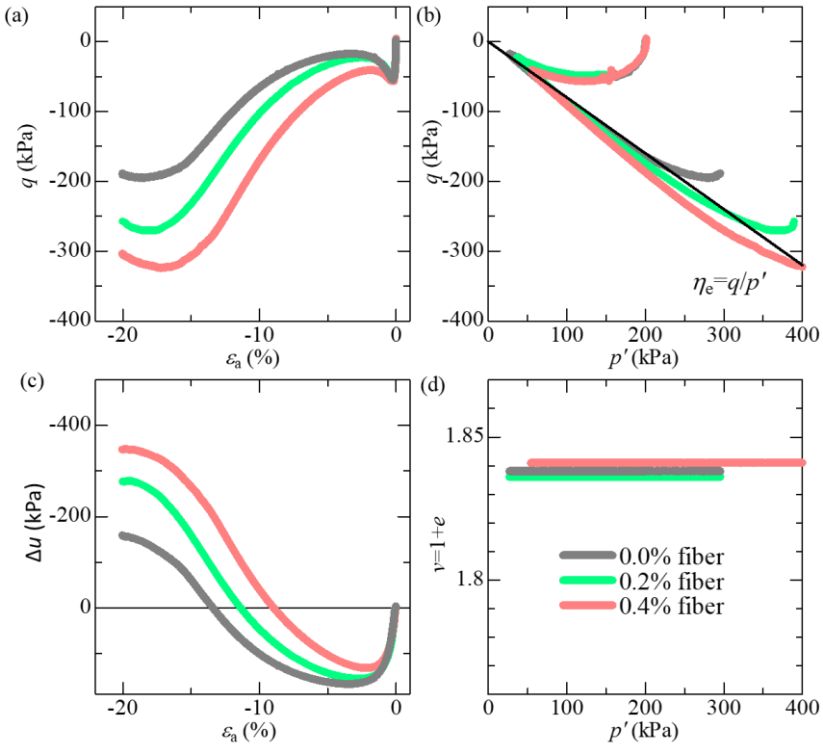

Fig. 4.34 Comparison of undrained triaxial extension test results of unreinforced, 0.2% and 0.4% fiber-reinforced specimens sheared under p_0'=200kPa

PWP generation has an opposite tendency from the undrained compressive behavior. Unreinforced sand initially experienced a higher positive PWP compared to fiber-reinforced sand, and finally the value of excess PWP reached to a smaller value. Furthermore, the intensity of the transformation of PWP from positive to negative value increased with the increase in confining pressure. Being more specific, the more the confining pressure the higher initial PWP and the higher the negative PWP at the end of the test. Such kind of tendency for the higher negative PWP generation in fiber-reinforced sand might be one of the possible effects on the tensile strength increase compared to drained condition, where no difference in the volumetric change behavior of unreinforced and fiber-reinforced sand in drained extension was observed.

4.5 Discussion based on failure mode analysis

Mechanism of fiber-reinforcement compared to unreinforced sand accompanied with more complicated interaction between sand particles and fibers. The effectiveness of fibers for improving compressive strength was observed in both drained and undrained conditions, while in extension the

impact of fiber on the tensile strength enhancement was observed only in undrained case. For the purpose of investigation of various aspects and factors about reinforcing effect of fibers, a macro mechanical analysis was performed through the failure mode analysis. Figs. 4.35 – 4.38 represent the failure modes of unreinforced and fiber-reinforced specimens at 20% of axial strain through triaxial compression test and at 15% axial strain through triaxial extension test for drained conditions under two different confining pressures. Figs. 4.39-4.42 illustrate similar series of failure modes for the undrained condition for compression and extension, respectively. It should be noted that the shear bands in unreinforced sand as well as in fiber-reinforced sand has started forming at smaller axial strains. The given failure modes are only the reference to fully formed shear bands at the end of the tests.

The failure modes of unreinforced and 0.2%, 0.4% fiber-reinforced sand specimens in compression tests were identical under both confining pressures in Figs. 4.35 and 4.36. The deformation occurred through the entire height of specimens with bulking in the central part. The number of shear bands was higher in the specimens with the higher fiber content, and it increased with more obvious strain localizations under higher confining pressures. On the other hand, 1% fiber-reinforced specimens that were prepared by moist tamping experienced a partial deformation on the upper part of the specimen. This might be one of the reasons for a significant difference in the mechanical behavior of 1% fiber-reinforced sand compared to specimen with lower fiber contents, especially in volumetric change behavior (Figs. 4.8, 4.16). Compared to failure modes in compression, the deformation shapes of fiber-reinforced specimens in triaxial extension tests were different from unreinforced ones even for a lower fiber content in Figs. 4.37 and 4.38. Unreinforced samples exhibited a “necking” in the center of the specimen, and the shear band became more predominant with clear doubled necking under higher confining pressure. However, the shear band in fiber-reinforced sand went down to the bottom part of the specimen without deformation on the upper part of the sample. In the case of a lower confining pressure no sharp strain localization was observed, while under higher confining pressure of 300kPa the strain localization occurred with explicit shear band formation. In order to make an assumption regarding a negligible effect of fibers to increase the tensile strength of sand in drained condition, and, where one of the reasons was considered to be somewhat “transferred” shear band to the bottom of the reinforced specimen, similar failure mode analysis performed in undrained case.

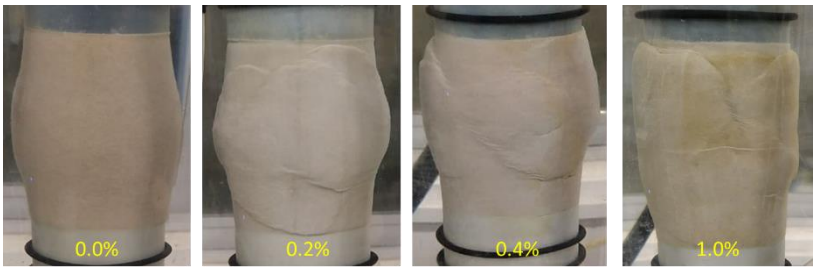

Fig. 4.35 Failure modes of specimens at 20% axial strain in drained triaxial compression sheared under 100kPa confining pressure (fiber content is given in yellow)

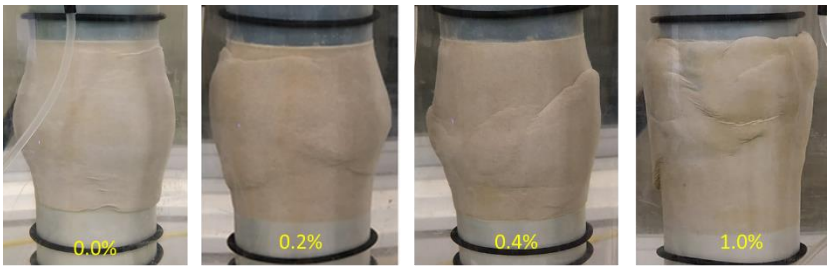

Fig. 4.36 Failure modes of specimens at 20% axial strain in drained triaxial compression sheared under 200kPa confining pressure (fiber content is given in yellow)

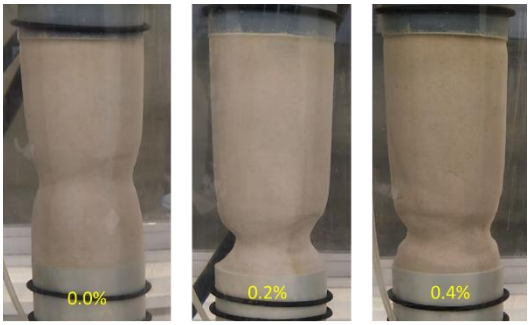

Fig. 4.37 Failure modes of specimens at 15% axial strain in drained triaxial extension sheared under 100kPa confining pressure (fiber content is given in yellow)

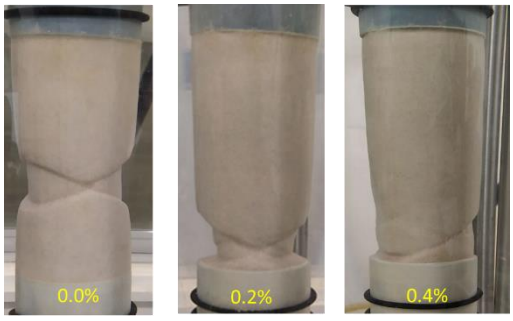

Fig. 4.38 Failure modes of specimens at 15% axial strain in drained triaxial extension sheared under 300kPa confining pressure (fiber content is given in yellow)

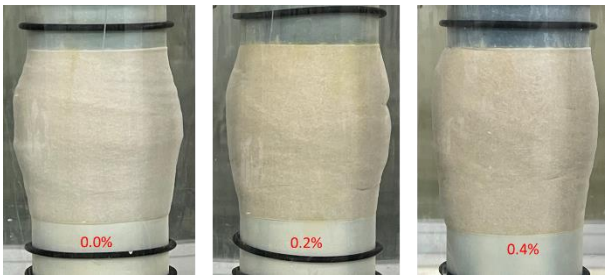

Fig. 4.39 Failure modes of specimens at 20% axial strain in undrained triaxial compression sheared under 100kPa confining pressure (fiber content is given in red)

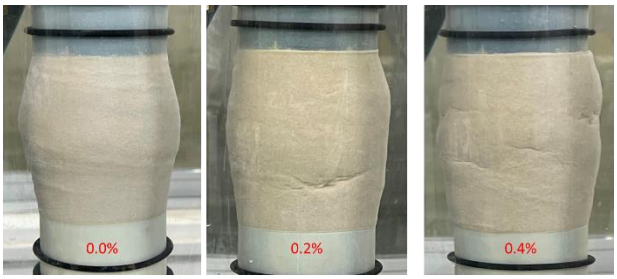

Fig. 4.40 Failure modes of specimens at 20% axial strain in undrained triaxial compression sheared under 200kPa confining pressure (fiber content is given in red)

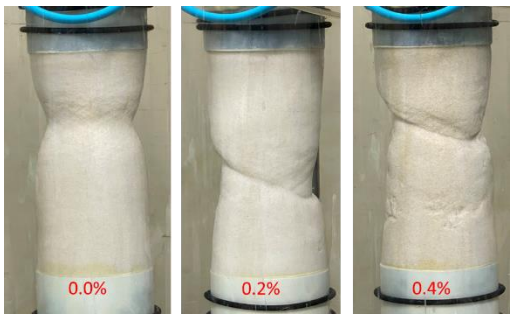

Fig. 4.41 Failure modes of specimens at 20% axial strain in drained triaxial extension sheared under 100kPa confining pressure (fiber content is given in red)

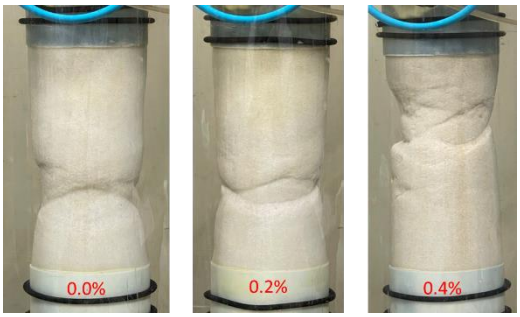

Fig. 4.42 Failure modes of specimens at 20% axial strain in undrained triaxial extension sheared under 200kPa confining pressure (fiber content is given in red)

Similar failure modes for unreinforced and fiber-reinforced sand were observed in undrained triaxial compression test as in drained condition as shown in Figs. 4.39 and 4.40. Especially, the deformation of both unreinforced and 0.2%, 0.4% fiber-reinforced sand specimens occurred through the entire height with bulking in the central part of the samples. From the deformation shapes under compression in drained and undrained condition and high reproducibility of test results, the relatively high uniformity of the fibers distribution within the whole sample can be additionally confirmed. Furthermore, the failure modes of fiber-reinforced sand specimens in undrained extension experiments were similar to the one of unreinforced specimen. Particularly, the deformation occurred in a relatively central part of the specimen with similar shear band formations for both unreinforced and fiber-reinforced specimens. In fact, the enhancement of tensile strength of sand with the increase in fiber content was clearly observed in undrained triaxial extension experiments. Based on the observed mechanical behavior of unreinforced and fiber-reinforced sands from experimental work and the deformation characteristics in drained and undrained conditions, it can be assumed that the one of the reasons for negligible effect of fiber in drained extension experiment is due to the transferred shear band to the bottom of the specimen.

4.6 Brief summary

In this chapter an extensive experimental results have been presented. Results and discussion were made according to isotropic compression, consolidated triaxial compression and extension tests under both drained and undrained condition. The followings are main conclusions based on observations and discussions:

1) Fiber-reinforcement decreased the value of N (NCL intercept) in isotropic consolidation experiment. Also, fiber-reinforced sand is more compressible at the initial stage of shearing with smaller initial stiffness and higher positive volumetric change. Furthermore, similarly to the tendency of NCL value N in isotropic compression, the value of the CSL parameter Γ has also a decreasing tendency with the increase in fiber content.

2) The drained shear behavior of fiber-reinforced sand with 0.2% and 0.4% of fiber content under the same confining pressure with different initial relative density exhibited similar behavior to unreinforced sand. At the end of shearing (20% axial strain), the respective deviatoric stresses were approximately the same; the specific volume reached almost the same value even if the initial relative

density was different. Hence, according to this observed mechanical behavior, it is considered that the stress state at the end of shearing is a near critical state.

3) The shear behavior of fiber-reinforced sand under different confining pressures also exhibited similar behavior to unreinforced sand. The test results of changing the confining pressure indicate that the critical state line exists in the fiber-reinforced sand as well as in unreinforced sand. It is a straight line through the origin in $q - p'$ plane and the slope of the critical state line increased as the fiber content increased. In $v - p'$ space, the specific volume decreased as the confining pressure increased. Furthermore, the shorter the fiber, the smaller the slope of the critical state line in $q - p'$ plane, which approaches that of unreinforced sand.

4) Effectiveness of fibers to improve the tensile strength of sand in drained condition was negligible, with possible explanation of the transferred shear band to the bottom of the reinforced specimen.

5) The undrained behavior of fiber-reinforced sand confirmed the existence of a unique critical state for a definite fiber content as well as for unreinforced sand. Furthermore, the values of stress ratios at the end of shearing from undrained tests are quite similar to those from compression testing in drained condition.

6) Two important observations from undrained triaxial compression complemented the observed mechanical behavior in drained compression tests. In fact, addition of fibers reduced the initial stiffness with a higher drop of effective stress paths and initially generated higher positive PWP, while brought a higher deviatoric stress with a higher stress ratios and a lower value of negative PWP at the end of shearing, similarly to volumetric change behavior in drained condition. This additionally confirmed that the effectiveness of fibers concludes in increasing the strength of host soil by positively contributing to confining pressure with produced tensile forces in fibers, and acting as a contracting agent to prevent the expansion.

7) Compared to drained extension behavior, contribution of fibers to improve the tensile strength of sand in undrained condition was obvious, with a higher deviatoric stress and a higher value of stress ratio at the end of shearing.

CHAPTER 5

CONSTITUTIVE MODELING OF FIBER-REINFORCED SAND

5.1 Introduction

From experimental study it was concluded that the effective stresses, q and p', and specific volumes v of both loose and dense sand sheared under the same confining pressure converged to a common value at the end of the tests with a small volumetric change independent of the initial relative density in Chapter 4. Therefore, the stress state was found to be a "near" critical state at the end of shearing ($\varepsilon_a \approx 20\%$), and even fiber-reinforced sand had its respective critical state as unreinforced sandy soil. Furthermore, the mechanical behavior of fiber-reinforced sand was quite similar to that of unreinforced sand, showing a similar tendency of softening/hardening and compression/expansion characteristics. Moreover, the values of residual stress ratios obtained from drained triaxial compression tests were also reached in undrained triaxial compression test for both unreinforced and fiber-reinforced sand. This suggested that the mechanical behavior of both unreinforced and fiber-reinforced sand could be expressed based on the critical state soil mechanics. However, fiber inclusions increased the strengths parameters as higher deviatoric and mean effective stresses with higher stress ratios at the end of the test, which indicates that unreinforced and fiber-reinforced specimens should be considered as different materials

5.2 Constitutive modeling based on a soil skeleton structure concept (SYS Cam-clay model)

The constitutive model used to reproduce the drained and undrained shearing behavior of both unreinforced and fiber-reinforced sand in triaxial compression is an elasto-plastic model based on the soil skeleton structure concept, called the super/subloading yield surface Cam-clay model, as SYS Cam-clay model for short. Before describing the super/subloading yield surfaces (SYS) Cam-clay model concept, limitations of the original and the modified Cam-clay models (Roscoe and Burland, 1968) should be mentioned. The modified Cam-clay model, the same as the original Cam-clay model, applies only to the loading/unloading of soils in which the soil is fully remolded, and loss of overconsolidation is completed. In other words, the modified Cam-clay model can only describe the mechanical behaviors of fully remolded and normally consolidated soils. The primary functions of the modified Cam-clay model are in simulation of hardening of soils that accompanies plastic volume

compression and softening with plastic volume expansion. Also, a borderline for hardening and softening in the stress space (phase transformation) expressed as a critical state line (CSL) q=Mp' is constant throughout the whole plastic deformation process. However, hardening can occur with plastic volume expansion above the CSL in the case of dense sand or overconsolidated clay, while softening of highly structured clay can occur with plastic volume compression below the CSL. The modified Cam-clay model cannot represent such kind of soil behaviors.

The SYS Cam-clay model can express 'soil skeleton structure' in terms of structure, overconsolidation and anisotropy, and describe the evolution of the soil skeleton structure associated with the development of plastic deformation. The SYS Cam-clay model is a constitutive model that describes elasto-plastic behaviors of soils by implementing two loading surfaces, superloading (Asaoka et al., 1998; Asaoka et al., 2000; Asaoka et al., 2002) and subloading (Hashiguchi, 1978; Hashiguchi, 1989) alongside the normal yield surface to describe the mechanical behavior of both structured and overconsolidated soils (Fig. 5.1).

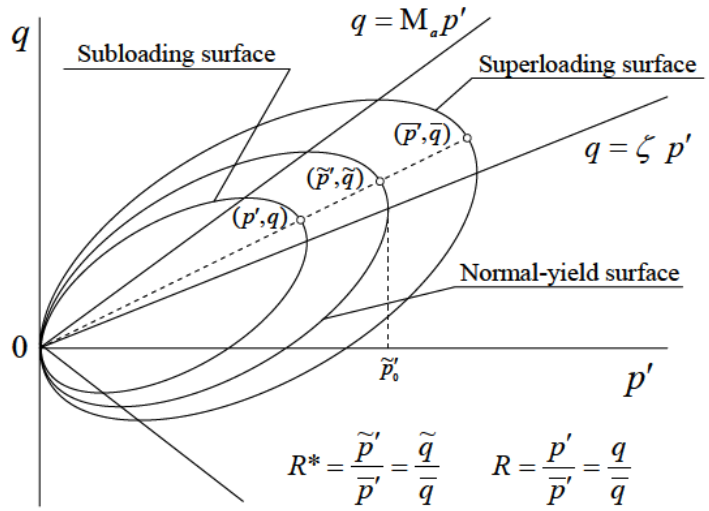

Fig. 5.1 Three yield surfaces (after Asaoka et al., 2002)

The current stress state is always on the subloading surface, where the soil is assumed to be in an overconsolidated state with a certain degree of structure. The stress parameters of the subloading surface are indicated by $p'$and q. R is the similarity ratio of the subloading surface to the superloading surface and R* is the similarity ratio of the normal-yield surface to the superloading surface in terms of stresses:

$$R = \frac{q}{\bar{q}} = \frac{p\prime}{\bar{p}\prime},\ R^* = \frac{\tilde{q}}{\bar{q}} = \frac{\tilde{p}\prime}{\bar{p}\prime} \tag{5.1}$$

R is the reciprocal of overconsolidation ratio, which develops as the soil is elastically unloaded from a certain stress state. When R becomes equal to 1.0 and the soil reaches a normally consolidated state, the subloading and superloading yield surfaces coincide, where the superloading surface ($\bar{p}'$, $\bar{q}$) represents a normally consolidated structured state of soil. The normal-yield surface ($\tilde{p}'$, $\tilde{q}$) is the same as a modified Cam-clay surface, which corresponds to a fully remolded and normally consolidated state of soil. When R^*, the degree of soil structure, becomes equal to 1.0 as the structure completely decays with the development of plastic deformation, the superloading surface comes to completely overlie the normal-yield surface.

The shape of the normal-yield surface of the modified Cam-clay model can be expressed as:

$$f(\tilde{p}', \tilde{\eta}^*) + \int_0^t J\mathrm{tr}\boldsymbol{D}^p d\tau = \mathrm{MDln}\frac{\widetilde{p'}}{\widetilde{p'}_0} + \mathrm{MDln}\frac{\mathrm{M}^2+\tilde{\eta}^{*2}}{\mathrm{M}^2} + \int_0^t J\mathrm{tr}\boldsymbol{D}^p d\tau = 0 \tag{5.2}$$

where $\tilde{\eta}^*$ is a stress ratio introduced to express anisotropic plastic behavior of soils (Sekiguchi and Ohta, 1977), $\widetilde{p'}_0$ is stress determined by the intersection between the initial yield surface and the central axis of normal yield surface (q=$\zeta p'$), M is the critical state index, D is the dilatancy parameter, $\boldsymbol{D}^p$ represents the plastic components of the stretching tensor $\boldsymbol{D}$, J is the Jacobian determinant of deformation gradient tensor $\boldsymbol{F}$.

$\tilde{\eta}^*$ is expressed as follows:

$$\tilde{\eta}^* = \sqrt{\frac{3}{2}}\|\hat{\boldsymbol{\eta}}\|, \hat{\boldsymbol{\eta}} = \boldsymbol{\eta} - \boldsymbol{\beta}, \boldsymbol{\eta} = \frac{\boldsymbol{S}}{p'}, \boldsymbol{S} = \boldsymbol{T}' + p'\boldsymbol{I}, p' = -\frac{1}{3}\,(\mathrm{tr}\boldsymbol{T}') \tag{5.3}$$

where $\boldsymbol{\beta}$ denotes the axis of the rotational tensor used in describing the anisotropy, and its magnitude is expressed as $\zeta = \sqrt{\frac{3}{2}}\|\boldsymbol{\beta}\|$. $\boldsymbol{I}$ is the identity tensor, and $\boldsymbol{T'}$ is the Cauchy effective stress tensor (positive in extension). $\|\ \ \|$ denotes the norm of a tensor ($\|\boldsymbol{A}\| = \sqrt{\boldsymbol{A}\cdot\boldsymbol{A}} = \sqrt{A_{ij}A_{ij}}$) and the operator "$\cdot$" denotes the inner product of the tensor.

J is expressed as follows:

$$J = \det\boldsymbol{F} = \frac{v}{v_0} \tag{5.4}$$

where v is the specific volume at the current and v_0 is at the reference state.

D is expressed as follows:

$$\mathrm{D} = (\tilde{\lambda} - \tilde{\kappa})/\mathrm{M}\mathrm{v}_0 \tag{5.5}$$

where $\tilde{\lambda}$ is compression index and $\tilde{\kappa}$ is the swelling index, noting that $(\tilde{\lambda} - \tilde{\kappa}) = (\mathrm{N} - \Gamma)/\ln 2$, and N and Γ are the material constants representing normal consolidation line (NCL) and critical state line (CSL) in $v - p'$ plane, respectively.

By alternatively substituting Eq. 5.1 into the modified Cam-clay yield surface, the superloading and subloading surfaces can be obtained as follows:

- superloading yield surface:

$$f(\bar{p}', \bar{\eta}^*) + \mathrm{MD}\ln R^* + \int_0^t J\mathrm{tr}\boldsymbol{D}^p d\tau = \mathrm{MD}\ln\frac{\bar{p}'}{\widetilde{p'}_0} + \mathrm{MD}\ln\frac{\mathrm{M}^2+\bar{\eta}^{*2}}{\mathrm{M}^2} + \int_0^t J\mathrm{tr}\boldsymbol{D}^p d\tau = 0 \tag{5.6}$$

- subloading yield surface:

$$f(p', \eta^*) + \mathrm{MD}\ln\frac{R^*}{R} + \int_0^t J\mathrm{tr}\boldsymbol{D}^p d\tau = \mathrm{MD}\ln\frac{p'}{\widetilde{p'}_0} + \mathrm{MD}\ln\frac{\mathrm{M}^2+\eta^{*2}}{\mathrm{M}^2} + \mathrm{MD}\ln\frac{R^*}{R} + \int_0^t J\mathrm{tr}\boldsymbol{D}^p d\tau = 0 \tag{5.7}$$

It is necessary to define the evolution rules associated with structure and overconsolidation to determine the magnitude of subsequent loading surfaces. The evolution rule of overconsolidation can be described by the following equation using the plastic stretching tensor $\boldsymbol{D}^p$:

$$\dot{R} = JU\|\boldsymbol{D}^p\| \tag{5.8}$$

U is defined following the dependency proposed by Hashiguchi (1989):

$$U = -\frac{m}{D}\ln R \tag{5.9}$$

where m is a positive material constant (degradation index of overconsolidation) that controls the rate of overconsolidation loss.

The evolution rule of structure can be expressed as follows (Asaoka et al., 1998; Asaoka et al., 2000; Asaoka et al., 2002):

$$\dot{R}^* = JU^*\left\{(1 - c_s)(-{D_v}^p) + c_s\sqrt{\frac{2}{3}}\|{\boldsymbol{D}_s}^p\|\right\} \tag{5.10}$$

where $D_v{}^p$ is plastic volumetric stretching and $\boldsymbol{D}_s{}^p$is deviation component of the plastic stretching tensor, $\boldsymbol{D}_s{}^p = \boldsymbol{D}^p - \frac{1}{3}(\mathrm{tr}\boldsymbol{D}^p)\boldsymbol{I}$. c_s is a material constant that represents the ratio of plastic shear deformation to plastic compression deformation ($0 \leq c_s \leq 1$). U^* is a positive scalar function of R^* and is defined as:

$$U^* = \frac{a}{D} R^{*b}(1 - R^*)^c \tag{5.11}$$

where *a*, *b*, and *c* are positive material constants (degradation indexes of structure) that control the rate of structure decay.

The following equations can describe the evolution rule of anisotropy (Hashiguchi and Chen, 1998):

$$\mathring{\boldsymbol{\beta}} = J \frac{b_r}{\mathrm{D}} \sqrt{\frac{2}{3}} \left\| \boldsymbol{D}_s^p \right\| \|\hat{\boldsymbol{\eta}}\| \boldsymbol{\eta}_b \tag{5.12}$$

where b_r is the material constant that controls the rate of the evolution of anisotropy (rotational hardening index), and $\boldsymbol{\eta}_b$ is expressed as:

$$\boldsymbol{\eta}_b = m_b \frac{\hat{\boldsymbol{\eta}}}{\|\hat{\boldsymbol{\eta}}\|} - \boldsymbol{\beta} \tag{5.13}$$

where m_b (≥ 0) is a material constant that represents the limitation of the evolution parameter of anisotropy. The sensitivity analysis of the evolution rule parameters is given in Appendix 2.

The following equation is essential to represent the relationship of CSL parameter M and the parameter M_a (the watershed of plastic compression and plastic expansion), where the anisotropy was considered (Fig. 5.1):

$$\mathrm{M}_a^2 \leq \mathrm{M}^2 + \zeta^2 \leq \mathrm{M}^2 + \frac{3}{2} m_b^2 \tag{5.14}$$

Additional information and the details of the SYS Cam-clay model formulation can be found in Asaoka et al., (1997); Asaoka et al., (1998); Asaoka et al., (2000); Asaoka et al., (2002); Asaoka, (2003) and for the essentials of the modified Cam-clay model, please refer to Muir Wood, (1990).

Put it simple, the 'structure' of clay is considered to be generated under long-term deposited process. As for sand, a very loose sand can be regarded as a highly structured soil. On the other hand, the 'overconsolidation' can be explained by comparing the current stress state with the most severe

loading state in the past. A very dense sand can be regarded as a heavily overconsolidated and less structured soil. The principal characteristic of the SYS Cam-clay model is that it is possible to explain the mechanical behavior of typical clays and sands and intermediate soils under a common theory of critical state soil mechanics.

5.2.1 Input parameters

In general, parameters utilized in the SYS Cam-clay model are divided into three groups. The first group are elasto-plastic parameters, that obtained from experimental results either from oedometer or isotropic compression test and drained or undrained triaxial tests in Table 5.1. Here, compression index $\bar{\lambda}$, swelling index $\bar{\kappa}$, and NCL index N were determined according to the performed isotropic compression experiments. The normal consolidation lines (NCL) of all specimens were parallel in isotropic compression test and NCL of fiber-reinforced sand lied lower and to the left compared to unreinforced sand. Behavior of unreinforced and fiber-reinforced sand in compression and swelling were similar, therefore, in both unreinforced and fiber-reinforced sand compression index $\bar{\lambda}$ and swelling index $\bar{\kappa}$ were set to be equal. Fiber inclusions increased the strength of sand by increasing residual stress ratios. Therefore, CSL parameter M is set to have an increasing tendency with the increase in fiber content additionally referring to Eq. 5.14 with consideration of the anisotropic parameters.

The second group includes the evolution rule parameters that were obtained according to the SYS Cam-clay formulation and through sensitivity analysis by "trial-and-error" method. In case of fiber-reinforced sand considering that it consisted of the same sand as unreinforced sand, initially we tried to use the same values of the evolution rule parameters. However, the typical shear behavior of fiber-reinforced sand exhibited a lower initial stiffness, higher peak, and post-peak stresses, and less volumetric expansion characteristics with an increase in the fiber content compared to unreinforced sand. Modifications to the evolution rule parameters of anisotropy were made based on the observed mechanical behavior. Further discussion with detailed explanation will be given in Chapter 6. Additional information on sensitivity analysis of each evolution rule parameters can be found in Appendix 2.

The third group consists of initial state values related to the initial state of samples and testing conditions (confining pressure, specific volume, degree of overconsolidation and structure, and initial anisotropy) in Table 5.2. According to the SYS Cam-clay model formulation, it is considered that

initially a looser sand has a higher degree of structure with less overconsolidation, while a denser sand has a higher degree of overconsolidation with less degree of structure. Initial degrees of overconsolidation $1/R$ and structure $1/R^*$ were calibrated and determined according to the initial relative density of sandy samples and the reproducibility of experimental results with particular attention to the volumetric change behavior.

Table 5.1 Elasto-plastic and evolution rule parameters of unreinforced and fiber-reinforced Toyoura sand

Material		Unreinforced sand	0.2% fiber-reinforced sand	0.4% fiber-reinforced sand
Elasto-plastic parameters				
Compression index	$\tilde{\lambda}$	0.075	0.075	0.075
Swelling index	$\tilde{\kappa}$	0.002	0.002	0.002
Critical state index	M	1.100	1.250	1.380
Normal consolidation line intercept (at p' = 98.1 kPa)	N	2.000	1.980	1.960
Poisson's ratio	υ	0.100	0.200	0.300
Evolution parameters				
Degradation index of overconsolidation	m	0.010	0.010	0.010
Degradation index of structure (b=c=1)	a	0.040	0.040	0.040
The ratio of plastic volume strain $-D_v^p$ to plastic deviatoric strain $\|\boldsymbol{D}_s^p\|$	c_s	1.000	1.000	1.000
Rotational hardening index	b_r	0.500	0.450	0.400
Limitation of rotational hardening	m_b	0.520	0.600	0.650

Table 5.2 Initial state values (CD test with different initial relative densities)

Fiber content	Confining pressure p'_0 (kPa)	Specific volume v_0	Reference relative density D_r	Degree of overconsolidation $1/R$	Degree of structure $1/R^*$	Degree of anisotropy ζ_0
0.0%	100	1.823	30	26.13	2.500	0.470
	100	1.771	60	46.47	2.400	0.470
	100	1.719	80	83.62	2.300	0.470
0.2%	100	1.829	30	17.19	2.500	0.420
	100	1.770	60	41.88	2.500	0.420
	100	1.713	80	78.55	2.300	0.420
0.4%	100	1.821	30	26.67	4.000	0.370
	100	1.772	60	52.40	3.700	0.370
	100	1.712	80	71.06	2.600	0.370

5.3 Simulation of drained compression behavior

5.3.1 Drained triaxial tests performed on specimens with different initial relative densities

Figs. 5.2-5.4 present the experimental and simulation results of isotropically consolidated drained triaxial compression experiments conducted on unreinforced, 0.2% and 0.4% fiber-reinforced sand under 100kPa confining pressure. The solid lines indicate experimental results, while dashed lines indicate simulated results in figures. The specimens were initially placed to meet the three different density conditions – loose (D_r=30%), medium dense (D_r=60%), and dense (D_r=80%). Initial state values for the simulation that determined according to the testing conditions and the SYS Cam-clay model formulation are summarized in Table 5.2. The results presented through the analysis of deviator stress q – axial strain ε_a, volumetric strain ε_v – axial strain ε_a, specific volume v – axial strain ε_a, and specific volume v – mean effective stress p' dependencies.

According to the critical state soil mechanics, sandy soils sheared under the same confining pressures with different initial relative densities initially experience different stress paths with different peak stress and finally reach the same critical state with the shear progression. Similar outcomes were obtained from the experiments for 0.2% and 0.4% fiber-reinforced sand as well as the unreinforced sand specimens observed in Figs. 5.2, 5.3, and 5.4 a, c, d (solid lines).

The mechanical behavior of the unreinforced sand was well–captured by the SYS Cam-clay model along the whole shearing process (dashed lines). Remarkably, the trend of simulated results, which means higher initial stiffness and peak stress with the increase in relative density and convergence of the deviator stress independently of the initial state at the end of shearing, was in good agreement with the experimental results. Furthermore, the volumetric change behavior of looser specimens with higher initial compression and less expansion with shear progression was well simulated by the model (Fig. 5.2b).

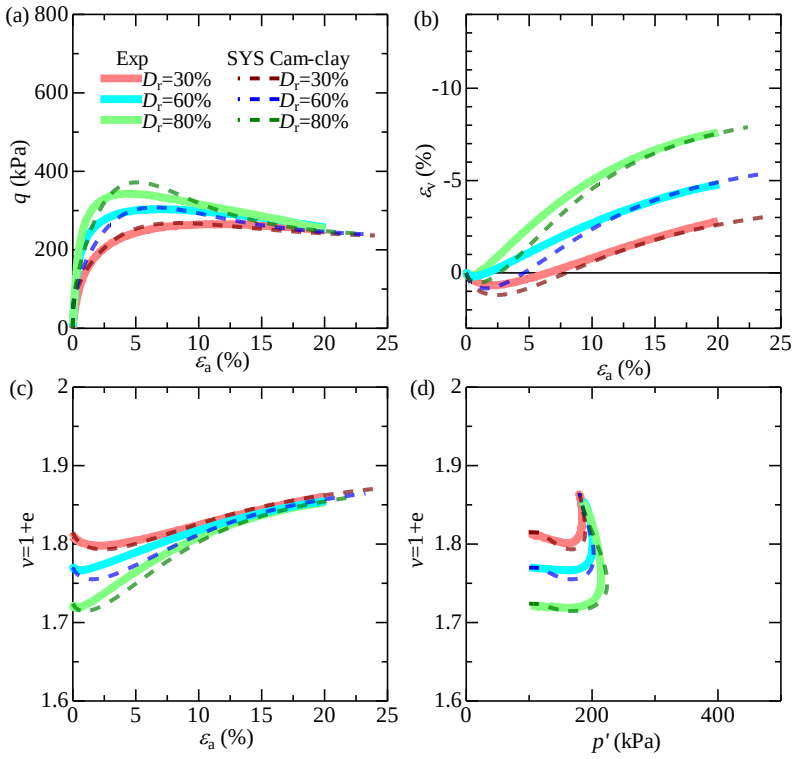

Fig. 5.2 Experimental results and model simulation for drained triaxial compression tests performed under 100kPa confining pressure on unreinforced sand with different initial relative densities

The SYS Cam-clay model accurately reproduced the experimental results with respect to the increase in initial stiffness, peak, and post-peak stresses with a relative density increase for 0.2% fiber-reinforced sand (Fig. 5.3a). Despite a slight difference in volumetric change, the trend of higher initial compression and less expansion at the end of the tests with relative density was well simulated (Fig. 5.3b). In the case of 0.4% fiber-reinforced sand, the peak stress reproduced by the model is slightly overestimated (Fig. 5.4a), especially for denser specimens, due to the higher value of the initial degree of structure ($1/R^*$) (Table 5.2) fixed to reproduce the volumetric change behavior. Following the peak, the characteristics were in good agreement, including post-peak and volumetric change behavior.

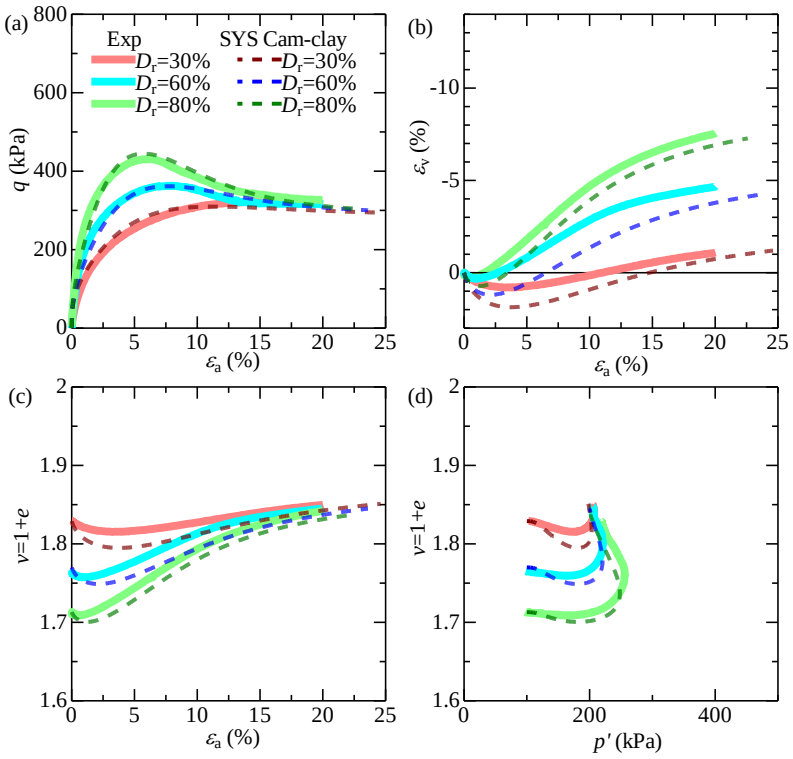

Fig. 5.3 Experimental results and model simulation for drained triaxial compression tests performed under 100kPa confining pressure on 0.2% fiber-reinforced sand with different initial relative densities

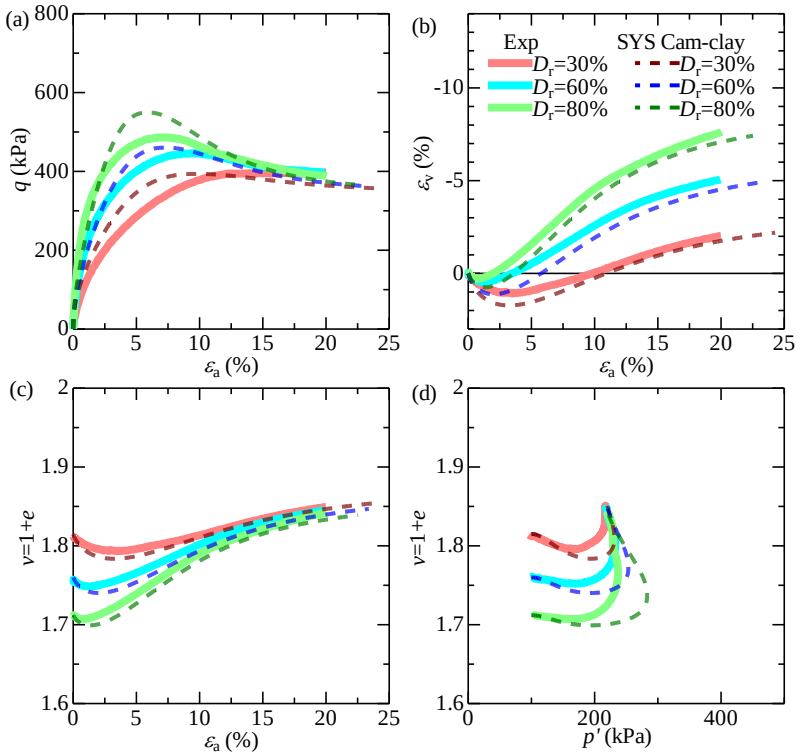

Fig. 5.4 Experimental results and model simulation for drained triaxial compression tests performed under 100kPa confining pressure on 0.4% fiber-reinforced sand with different initial relative densities

Initially, considering that fiber-reinforced specimens consisted of the same host soil as unreinforced sand, the same evolution rule parameters were utilized. However, the shear behavior of fiber-reinforced sand exhibited a lower initial stiffness, higher peak, and post-peak stresses, and less volumetric expansion with an increase in the fiber content compared to unreinforced sand. These characteristics indicated that the fiber inclusions decreased the initial anisotropy of fiber-unreinforced sand, that will be explained in detail in section 5.5. Therefore, the evolution rule parameters of anisotropy were modified based on the formulation of the SYS Cam-clay model and determined based on the sensitivity analysis (Appendix 2) to appropriately reproduce the shear behavior of fiber-reinforced sand. Poisson's ratio v and the initial anisotropy (expressed by the initial state value ζ_0) govern the initial stiffness characteristics, i.e., v increased and ζ_0 decreased with the increase in fiber content (Tables 5.1, 5.2). Peak and post-peak stresses are controlled by CSL parameter M and limitation of rotational hardening index m_b, where both M and m_b increased with the increase in fiber content.

Comparative analysis of experimental results and model simulation in terms of stress ratio (=q/p') against the axial strain and dilatancy response of both unreinforced and fiber-reinforced sand are given in Figs. 5.5 and 5.6, respectively. The features of sandy soils with different initial relative densities, experiencing different stress-strain-volumetric changes at smaller axial strains and converging at higher axial strains observed in fiber-reinforced sand, were reasonably reproduced by the model. As can be observed from Fig. 5.5, all stresses converged at the end of shearing and reached the respective stress ratios. Fiber-reinforced sand was less dilative compared to unreinforced sand, and the dilatancy ratio decreased with the increase in fiber content in Fig. 5.6. The deformation shapes of unreinforced and fiber-reinforced sand specimens were similar with bulking of the specimens in the central part as shown in section 4.4. Some local shear bands appeared in all specimens, and as a consequence, the volumetric strain did not reach a zero dilation. Therefore, the behavior of the specimens cannot be regarded as an element behavior even when the axial strain reached 20%. Overall, the tendency of decreased dilation in fiber-reinforced sand was accurately simulated.

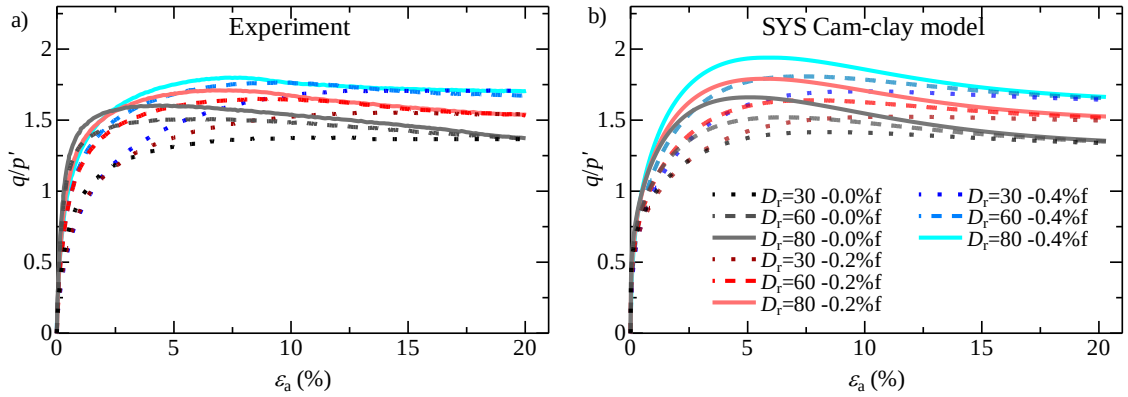

Fig. 5.5 Normalized deviatoric stress against the axial strain for specimens prepared with different relative densities

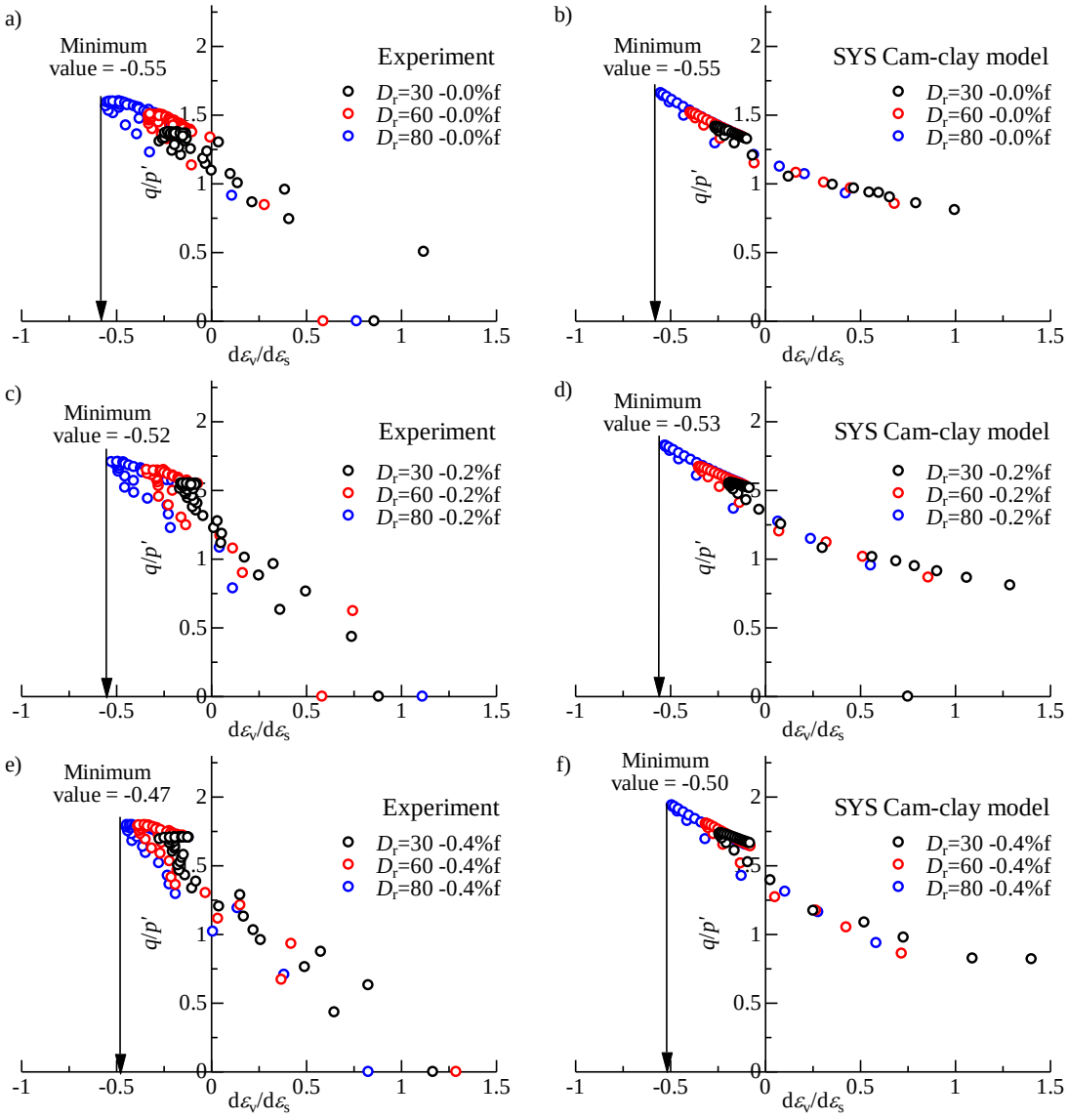

Fig. 5.6 Stress-dilatancy response for specimens prepared with different relative densities

5.3.2 Drained triaxial tests performed under different confining pressures

Experimental results of consolidated drained triaxial tests conducted under five different confining pressures on unreinforced, 0.2% and 0.4% fiber-reinforced sands, and the respective model responses are presented in Figs. 5.7-5.9. The material parameters (Table 5.1), including elasto-plastic and evolution rule parameters, are the same as those obtained from isotropic consolidation tests and drained triaxial tests with different initial relative densities (section 5.2.1). Initial state values, including testing conditions and specimen characteristics, are summarized in Table 5.3.

Table 5.3 Initial state values (CD tests under different confining pressures)

Fiber content	Confining pressure p'_0 (kPa)	Specific volume v_0	Reference relative density D_r	Degree of overconsolidation $1/R$	Degree of structure $1/R^*$	Degree of anisotropy ζ_0
0.0%	50	1.721	80	92.46	1.300	0.470
	100	1.719	80	83.62	2.300	0.470
	200	1.717	80	74.49	3.900	0.470
	400	1.712	80	58.79	5.700	0.470
	600	1.708	80	50.28	7.000	0.470
0.2%	50	1.715	80	81.28	1.200	0.420
	100	1.713	80	78.55	2.300	0.420
	200	1.709	80	72.56	4.100	0.420
	400	1.699	80	55.43	5.800	0.420
	600	1.695	80	44.38	6.400	0.420
0.4%	50	1.712	80	78.01	1.400	0.370
	100	1.712	80	71.06	2.600	0.370
	200	1.705	80	66.42	4.500	0.370
	400	1.698	80	55.78	7.000	0.370
	500	1.696	80	46.89	7.200	0.370

The mechanical behavior of unreinforced sand sheared under different confining pressures was accurately reproduced by the SYS Cam-clay model, capturing all elasto-plastic features along the whole shearing process in Fig. 5.7. Mainly, initial stiffness, peak, and post-peak stress values on the q–ε_a curve, volumetric change behavior in both ε_v–ε_a and v–p' curves were well simulated by the model. The CSL parameter M obtained from the previous case with different initial relative densities was validated with experimental results of shearing under different confining pressure. All five stress curves reached the same CSL within the considered axial strain range. The model response for the stress path in the q–p' curve upon reaching the same CSL was in satisfactory agreement.

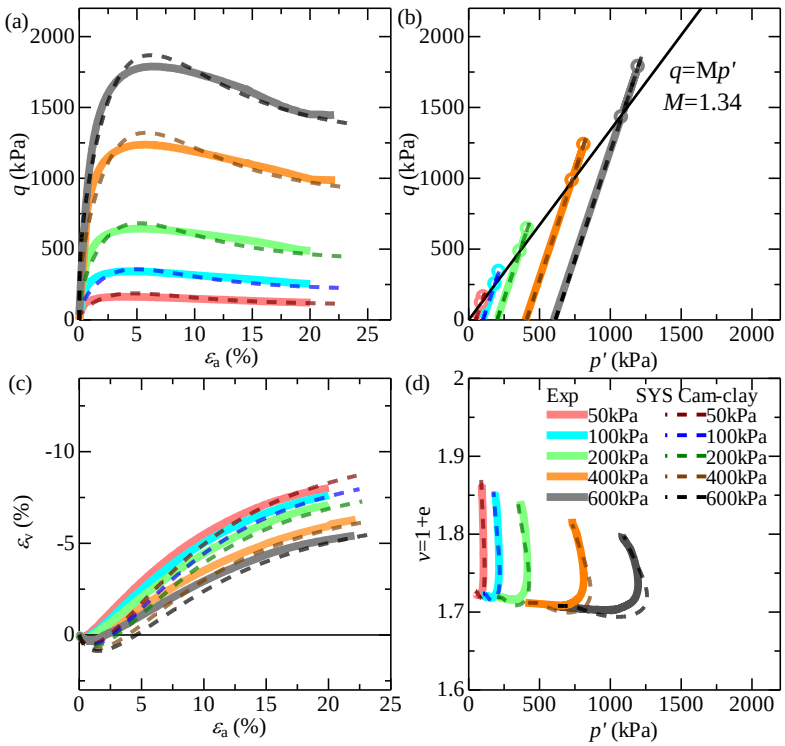

Fig. 5.7 Experimental results and model simulation for drained triaxial compression tests performed under different confining pressures on unreinforced sand with 80% initial relative density

In the case of cohesionless soils like sand, the relationship between CSL parameter M and internal friction angle ϕ' can be expressed by the following equation:

$$\sin\phi' = \frac{3\mathrm{M}}{6+\mathrm{M}} \tag{5.15}$$

The fiber-reinforced sands can be regarded as cohesionless soils, and therefore, including the fibers in sand increases internal friction angle based on experimental and simulated results.

Negligible difference can be noticed in the volumetric change response of the model on the ε_v–ε_a curve during the initial shearing stage with higher compression. This difference represents the limit of the reproduction performance of the SYS Cam-Clay model and the influence of the anisotropy related to the sample preparation method.

The effect of fibers in reinforced specimens was in a higher peak and post-peak stress (higher CSL) for all considered confining pressure values as shown in Figs. 5.8 and 5.9. Each unreinforced sandy soil, 0.2% and 0.4% fiber-reinforced sand reached the respective CSL within 20% axial strain,

i.e., the residual stress ratio was the same despite the different stress paths. This tendency can be clearly observed in Fig. 5.10, where normalized deviator stress was plotted against the axial strain. In general, the SYS Cam-clay model could reproduce and fit the experimental results for all considered series with different confining pressures. It is worth noting that the model utilized an equal number of parameters to reproduce the mechanical behavior of fiber-reinforced sand as for unreinforced sand. The model response's limitation was in slightly overestimating the peak stress and volumetric change at the phase transformation point.

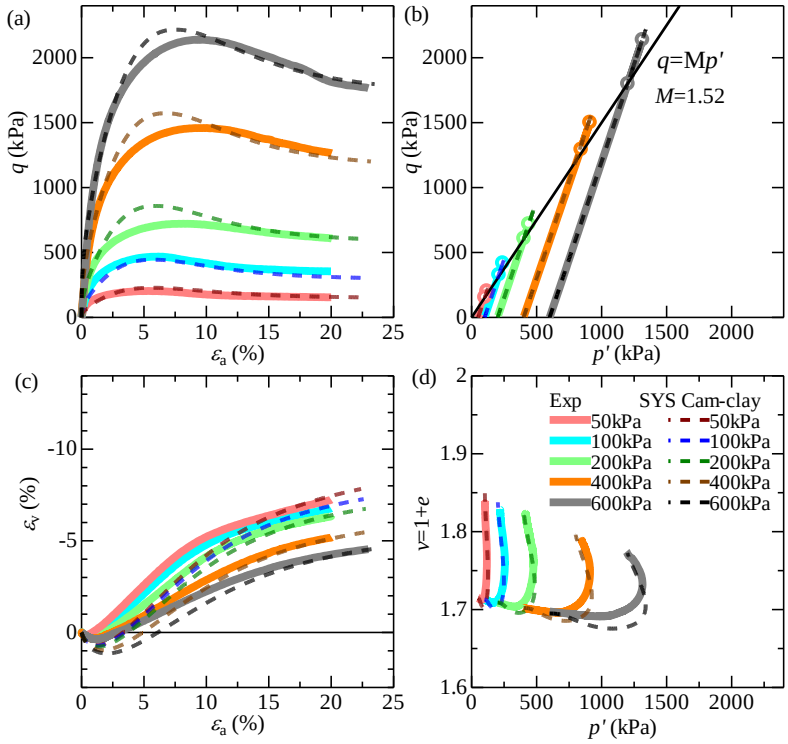

Fig. 5.8 Experimental results and model simulation for drained triaxial compression tests performed under different confining pressures on 0.2% fiber-reinforced sand with 80% initial relative density

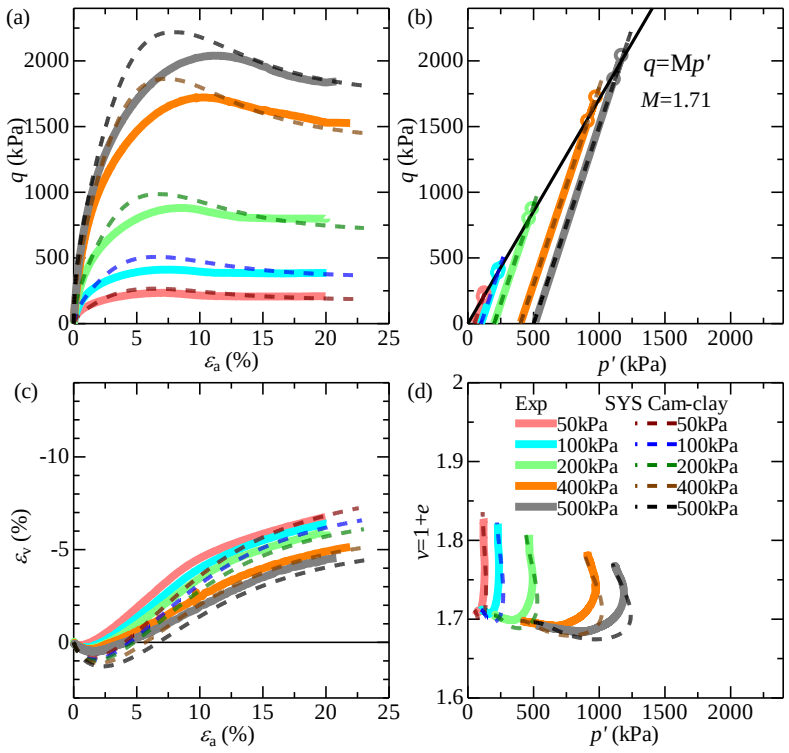

Fig. 5.9 Experimental results and model simulation for drained triaxial compression tests performed under different confining pressures on 0.4% fiber-reinforced sand with 80% initial relative density

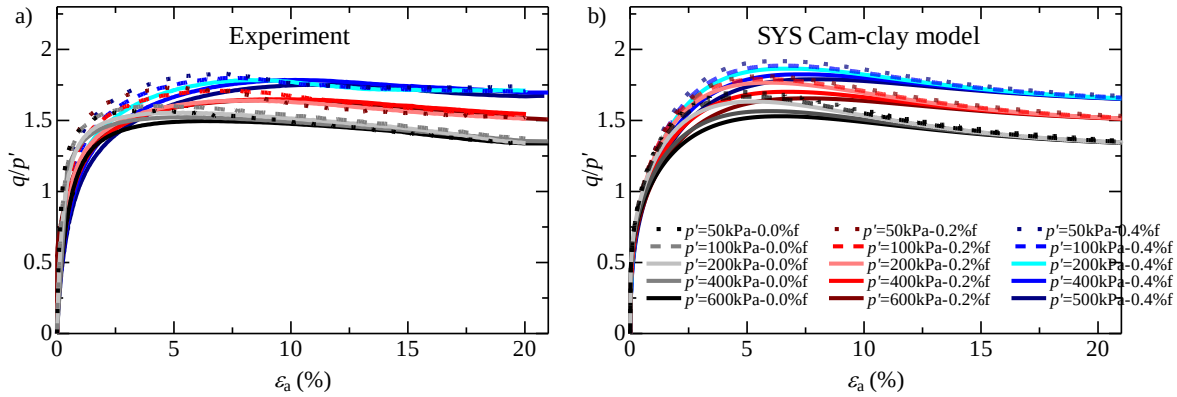

Fig. 5.10 Normalized deviatoric stress against the axial strain for specimens sheared under different confining pressures

Fig. 5.11 shows the experimental and simulatied results of dilatancy behavior of both unreinforced and fiber-reinforced sand. As can be observed from the Fig. 5.11, unreinforced soil showed more dilative behavior compared with fiber-reinforced sand, and the dilatancy ratio increased

with lower confining pressure. A similar tendency was observed in fiber-reinforced sand for confining pressure variations. The SYS Cam-clay model captured relatively well the dilatancy behavior of both unreinforced and fiber-reinforced sand with a decreased dilatancy tendency accompanying an increase in confining pressure.

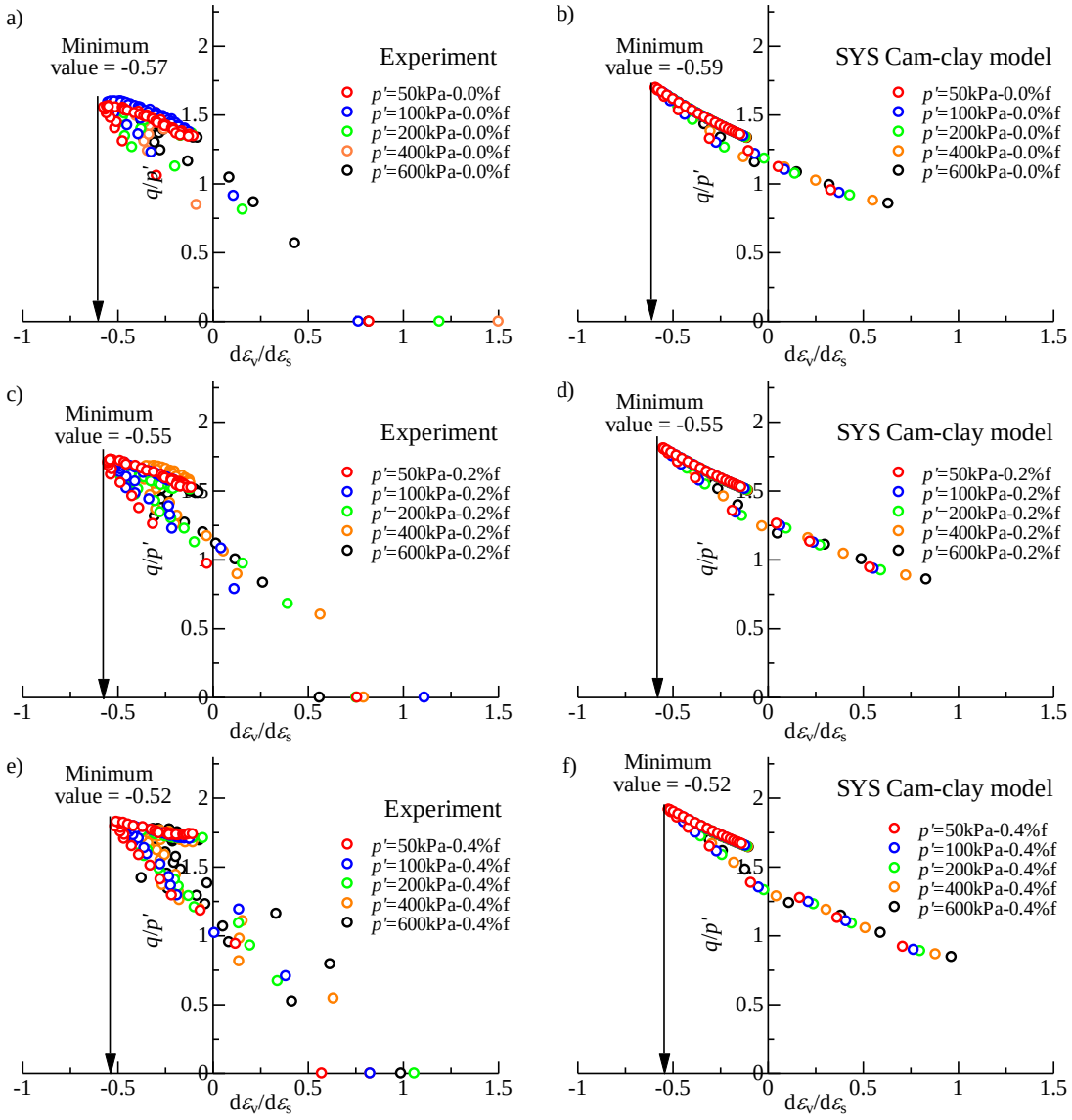

Fig. 5.11 Stress-dilatancy response for specimens sheared under different confining pressures

It should be noted that the initial stiffness decreased with the increase in fiber content, i.e., the higher the fiber content – the smaller the initial stiffness. Such a decrease was associated with the reinforcing material's nature, where the reinforced soils experienced a reduction in the initial stiffness

in some cases (Michalowski and Ĉermak, 2003; Heineck et al., 2005). Also, the reason for decreased initial stiffness was concluded as an interaction mechanism between soil particles and fibers, where higher strain rate is necessary to reveal the positive contribution of fibers to reinforce the soils (Li et al., 2017; Li and Senetakis, 2017; Li et al., 2019). Another reason includes the impact of fibers on the compaction of sample and, consequently, the anisotropic characteristics of sandy soils. The Chapter 6 will discuss the effect of sample preparation and the inclusion of fibers as a reinforcing material on the anisotropic behavior of sand.

5.4 Simulation of undrained compression behavior

Simulation results of consolidated undrained triaxial tests conducted under three different confining pressures on unreinforced, 0.2% and 0.4% fiber-reinforced sands are presented in Figs. 5.12-5.14. The material parameters (Table 5.1), including elasto-plastic and evolution rule parameters, are the same as those obtained from isotropic consolidation tests and drained triaxial tests with different initial relative densities (section 5.2.1) and used for the simulation of drained response of both unreinforced and fiber-reinforced sand. Initial state values, including testing conditions and specimen characteristics, are summarized in Table 5.4. Some of the initial state values (initial degree of overconsolidation and structure) used to reproduce the mechanical behavior of undrained traixial compression test differed from the initial state value in drained condition. As the reproducibility of experimental results are in high priority, small corrections to the initial state values of overconsolidation and structure have been implemented through the trial-and-error method to get closer fitting of the results. In fact, the modification was done following the formulation of SYS Cam-clay model.

Table 5.4 Initial state values (CU tests under different confining pressures)

Fiber content	Confining pressure p'_0 (kPa)	Specific volume v_0	Reference relative density D_r	Degree of overconsolidation $1/R$	Degree of structure $1/R^*$	Degree of anisotopy ζ_0
0.0%	50	1.845	40	169.2	9.700	0.470
	100	1.844	40	85.57	10.00	0.470
	200	1.840	40	46.18	11.00	0.470
	100	1.763	60	198.1	9.500	0.470
0.2%	50	1.837	40	152.1	11.00	0.420
	100	1.827	40	85.98	12.00	0.420
	200	1.827	40	42.18	12.00	0.420
0.4%	50	1.838	40	185.2	15.00	0.370
	100	1.835	40	81.38	14.00	0.370
	200	1.826	40	50.39	16.50	0.370

The initial relative density was chosen so that the investigation of undrained behavior of both unreinforced and fiber-reinforced sand was possible at higher axial strains (approximately ε_a=20%) without cavitation regarding the PWP generation, as it was mentioned in previous Chapter. The triaxial cell limitation is 700kPa, for this reason the maximum of 500kPa back pressure can be applied when the confining pressure equals to 200kPa. Practical illustration of the case of cavitation is given in Fig. 5.12 as an example of experimental and SYS Cam-clay model simulation of an undrained response of unreinforced medium dense specimen prepared with approximately 60% initial relative density and sheared under 100kPa confining pressure. The rest of simulation results on medium loose unreinforced specimens sheared under 50kPa, 100kPa and 200kPa confining pressures is also presented in Fig. 5.12. The simulation results for the unreinforced sand are in a quite good agreement with experimental data. Especially for the denser specimen the SYS Cam-clay model was able to fully capture the mechanical behavior including stress-strain, effective stress path and PWP generation. For the looser specimens with 40% initial relative density the undrained behavior showed a higher decrease of mean effective stress (strain-softening) and the intensity of the deviatoric stress at lower axial strain was low and the increase of the deviatoric stress occurred in convex trajectory. Even the SYS Cam-clay model was able to capture the tendency of the initial drop of the effective stress path and to describe the strain-softening behavior through the whole shearing process, however, a small difference between experimental and model response during small strains was observed. Particularly, the difference is in the initial deviatoric stress and excess PWP generation curve. Overall, for a considered range of confining pressures and different initial relative densities the SYS Cam-clay model fairly reproduced the experimental results and captured all the tendencies.

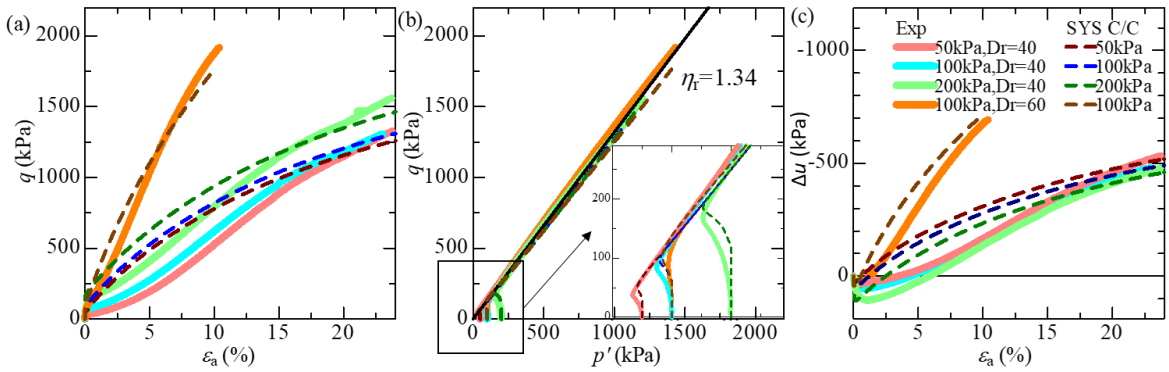

Fig. 5.12 Experimental results and model simulation for undrained triaxial compression tests performed under different confining pressures on unreinforced sand with 40% and 60% initial relative density

Figs. 5.13 and 5.14 reports the model response for the reinforced sand specimens with 0.2% and 0.4% fiber contents, respectively. The overall tendency for the mechanical behavior of 0.2% and 0.4% fiber-reinforced sand in undrained compression was fairly reproduced by the considered model. It should be noted that the intermediate behavior with initial stiffness decrease in sand due to the increase in fiber content was not captured by the model. As it was observed in experimental work, inclusions of fibers reduce the initial stiffness of sand and fiber-reinforced specimens experience a higher drop of effective stress path with more pronounced strain-softening behavior. For this purpose, the evolution rule of anisotropy and initial values of anisotropy were determined to make the description of initial stiffness decrease possible. The value initial degree of anisotropy was set to have a decreasing tendency with the increase in fiber content (Table 5.4). However, despite considering all possible variations of the evolution rule parameters and initial state values including initial degree of anisotropy, the considered model at the current stage is not capable to capture the high intermediate reduction of the initial stiffness in reinforced sands as an influence of the fiber inclusions on a medium loose relative density condition in undrained triaxial compression. Further elaborations and modifications in the model are needed to improve the reproduction of a small strain behavior of a loose fiber-reinforced sand specimens.

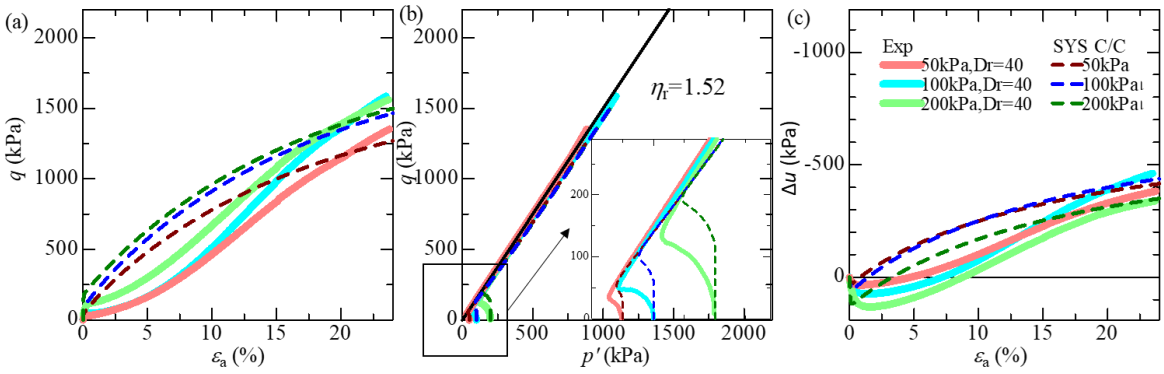

Fig. 5.13 Experimental results and model simulation for undrained triaxial compression tests performed under different confining pressures on 0.2% fiber-reinforced sand with 40% initial relative density

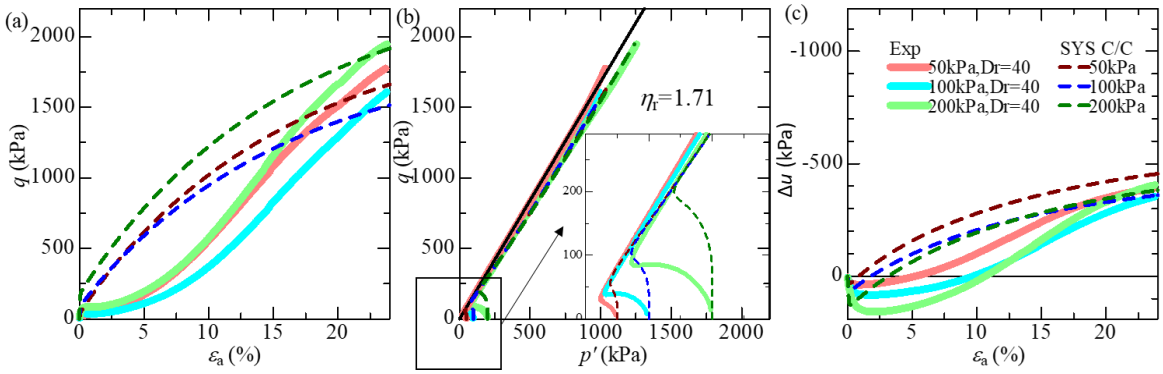

Fig. 5.14 Experimental results and model simulation for undrained triaxial compression tests performed under different confining pressures on 0.4% fiber-reinforced sand with 40% initial relative density

5.5 Importance of consideration of anisotropy in simulation of the mechanical behavior of unreinforced and fiber-reinforced sand

In order to show the importance of consideration of the effect of anisotropy in the considered constitutive model, Figs. 5.15 and 5.16 show the comparison of drained and undrained shearing response of unreinforced sand simulated by the SYS Cam-clay model with and without applying the anisotropy. As can be observed in Fig. 5.15a, effect of the initial anisotropy ζ_0 is concluded in the influence on the initial stage of shearing with higher initial stiffness and lower volumetric compression, i.e. the higher the value of the initial anisotropy – the higher initial stiffness close to the experimental results. In order to describe the subsequent characteristics of fiber-reinforced soil, the effect of evolution rule parameters of anisotropy b_r and m_b should be additionally considered as shown in Fig. 5.15. When the evolution rule parameters b_r and m_b were considered, the impact of initial anisotropy ζ_0 was concluded in the influence on the initial stage. That is, the higher the value of the initial anisotropy the higher initial stiffness (a comparison of a black and red dashed lines), which was close to the experimental results. In the case of a total exclusion of the consideration of anisotropic parameters (b_r=0, m_b=0), the mechanical behavior was reflected in a difference of the initial stage and affected the final state with smaller post-peak stress and less volumetric expansion (a blue dashed line). Evolution rule parameter b_r governs a development/diminishing of anisotropy in soils, and a smaller value of b_r means a slower evolution of anisotropy. In Fig. 5.15b, a smaller value of b_r brought a higher initial compression and less subsequent volumetric expansion at higher strains.

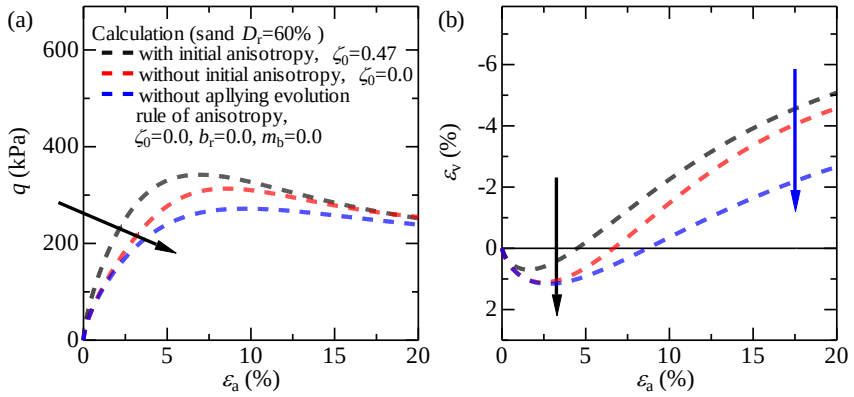

Fig. 5.15 Effect of initial anisotropy and evolution rule of anisotropy on the drained shearing behavior of sand by the SYS Cam-clay model (example of D_r=60%, p'_0=100kPa)

In case of undrained shearing behavior, the effect of initial anisotropy and the parameters of the evolution rule of anisotropy on the model response was obvious. At first, exception of the initial degree of anisotropy (red dashed line) might seem that stress-strain-PWP response does not affected. However, on the stress path curve it is clear that the exclusion of the initial anisotropy ζ_0 (i.e. ζ_0=0) led to larger difference between effective stress path from experimental and model results at the initial stages. Also, the calculated specimen without initial anisotropy reached a smaller CSL. Moreover, a totally exclusion of the evolution rule parameters of anisotropy and initial degree of anisotropy affected the model response for all dependencies, i.e. a lower deviatoric stress value, a higher drop in effective stress path with further difference in CSL, and smaller value of the generated negative PWP.

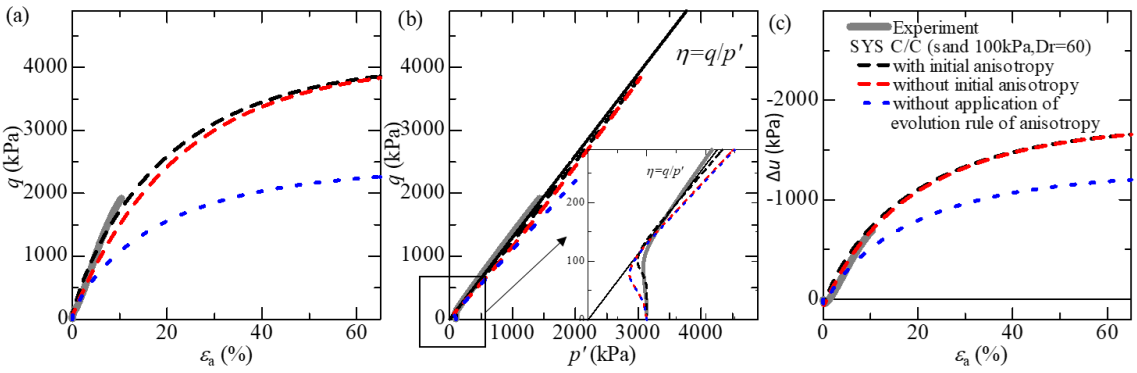

Fig. 5.16 Effect of initial anisotropy and evolution rule of anisotropy on the undrained shearing behavior of sand by the SYS Cam-clay model (example of D_r=60%, p'_0=100kPa)

5.6 Brief summary

The SYS Cam-clay model simulated the drained and undrained triaxial compression tests performed on both unreinforced and fiber-reinforced sand with different initial relative densities under various confining pressures. Based on the experimental and reproduced results, along with discussion of the elasto-plastic constitutive model response for predicting mechanical behavior of unreinforced sand and sand reinforced with fibers, the followings are the main conclusions:

- The simulation results of drained triaxial compression tests with different initial relative densities sheared under the unique confining pressure were in good agreement with experimental results. As with experimental results, the simulated results showed that despite initially experiencing different stress paths and volumetric change behavior attributed to different initial relative densities, all post-peak stresses and specific volumes of fiber-reinforced sand converged to the respective values with the shear progression as well as in unreinforced sand.
- Using elasto-plastic parameters obtained from isotropic consolidation and drained triaxial compression with different initial relative densities, the SYS Cam-clay model reproduced the drained triaxial compression test results under five different confining pressures. In general, the mechanical behavior of both unreinforced and fiber-reinforced sands was well-reproduced by the model. However, a slight overestimation of the peak stress for the fiber-reinforced sand due to the nature of reinforcing material and the anisotropic behavior of reinforced sand was observed. Both experimental and simulated results for the fiber-reinforced sand showed that each specimen reached the same respective CSL for definite fiber content despite shearing under five different confining pressures. The inclusion of fibers in sand increased internal friction angle ϕ' based on the relationship between M and $\phi'$for cohesionless soil.
- Undrained behavior of unreinforced and fiber-reinforced sand was also reproduced by using the material and evolution rule parameters obtained from simulation results under drained condition. The tendency for the shearing behavior of both unreinforced and fiber-reinforced sand in undrained triaxial compression was well captured by the model. Some limitations of the considered model were observed in the response to the intermediate undrained shearing behavior of medium loose specimens, where the experimental results showed a “convex” type change of devitoric stress and smaller initial stiffness compared to the model simulation.

Overall, the SYS Cam-clay model was able to reproduce and predict the trend of stress-strain-volumetric change behavior of the fiber-reinforced and unreinforced sand in drained and undrained

compression under various initial conditions. From the existing data and obtained parameters, the mechanical behavior of fiber-reinforced sand can be predicted for a wide range of initial conditions, including relative density and confining pressure.

CHAPTER 6

ANISOTROPY IN SANDS AND THE EFFECT OF FIBERS ON THE DEGREE OF ANISOTROPY

6.1 Introduction

It is well-known that unreinforced sand has initial anisotropy due to the sample preparation (Oda, 1972). According to the previous studies (Miura and Toki, 1982; Wood et al., 2008), unreinforced sand specimens experienced different mechanical behaviors associated with the difference in sample preparation methods. For example, different placement methods of sandy soils (tamping/vibration in dry/moist conditions) produced different anisotropic behavior. The effect of anisotropy was mainly reflected in different initial stiffness characteristics and volumetric change behavior in drained triaxial compression tests and the difference in stress paths in undrained triaxial compression and extension experiments. Accordingly, additional experimentations were performed to make a comparison of the shear behavior between unreinforced sand specimen of high initial anisotropy and the specimen that has less initial anisotropy. Also, the effect of the particles' shape of the host soil and the type of fibers with varying the aspect ratios on the initial and the subsequent mechanical behavior of sand in term of the anisotropy were discussed.

6.2 Effect of fibers on the anisotropic behavior of sands (general observation)

At first, before going to the detailed explanation of the anisotropic behavior of unreinforced sand and the effect of fibers on the initial anisotropy of reinforced sand, the comparison of a typical mechanical behavior of unreinforced and fiber-reinforced sand in drained triaxial compression and undrained triaxial compression/extension tests are given. The drained compression behavior of unreinforced, 0.2% and 0.4% fiber-reinforced sand prepared with 60% initial relative density and sheared under 100kPa confining pressure is given in Fig. 6.1, using experimental data from Figs. 4.5-4.7. The shear behavior of fiber-reinforced sand featured the increase in the strength of sandy soil by increasing the peak and post-peak stresses. Consequently, the residual stress ratio or CSL parameter M was higher for samples with a higher percentage of fiber inclusions. Additionally, fiber-reinforced sand initially showed higher compression and less volumetric expansion at the end of the test, i.e., fiber-reinforced sand was less dilative. Another point should be noted, that an increase in fiber content led to decreased initial stiffness ($q - \varepsilon_a$ curve). Similar outcomes of initial stiffness reduction were

obtained in previous studies performed to investigate the anisotropic behavior of fiber-reinforced sand and its effect on the mechanical behavior of reinforced sand (Michalowski and Ĉermak, 2002; Mandolini et al., 2019).

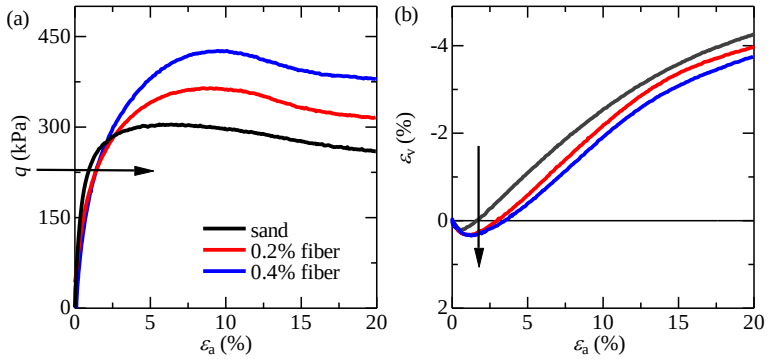

Fig. 6.1 Experimental results of drained triaxial compression tests performed under 100kPa confining pressure on unreinforced, 0.2% and 0.4% fiber-reinforced sand with 60% initial relative density

The undrained triaxial compression and extension behavior of unreinforced and 0.2%, 0.4% fiber-reinforced specimens prepared with 40% initial relative densities and sheared under 200kPa confining pressure is given in Fig. 6.2, using experimental data from Figs. 4.29-4.34. The effectiveness of fibers on the higher shear strength was shown previously, and here the scale of the graph was set to have an enlarged image of the initial state shearing characteristics. In compression, deviatoric stress – axial strain response is similarly to the drained case, where an increase in fiber content led to smaller initial stiffness. Furthermore, PWP generation during the compression is identical with the volumetric change behavior in drained compression, i.e. fiber-reinforced sand initially experienced a higher positive PWP generation and turned to negative PWP at higher axial strains, and eventually reached to a smaller value of negative PWP. From this observation it was concluded that fibers act as a contacting agent and prevent expansion of specimens. On the effective stress path fiber-reinforced specimens showed a higher drop of mean effective stress with more pronounced strain-softening behavior in compression. In contrast, in triaxial extension side the fiber-reinforced specimen showed less decrease in mean effective stress. From this observation on the difference of the effective stress paths it can be concluded that the fiber-reinforced specimens had a smaller degree of initial anisotropy compared to unreinforced sand. In order to closer investigate and prove this assumption the following

section describes the effect of sample preparation on the anisotropic behavior of sand and the effect of initial anisotropy on the shearing properties.

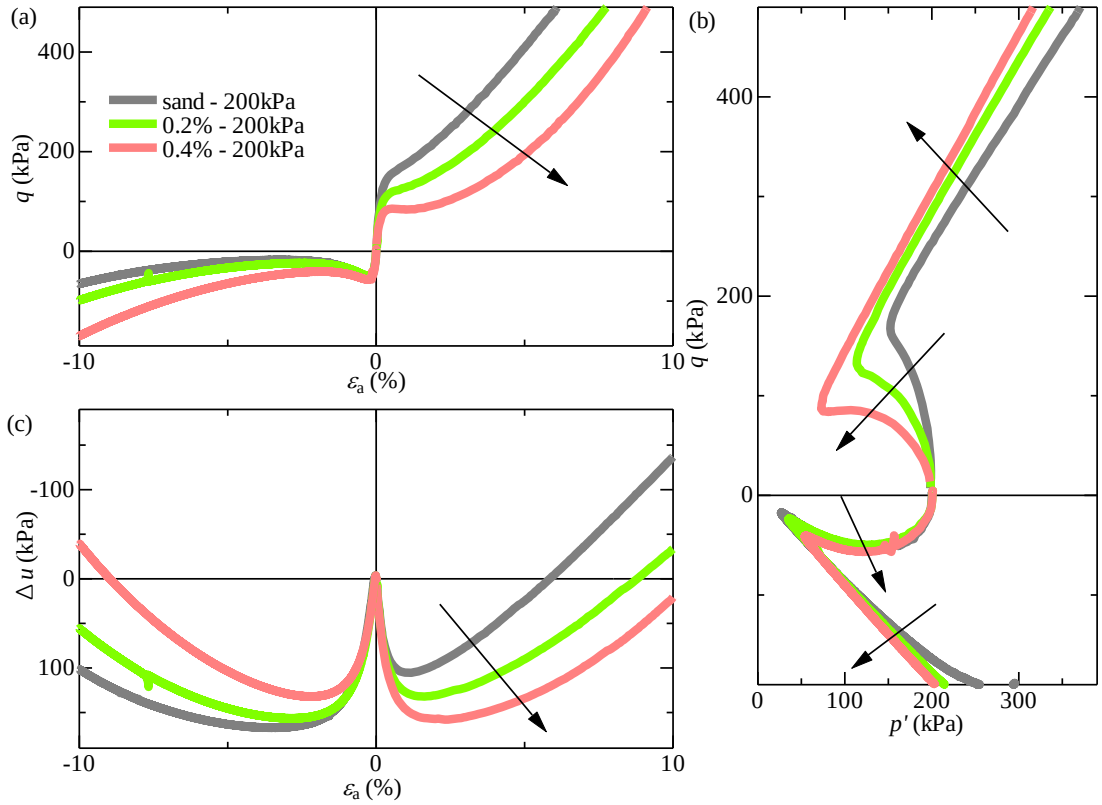

Fig. 6.2 Experimental results of undrained triaxial compression and extension tests performed under 200kPa confining pressure on unreinforced, 0.2% and 0.4% fiber-reinforced sand with 40% initial relative density

6.3 Effect of sample preparation on the anisotropic behavior of unreinforced sand

An initial anisotropy of unreinforced sand was considered to explain the mechanism of the observed behavior in Figs. 6.1 and 6.2 for fiber-reinforced sand. Fig. 6.3 represents the comparison of drained triaxial compression behavior of sand prepared by two different methods. The sample preparation #1, the same as for the rest experimentations in this study, was conducted by dry deposition through vibration. The specimens prepared by this method possibly has a higher initial anisotropy as was shown by Miura and Toki, (1982), due to more horizontally preferred orientation of sand particles. In contrast, the sample preparation #2 that included an extra step of stirring of sand particles with a "stick" during placement, imitating a similar sample preparation method of "mixed

dry deposition" as in Wood et al., (2008), possibly produced less preferred orientation of sand particles, i.e., the sample was less anisotropic. The sample that was initially stirred during the placement procedures exhibited a smaller value of initial stiffness (Fig. 6.3a) and a higher initial volumetric compression (Fig. 6.3b).

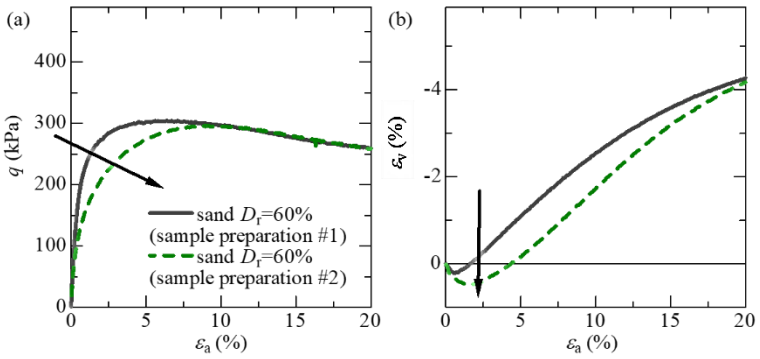

Fig. 6.3 Experimental results on the effect of sample preparation on the anisotropic behavior of sand with 60% initial relative density in drained triaxial compression

From comparison of Figs. 6.1 and 6.2, it is obvious that the shearing behavior of unreinforced sand with stirring (sample preparation #2) was similar to that of fiber-reinforced sand specimens. The fiber-reinforced sand specimens exhibited a lower initial stiffness and a higher initial volumetric compression than the unreinforced sand in Fig. 6.1, which was similar to the behavior of the unreinforced sand specimen prepared with and without initial stirring in Fig. 6.3. Therefore, it was implied that the fiber inclusions decreased the initial anisotropy of fiber-unreinforced sand. As the shear progressed, the subsequent behavior of unreinforced specimens prepared by two different methods became similar (Fig. 6.3), and stress-strain–volumetric responses converged at the end of shearing. However, the subsequent behavior of unreinforced and fiber-reinforced sand did not converge due to contractive contribution of fibers that possibly increase the confining pressure by producing tensile forces (Fig. 6.1).

Additionally, the effect of sample preparation on the anisotropic behavior was also proved in undrained shearing, where the similar sample preparation methods has been followed. Fig. 6.4 shows the results of undrained triaxial compression and extension where the samples were prepared by both methods #1 and #2. As can be seen from Fig. 6.4, when the compression tests compared to extension experiments on the unreinforced sample prepared by the method #1 (gray line), the obvious difference in stress paths appeared. This means that the specimen had a high initial anisotropy. On the other

hand, the specimens prepared with the initial stirring following the sample preparation method #2, the stress paths were approximately the same despite being either compressed or extended. This means that the specimens were less anisotropic. The comparison of Figs. 6.2 and 6.4 shows that the fiber-reinforced sand specimens prepared by dry vibration (sample preparation #1) has an identical effective stress paths in compression and extenstion to the unreinforced specimen preparation by additional stirring (sample preparation #2). Based on the observed mechanical behavior of unreinforced sand prepared by two different methods, the mechanism of fiber-reinforcement (where a lower initial stiffness and higher initial volumetric compression in drained shearing, a higher drop of the effective stress paths in undrained compression (more obvious strain-softening) and higher initial positive PWP, identical effective stress paths in compression and extension was observed) can be assumed to be caused by the influence of fibers on the less preferred orientation of sand particles, which led to less anisotropic behavior as in case of specimen prepared by method #2.

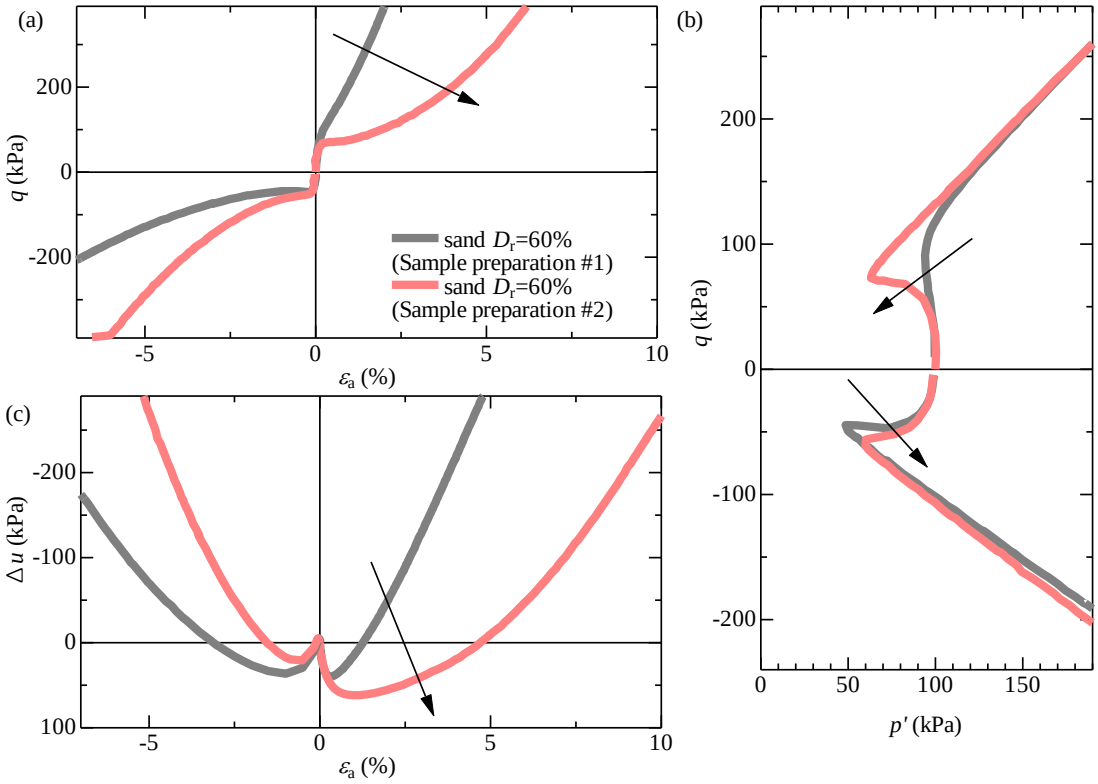

Fig. 6.4 Experimental results on the effect of sample preparation on the anisotropic behavior of sand with 60% initial relative density in undrained triaxial compression and extension

The schematic illustration of the orientation of sand particles and its effect on anisotropic behavior of unreinforced and fiber-reinforced sand is shown in Fig. 6.5. The sample preparation #1 possibly has a higher initial anisotropy as was shown by Miura and Toki, (1982) and the sand particles have more preferred horizontal orientation (Fig. 6.5a). Stirring offers the possibility of less preferred orientation of sand particles, i.e., the sample is less anisotropic (Fig. 6.5b). Similarly, when the fibers are added to sand, the fibers affect the compaction of sand particles. The sand particles in fiber-reinforced sand are assumed to have less preferred orientation and the fiber-reinforced specimen has a lower initial anisotropy.

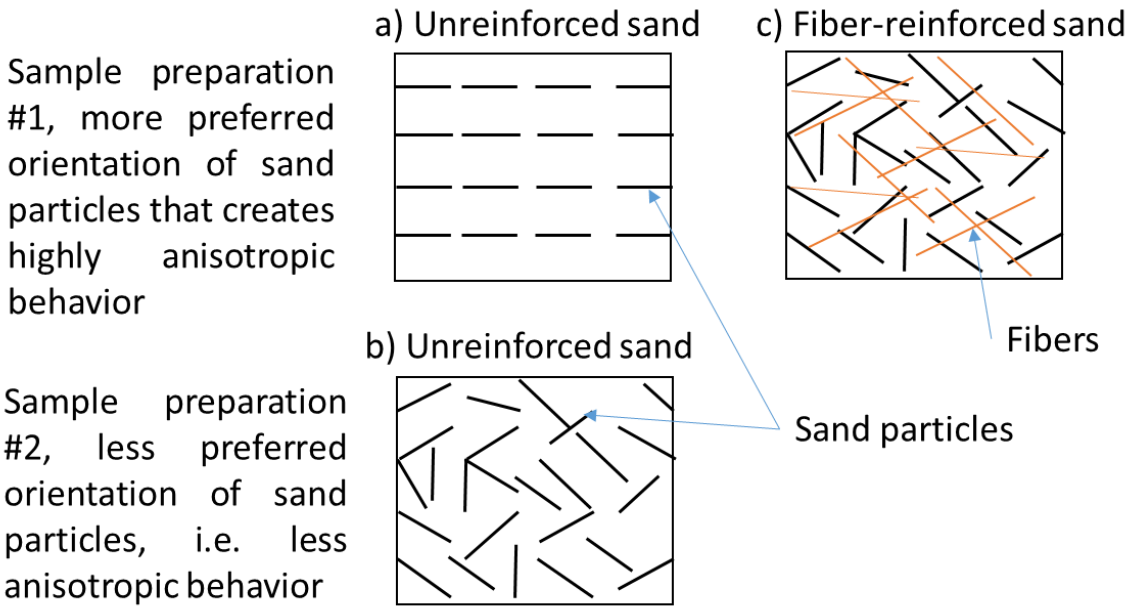

Fig. 6.5 Schematic illustration of the sand particles' orientation due to the sample preparation method

A similar tendency for shearing behavior was obtained from the SYS Cam-clay model calculations performed on unreinforced, 0.2% and 0.4% fiber-reinforced sands as shown in Fig. 6.6. The elasto-plastic parameters were fixed to simulate the initial and final states' tendency simultaneously. The fibers brought a lower initial stiffness and a higher initial volumetric compression, whereas a composite material experienced a higher peak and post-peak stresses, i.e., higher CSL parameter M. The value of initial anisotropy ζ_0, which is the norm of the axis of the rotation tensor used in describing the anisotropy, affects and respondent for the decreased initial stiffness with the increase in fiber content. The SYS Cam-clay model fully reproduced the tendency

of the mechanical behavior of unreinforced sand as well as fiber-reinforced sand by considering the effect of anisotropy on the initial states and CSL parameters for peak and post-peak states. Moreover, a higher peak and post-peak stresses in fiber-reinforced sands cannot be attributed to the effect of anisotropy, but to the effect of fiber inclusion itself that increased internal friction angle ϕ' of composite material (section 4.2).

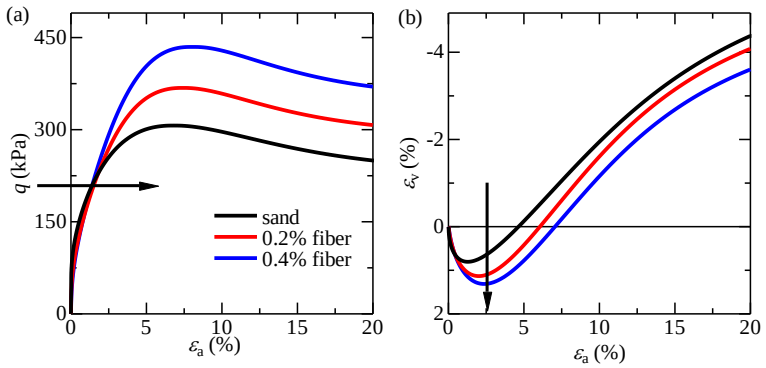

Fig. 6.6 Calculation results of the experimental results shown in Fig. 6.1 by the SYS Cam-clay model

6.4 Effect of the shape of host soil and type of fibers on the anisotropic behavior of fiber-reinforced sand

Toyoura sand was supposed to be a highly anisotropic depending on the sample preparation methods. More or less preferred orientation of sand particles were conditioned with prolonged sub-angular and angular shaped particles. In order to examine the effect of shape of the host soil with more rounded particles and possibly prevent a more preferred orientation of sand particles, Mikawa sand #6 with rounded shape (Fig. 3.4 b) was used.

Firstly, before considering the effect of the shape of sand particles and sample preparation method on anisotropy, a comparison of the shearing behavior of Toyoura sand, Mikawa sand #6 normal (Mikawa N) and Mikawa sand #6 rounded (Mikawa R) has been performed. Figs. 6.7 and 6.8 present experimental results from drained and undrained triaxial compression tests performed on three different sands prepared by side tapping/vibration (sample preparation #1). Despite having a different grain size distribution and physical properties, the results of the stress-strain-volumetric response in drained condition and effective stress path with PWP generation in undrained condition was quite similar in all three sands. Based on this observation, further experimentations were performed on

Mikawa N and Mikawa R with two different sample preparation methods in undrained condition (Fig. 6.9). As can be seen in Fig. 6.9, different sample preparation methods influenced both soils shearing behavior, despite Mikawa R sand was sand with more spherical particles' shape. Both types of Mikawa sand experienced different mechanical behavior with more pronounced softening behavior of initial stiffness decrease and higher decrease of effective stress path for a sample preparation with additional stirring (sample preparation #2) same as an undrained compression behavior of Toyoura sand. However, it should be noted that the difference in shearing response of more spherical Mikawa R sand (initial stiffness reduction and more obvious softening in effective stress path) was less influenced by the sample preparation method. The initial degree of anisotropy of Mikawa R sand is assumed to be less affected due to the less preferred orientation of sand particles with more rounded/spherical shapes. Similar conclusion was presented in previous studies on glass beads (Miura and Toki, 1982).

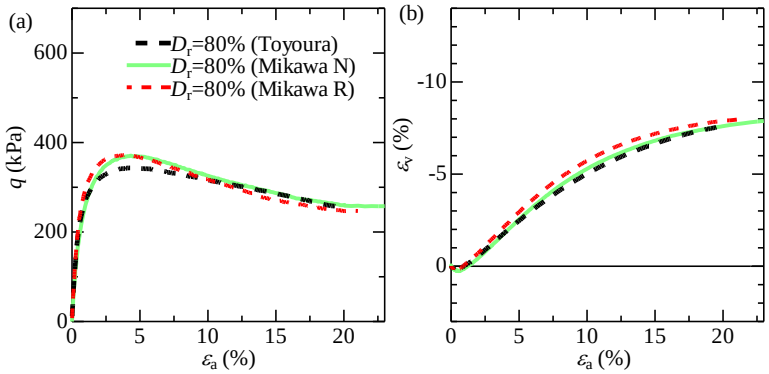

Fig. 6.7 Stress-strain response of Toyoura, Mikawa #6 normal, Mikawa #6 rounded sand in drained triaxial compression (D_r=80%, p'_0=100kPa) prepared by sample preparation #1

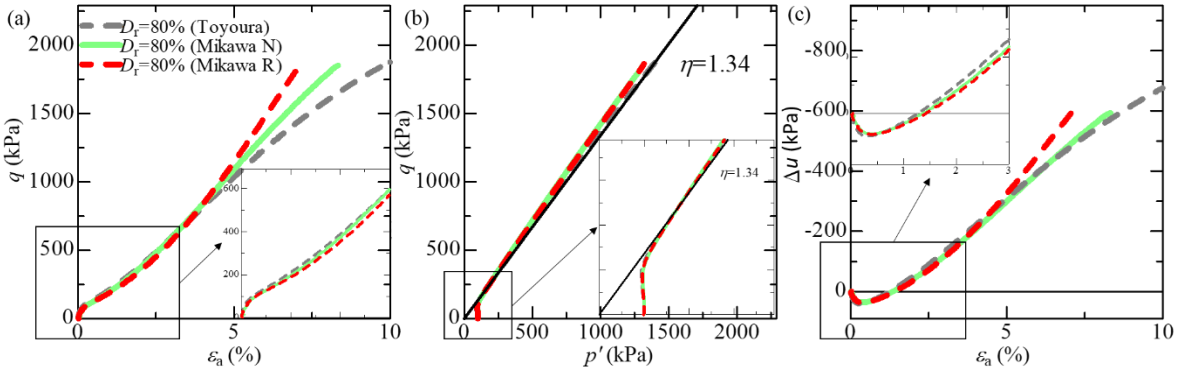

Fig. 6.8 Stress-strain response of Toyoura, Mikawa #6 normal, Mikawa #6 rounded in undrained triaxial compression (D_r=60%, p'_0=100kPa) prepared by sample preparation #1

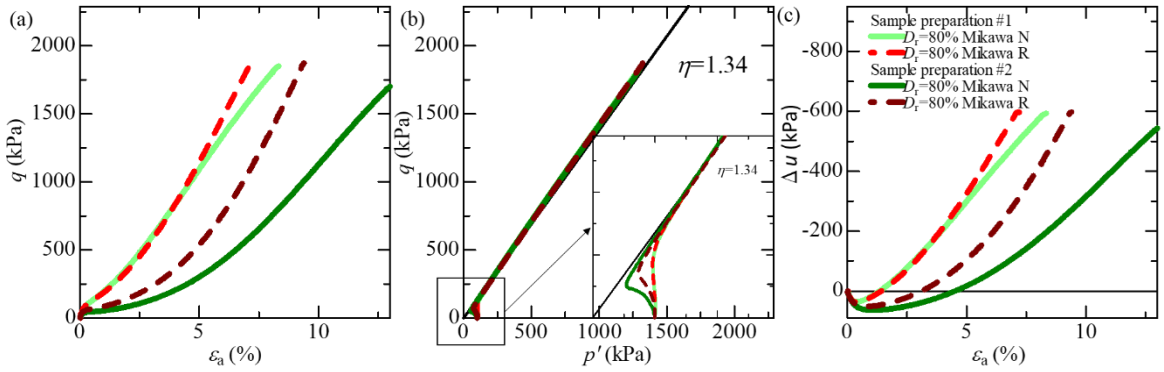

Fig. 6.9 Comparison of the effect of sample preparation on the undrained shear behavior of normal and rounded Mikawa sand #6 (D_r=60%, p'_0=100kPa)

Making sure that the more rounded/spherical Mikawa sand was less influenced by the sample preparation method, an undrained triaxial compression test on 0.4% fiber-reinforced Mikawa R sand was performed to compare the effect of fibers on the mechanical behavior with attention to an anisotropic effect. Fig 6.10 shows the comparison of undrained shearing tests performed on unreinforced and 0.4% fiber-reinforced Mikawa R sand. Indeed, the inclusions of fibers even affected the shearing behavior of Mikawa R sand with difference in initial stiffness and effective stress path. In fact, the intensity of the difference in initial stage is smaller in fiber-reinforced sand with more rounded shape (Fig. 6.10) compared to reinforced Toyoura sand of angular and sub-angular shape (Fig. 6.2). From the experimental results it can be confirmed that the anisotropic behavior of unreinforced sand depends on the particles' shape with less/more horizontally-oriented distribution due to the sample preparation. Moreover, it is assumed that fiber inclusions prevent a preferred orientation of sand particles and reduce the degree of initial anisotropy. One of the reasons in reduction of initial stiffness or more pronounced softening behavior without doubts is occurred due to the anisotropy. However, interaction between sand particles and fibers is also assumed to be a key factor, where fiber inclusions weakened the contact forces between sand particles affecting the initial shearing characteristics of fiber-reinforced sand.

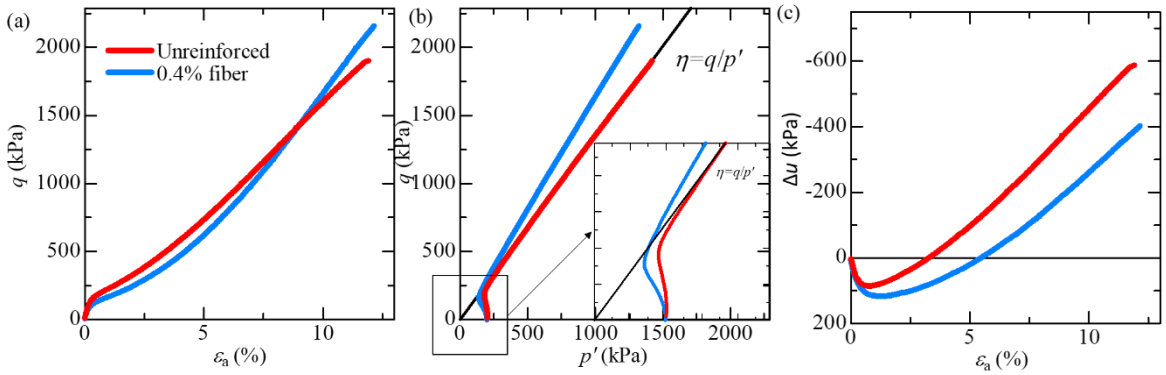

Fig. 6.10 Undrained triaxial compression performed under 200kPa confining pressure on unreinforced and 0.4% fiber-reinforced Mikawa sand #6 (rounded) with 40% initial relative density

Finally, experimentations with different fibers (PVA and VF) were performed to check the effect fibers' type on shearing properties and the anisotropy of Toyoura sand. Figs. 6.11 and 6.12 show the triaxial compression test results for drained and undrained conditions, respectively. Both types of fibers were effective to enhance the strength of sand with higher residual stresses and stress ratios. Making any conclusions on the effectiveness of considered types of fiber is quite complicated at the current stage due to relatively similar mechanical behaviors. Moreover, despite some differences in the strength properties of PVA and VF fibers (Table 3.1) the values of them were of the same order, and geometry including the aspect ratio was also similar (l_f=12mm and d=0.04mm). Further investigations are needed to make a comparative analysis and propose conclusions on the effect of fibers with various strength properties and various geometries.

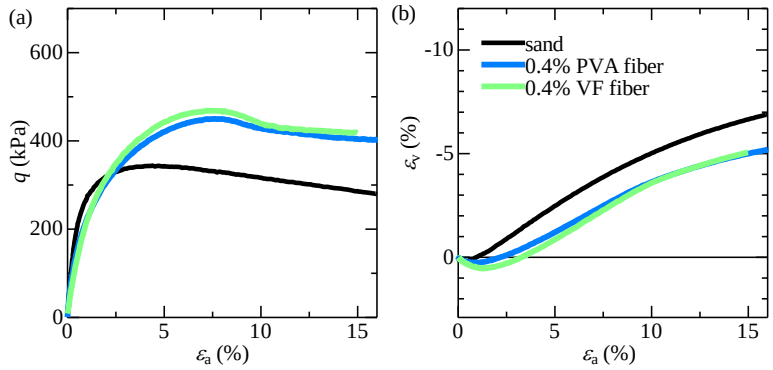

Fig. 6.11 Drained triaxial compression tests performed on unreinforced sand and sand reinforced with 0.4% PVA and 0.4% VF fibers (D_r=80%, p'_0=100kPa)

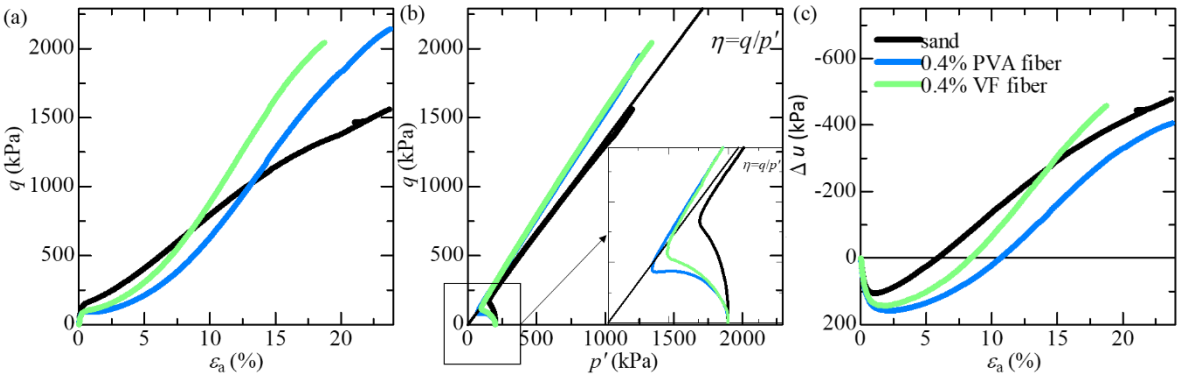

Fig. 6.12 Undrained triaxial compression tests performed on unreinforced sand and sand reinforced with 0.4% PVA and 0.4% VF fibers (D_r=40%, p'_0=200kPa)

6.5 Brief summary

Experimental investigation of the anisotropy of unreinforced and fiber-reinforced sand has been performed. According to the results it was revealed that the unreinforced sands independently of the shape of particles produce different degree of initial anisotropy depending on the sample preparation methods. Compaction through the side tapping/vibration is assumed to produce higher degree of initial anisotropy compared to sample preparation way with additional stirring. The high initial anisotropy is assumed to be due to the more horizontally preferred orientation of sand particles. In case of fiber-reinforced sands, fiber inclusions reduced the preferred orientation of sand particles, and as a results, reduce the degree of initial anisotropy. The effect of lower anisotropy was on the shearing behavior in both drained and undrained conditions attributed to decrease in initial stiffness characteristics and more pronounced softening behavior in fiber-reinforced sands compared to unreinforced sand. Also, with the increase in fiber content the initial anisotropy decreased within the considered fiber contents. As in previous studies, there is an effect of the shape of host soil, where the shearing behavior of more spherical/rounded sand was less influenced by the sample preparation methods and fiber inclusions.

From the observed behavior and discussions, it is assumed that the mechanical behavior of both unreinforced and fiber-reinforced sand is highly anisotropic. To evaluate the effect of anisotropy of fiber-reinforced sand not only the effect of fibers on the less preferred orientation of sand particles should be considered, but also the interaction mechanism between sand particles and fibers regarding the contact forces.

CHAPTER 7

CONCLUSIONS AND FUTURE WORKS

7.1 Conclusions

Experimental and numerical study have been performed in this study with the wide range of experimental testing and calculation. Based on the observed mechanical behavior and discussion the followings are main conclusion from the considered chapters.

In Chapter 3, an optimum sample preparation method out of four different methods was proposed for a considered fiber type and host soil, i.e. dry deposition through side tabooing/vibration. The proposed method of sample preparation is assumed to make the distribution of fibers more uniform (homogeneous) with random distribution through the entire specimens. This way of sample preparation showed that the experimental work can be conducted with a high reproducibility.

In Chapter 4, an extensive experimental results have been presented. Results and discussions were made according to isotropic compression, consolidated triaxial compression and extension tests under both drained and undrained conditions. In isotropic compression tests the fiber-reinforcement decreased the value of N (NCL intercept), where fiber-reinforced sand was more compressible at the initial stage of shearing with smaller initial stiffness and higher positive volumetric change.

The drained shear behavior of fiber-reinforced sand with 0.2% and 0.4% of fiber content under the same confining pressure with different initial relative density exhibited similar behavior to unreinforced sand. At the end of shearing (20% axial strain), the respective deviatoric stresses were approximately the same; the specific volume reached almost the same value even if the initial relative density was different. Hence, according to this observed mechanical behavior, it is considered that the stress state at the end of shearing is a near critical state.

The shear behavior of fiber-reinforced sand under different confining pressures also exhibited similar behavior to unreinforced sand. The test results of changing the confining pressure indicate that the critical state line exists in the fiber-reinforced sand as well as in unreinforced sand. It is a straight line through the origin in $q - p'$ plane and the slope of the critical state line increased as the fiber content increased. In $v - p'$ space, the specific volume decreased as the confining pressure increased. Furthermore, the shorter the fiber, the smaller the slope of the critical state line in $q - p'$

plane, which approaches that of unreinforced sand. Effectiveness of fibers to improve the tensile strength of sand in drained condition was negligible, with possible explanation of the transferred shear band to the bottom of the reinforced specimen.

The undrained behavior of fiber-reinforced sand confirmed the existence of a unique critical state for a definite fiber content as well as for unreinforced sand. Furthermore, the values of stress ratios at the end of shearing from undrained tests are quite similar to those from drained tests. Two important observations from undrained triaxial compression complemented the observed mechanical behavior in drained compression tests. In fact, addition of fibers reduced the initial stiffness with a higher drop of effective stress paths and initially generated higher positive PWP, while brought a higher deviatoric stress with a higher stress ratios and a lower value of negative PWP at the end of shearing, similarly to volumetric change behavior in drained condition. This additionally confirmed that the effectiveness of fibers concludes in increasing the strength of host soil by positively contributing to confining pressure with produced tensile forces in fibers, and acting as a contracting agent to prevent the expansion. Compared to drained extension behavior, contribution of fibers to improve the tensile strength of sand in undrained condition was obvious, with a higher deviatoric stress and a higher value of stress ratio at the end of shearing.

In Chapter 5, the simulation of drained and undrained triaxial compression tests performed on both unreinforced and fiber-reinforced sands with different initial relative densities under various confining pressures through the SYS Cam-clay model was presented. The simulation results of drained triaxial compression tests were in good agreement with experimental results. As with experimental results, the simulated results showed that despite initially experiencing different stress paths and volumetric change behavior attributed to different initial relative densities, all post-peak stresses and specific volumes of fiber-reinforced sand converged to the respective values with the shear progression as well as in unreinforced sand. Also, both experimental and simulated results for fiber-reinforced sand showed that each specimen reached the same respective CSL for definite fiber content despite shearing under five different confining pressures. The inclusion of fibers in sand increased internal friction angle ϕ' based on the relationship between M and $\phi'$for cohesionless soil.

Undrained behavior of unreinforced and fiber-reinforced sand was also reproduced by using the material and evolution rule parameters obtained from simulation results under drained condition. The tendency for the shearing behavior of both unreinforced and fiber-reinforced sand in undrained triaxial compression was well captured by the model. Some limitations of the considered model were

observed in the response to the intermediate undrained shearing behavior of medium loose specimens, where the experimental results showed a “convex” type change of devitoric stress and smaller initial stiffness compared to the model simulation.

In Chapter 6, a comprehensive analysis of the anisotropy in unreinforced and fiber-reinforced sand has been performed. According to the results it was revealed that the unreinforced sands independently of the shape of particles produce different degree of initial anisotropy depending on the sample preparation methods. The high initial anisotropy is assumed to be due to the more horizontally preferred orientation of sand particles. In case of fiber-reinforced sands, fiber inclusions reduced the preferred orientation of sand particles, and as a results, reduce the degree of initial anisotropy. From the observed behavior and discussions, it is assumed that the mechanical behavior of both unreinforced and fiber-reinforced sand is highly anisotropic. To evaluate the effect of anisotropy of fiber-reinforced sand not only the effect of fibers on the less preferred orientation of sand particles should be considered, but also the interaction mechanism between sand particles and fibers regarding the contact forces.

7.2 Future works

In the current research some important points regarding the experimental work has been presented. From the experimental results, it is recommended to perform further experimentations on a totally different type of soils as gravel and silt/clay to make the possibility of the implementation of fiber-reinforcement for a wide range construction works and investigate the influence of different fibers with respect the fiber’s physical properties and geometry.

In numerical analysis some limitation of the considered model was revealed, which is also in a high demand in further elaboration to overcome the limitations either by further reconsideration of the existing model parameters or, if necessary, by introducing additional parameters to make the constitutive model applicable to reproduce a variety of mechanical properties of both unreinforced and fiber-reinforced soils.

Finally, once the modifications of the constitutive model are performed, FEM/DEM analysis of various geo-structures reinforced with fibers can be performed to bring closer the practical implementation of this promising alternative soil improvement technique.

REFERENCES

Ajayi, O., Le Pen, L., Zervos, A., Powrie, W., 2017. A behavioural framework for fibre-reinforced gravel. Géotechnique 67 (1), 56-68.

Asaoka, A., 2003. Consolidation of clay and compaction of sand – An elasto-plastic description. In: Proceedings of the 12th Asian Regional Conference on Soil Mechanics and Geotechnical Engineering, Singapore, 2, 1157-1195.

Asaoka, A., Nakano, M., Noda, T., 1997. Soil water coupled behavior of heavily overconsolidated clay near/at critical state. Soils Found. 37 (1), 13–28.

Asaoka, A., Nakano, M., Noda, T., 1998. Super loading yield surface concept for the saturated structured soils. In: Proceedings of the 4th European Conference on Numerical Methods in Geotechnical Engineering, NUMGE98, pp. 232–242.

Asaoka, A., Nakano, M., Noda, T., 2000. Super loading yield surface concept for highly structured behavior. Soils Found. 40 (2), 99–110.

Asaoka, A., Noda, T., Yamada, E., Kaneda, K., Nakano, M., 2002. An elasto-plastic description of two distinct volume change mechanisms of soils. Soils Found. 42 (5), 47–57.

Atkinson, J.H., Bransby, P.L., 1978. The Mechanics of Soils: An Introduction to Critical State Soil Mechanics. McGraw-Hill, London.

Babu, G.L., Chouksey, S.K., 2010. Model for analysis of fiber-reinforced clayey soil. Geomech. Geoeng. 5 (4), 277–285.

Babu, G.L., Vasudevan, A.K., Haldar, S., 2008. Numerical simulation of fiber-reinforced sand behavior. Geotext. Geomembranes 26 (2), 181-188.

Chen, C., 2010. Triaxial compression and extension for fiber-reinforced silty sand. GeoShanghai International Conference 2010. Ground Improvement and Geosynthetics ASCE, 367-376.

Consoli, N.C., Casagrande, M.D.T., Coop, M.R., 2005. Effect of fiber reinforcement on the isotropic compression behavior of sand. J. Geotech. Geoenviron. Eng. ASCE 131 (11), 1434-1436.

Consoli, N.C., Heineck, K.S., Casagrande, M.D.T., Coop, M.R., 2007a. Shear strength behavior of fiber-reinforced sand considering triaxial tests under distinct stress path. J. Geotech. Geoenviron. Eng. ASCE 133 (11), 1466-1469.

Consoli, N.C., Casagrande, M.D.T., Coop, M.R., 2007b. Performance of fiber-reinforced sand at large shear strains. Géotechnique 57 (9), 751-756.

Consoli, N.C., Festugo, L., Heineck, K.S., 2009. Strain-hardening behaviour of fibre-reinforced sand in view of filament geometry. Geosynth. Int. 16 (2), 109-115.

di Prisco, C., Nova, R., 1993. A constitutive model for soil reinforced by continuous threads. Geotext. Geomembranes 12 (2): 161–178

Diambra, A., Ibraim, E., 2014. Modelling of fibre–cohesive soil mixtures. Acta Geotech. 9 (6), 1029–1043.

Diambra, A., Ibraim, E., 2015. Fibre-reinforced sand: interaction at the fibre and grain scale. Géotechnique 65 (4), 296–308.

Diambra, A., Ibraim, E., Muir Wood, D., Russell, A.R., 2010. Fibre reinforced sands: experiments and modelling. Geotext. Geomembranes 28 (3), 238-250.

Diambra, A., Ibraim, E., Russell, A.R., Muir Wood, D., 2011. Modelling the undrained response of fibre reinforced sands. Soils Found. 51 (4), 625–636.

Diambra, A., Ibraim, E., Russell, A.R., Muir Wood, D., 2013. Fibre reinforced sands: from experiments to modelling and beyond. Int. J. Numer. Anal. Meth. Geomech. 37 (5), 2427-2455.

Dos Santos, A.P.S., Consoli, N.C., Baudet, B.A., 2010. The mechanics of fibre-reinforced sand. Géotechnique 60 (10), 791-799.

Eldesouky, H.M., Morsy, M.M., Mansour, M.F., 2016. Fiber-reinforced sand strength and dilation characteristics. Ain Shams Eng. J. 7 (2), 517-526.

Falorca, I.M.C.F.G, Pinto, M.I.M., 2011. Effect of short, randomly distributed polypropylene microfibers on shear strength behaviour of soils. Geosynth. Int. 18 (1), 2-11.

Falorca, I.M.C.F.G., Gomes, L.M.F., Pinto, M.I.M., 2011. A full-scale trial embankment construction with soil reinforced with short randomly distributed polypropylene microfibers. Geosynth. Int. 18 (5), 280-288.

Gajo, A., Muir Wood, D., 1999. Severn-trent sand: A kinematic-hardening model for sands: the q-p formulation. Géotechnique, 49 (5), 595–614.

Gao, Z.W., Diambra, A., 2020. A multiaxial constitutive model for fibre-reinforced sand. Géotechnique 71 (6), 548-560.

Gao, Z., Huang, M., 2021. Effect of sample preparation on mechanical behavior of fibre-reinforced sand. Comput. Geotech. 133:104007.

Gao, Z. W., Lu, D., Huang, M., 2020. Effective skeleton stress and void ratio for constitutive modeling of fiber-reinforced sand. Acta Geotech. 15, 2797–2811.

Gray, D.H., Ohashi, H., 1983. Mechanics of fiber reinforcement in sands. J. Geotech. Eng. ASCE 109 (3), 335-353.

Gray, D.H., Al-Refeai, T., 1986. Behavior of fabric-versus fiber-reinforced sand. J. Geotech. Eng. ASCE 112 (8), 804-820.

Hashiguchi, K., 1978. Plastic constitutive equations of granular materials, In: S.C. Cowin, M. Satake (Eds.). In: Proceedings of the US-Japan Seminar on Continuum Mechanics and Statistical Approaches in the Mechanics of Granular Materials, JSSMFE, Sendai, 321–329.

Hashiguchi, K., 1989. Subloading surface model in unconventional plasticity. Int. J. Solids Struct. 25, 917–945.

Hashiguchi, K., Chen, Z.P., 1998. Elastoplastic constitutive equations of soils with the subloading surface and the rotational hardening. Int. J. Numer. Anal. Meth. Geomech. 22, 197-227.

Heineck, K.S., Coop, M.R., Consoli, N.C., 2005. Effect of microreinforcement of soils from very small to large shear strains. J. Geotech. Geoenviron. Eng. ASCE 131 (8), 1024-1033.

Ibraim, E., Fourmont, S., 2007. Behaviour of sand reinforced with fibres. In: Ling, Callisto, Leshchinsky, Koseki (Eds.), Soil stress–strain behavior: measurement, modelling and analysis, Geotechnical Symposium, Rome, March 16–17, 2006. Springer, 807–918.

Ibraim, E., Maeda, K., 2007. Numerical analysis of fibre-reinforced granular soils. In: Otani J, Miyata Y, Mukunoki T (Eds.). New horizons in earth reinforcement, Proceedings of 5th international symposium on earth reinforcement, IS Kyushu'07. Balkema, Rotterdam, pp. 387–393.

Ibraim, E., Diambra, A., Muir Wood, D., Russell, A.R., 2010. Static liquefaction of fibre reinforced sand under monotonic loading. Geotext. Geomembranes 28 (4), 374–385.

Ibraim, E., Diambra, A., Russell, A.R., Muir Wood, D., 2012. Assessment of laboratory sample preparation for fibre reinforced sands. Geotext. Geomembranes 34, 69-79.

Jamie, M., Villard, P., Guiras, H., 2013. Shear failure criterion based on experimental and modeling results for fiber-reinforced clay. Int. J. Geomech. 13 (6), 882-893.

Jewell, R.A., Wroth, C.P., 1987. Direct shear tests on reinforced sand. Géotechnique 37 (1), 53-68.

Jie, Y.X., Zhang, B., Li, G.X., 2012. A new method for numerical analysis of reinforced soil. J. Test. Eval. 40 (4), 586–596.

JGS Standards, 2020. Test method for particle size distribution of soils. JGS 0131, Tokyo, Japan.

JGS Standards, 2020. Test method for minimum and maximum densities of sands. JGS 0161, Tokyo, Japan.

JGS Standards, 2020. Method for consolidated-undrained triaxial compression test on soils with pore water pressure measurements. JGS 0523, Tokyo, Japan.

JGS Standards, 2020. Method for consolidated-drained triaxial compression test on soils. JGS 0524, Tokyo, Japan.

Kar, R.K., Pradhan, P.K., Naik, A., 2012. Consolidation characteristics of fiber-reinforced cohesive soil. Electron J. Geotech. Eng. 7: 3861-3874.

Kanchi, G.M., Neeraja, V.S., Babu, G.L.S., 2015. Effect of anisotropy of fibers on the stress-strain response of fiber-reinforced soil. Int. J. Geomech. ASCE 15(1): 06014016.

Kuerbis, R.H., Negussey, D., Vaid, Y.P., 1988. Effect of gradation and fines content on the undrained response of sand. In: Proceedings of the ASCE Conference on Hydraulic Fill Structures, Geotechnical Special Publication, vol. 21, pp. 330–345.

Li, X. S., Dafalias, Y. F., 2002. Constitutive modelling of inherently anisotropic sand behaviour. J. Geotech. Geoenviron. Eng. 128(10), 868–880.

Li, H., Senetakis, K., 2017. Dynamic properties of polypropylene fibre-reinforced silica quarry sand. Soil Dyn. Earthq. Eng. 100, 224-232.

Li, J., Tang, C., Wang, D., Pei, X., Shi, B., 2014. Effect of discrete fibre reinforcement on soil tensile strength. J. Roch Mechanics and Geotech. Eng. 6, 133-137.

Li, M., He, H., Senetakis, K., 2017. Behavior of carbon fiber-reinforced recycled concrete aggregate. Geosynth. Int. 24 (5), 480-490.

Li, H., Senetakis, K., Coop., M.R., 2019. Medium-strain dynamic behavior of fiber-reinforced sand subjected to stress anisotropy. Soil Dyn. Earthq. Eng. 126, 105764.

Lirer, S., Flora, A., Consoli, N.C., 2011. On the strength of fibre-reinforced soils. Soils Found. 51 (4), 601-609.

Liu, J., Wang, G., Kamai, T., Zhang, F., Yang, H., Shi, B., 2011. Static liquefaction behavior of saturated fiber-reinforced sand in undrained ring-shear tests. Geotext. Geomembranes 29 (5), 462-471.

Maeda, K., Ibraim, E., 2008. DEM analysis of 2D fibre-reinforced granular soils. In Vol. 2 of Proc., 4th Int. Symp. on Deformation Characteristics of Geomaterials, 623–628. Amsterdam, Netherlands: IOS Press.

Maher, M.H., Gray, D.H., 1990. Static response of sands reinforced with randomly distributed fibers. J. Geotech. Eng. ASCE 116 (11), 1661-1677.

Mandolini, A., Diambra, A., Ibraim, E., 2019. Strength anisotropy of fibre-reinforced sands under multiaxial loading. Géotechnique 69 (3), 203-216.

Michalowski, R.L., 2008. Limit analysis with anisotropic fiber-reinforced soil. Géotechnique 58(6), 489-501.

Michalowski, R.L., Ĉermak, J., 2002. Strength anisotropy of fiber-reinforced sand. Comput. Geotech. 29, 279-299.

Michalowski, R.L., Ĉermak, J., 2003. Triaxial compression of sand reinforced with fibers. J. Geotech. Geoenviron. Eng. ASCE 129 (2), 125-136.

Michalowski, R.L., Zhao, A., 1996. Failure of fiber-reinforced granular soils. J. Geotech. Eng. ASCE 122(3), 226–234.

Mirzababaei, M., Arulrajah, A., Haque, A., Nimbalkar, S., Mohajerani, A., 2018. Effect of fiber reinforcement on shear strength and void ratio of soft clay. Geosynth. Int. 25 (4), 471-480.

Miura, S., Toki, S., 1982. A sample preparation method and its effect on static and cyclic deformation-strength properties of sand. Soils Found. 22 (1), 61–77.

Muir Wood, D., 1990. Soil behavior and critical state soil mechanics. Cambridge University Press, Cambridge.

Muir Wood, D., Diambra, A., Ibraim, E., 2016. Fibres and soils: a route towards modelling of root-soil systems. Soils Found. 56 (5), 765-778.

Oda, M., 1972. Initial fabrics and their relations to mechanical properties of granular material. Soils Found. 12 (1), 17-36.

Palacios, M., Casagrande, M., Consoli, N., 2012. Behavior of a polypropylene renforced sand under triaxial extension tests. Rio de Janeiro, 2012. 101p. MSc. Dissertation – Civil Engineering Department, Pontifical Catholic University of Rio de Janeiro.

Pitman, T.D., Robertson, P.K., Sego, D.C., 1994. Influence of fines on the collapse of loose sands. Can. Geotech. J. 31 (5), 728–739.

Roscoe, K.H., Schofield, A.N., Wroth, C.P., 1958. On the yielding of soils. Géotechnique 8 (1), 22–53.

Roscoe, K.H., Burland, J.B., 1968. On the generalized stress-strain behavior of 'wet' clay. Engineering Plasticity (ed. By Hey-man, J. and Leckie, F. A.), Cambridge University Press, 535-609.

Santoni, R.L., Webster, S.L., 2001. Air field sand road construction using fiber stabilization of sands. J. Transp. Eng. 127(2), 96–104.

Sadek, S., Najjar, S.S., Freiha F., 2010. Shear strength of fiber-reinforced sands. J. Geotech. Geoenviron. Eng. ASCE 136 (3), 490-499.

Schofield, A.N., Wroth, C.P., 1968. Critical State Soil Mechanics. McGraw-Hill, Cambridge.

Shukla, S.K., 2017. Fundamentals of fibre-reinforced soil engineering. Springer, Singapore.

Shukla, S.K., Sivakugan, N., Singh, A.K., 2010. Analytical model for fiber-reinforced granular soils under high confining stresses. J. Mater. Civ. Eng. 22 (9), 935–942.

Sekiguchi, H., Ohta, H., 1977. Induced anisotropy and time dependency in clays. 9th ICSMFE, Proc. Specialty Session 9, Tokyo, 229-238.

Tang, C., Shi, B., Cui, Y., Wang, D, 2016. Tensile Strength of Fiber-Reinforced Soil. Journal of Materials in Civil Engineering, 2016, 28(7):04016031.

Thevanayagam, S., 1998. Effect of fines and confining stress on undrained shear strength of silty sands. J. Geotech. Geoenviron. Eng. ASCE 124 (6), 479–491.

Verdugo, R., Ishihara, K., 1996. The Steady State of Sandy Soils. Soils Found. 36 (2), 81–91.

Wang, Y., Guo, P., Dai, F., Li, X., Zhao, Y., Liu, Y., 2018. Behavior and modeling of fiber-reinforced clay under triaxial compression by combining the superposition method with the energy-based homogenization technique. Int. J. Geomech. ASCE 18 (12): 04018172.

Wang, Y., Guo, P., Lin, H., Li, X., Zhao Y., Yuan, B., Liu, Y., Cao, P., 2019. Numerical analysis of fiber-reinforced soils based on the equivalent additional stress concept. Int. J. Geomech. ASCE 19 (11): 04019122.

Wood, F.M., Yamamuro, J.A., Lade, P.V., 2008. Effect of depositional method on the undrained response of silty sand. Can. Geotech. J. 45 (11), 1525-1537.

Wu, T.H., Mckinnel, W.P.III, Swanston, D.N., 1979. Strength of tree roots and landslides on Prince of Wales Island, Alaska. Can. Geotech. J. 16 (1), 19–33.

Yang, J., Wei, L.M., Dai, B.B., 2015. State variables for silty sand: Global void ratio or skeleton void ratio? Soils Found. 55 (1), 99-111.

Yetimoglu, T., Salbas, O., 2003. A study on shear strength of sands reinforced with randomly distributed discrete fibers. Geotext. Geomembranes 21 (2), 103-110.

Zhang, J.L., Yuan, M., Jiang, Z.G., Yang, Q., 2013. Triaxial test and numerical analysis on the fiber reinforced laterite clay. Appl. Mech. Mater. I, 1219–1224.

Zornberg, J.G., 2002. Discrete framework for equilibrium analysis of fibre reinforced soil. Géotechnique 52 (8), 593–604.

APPENDIX

A1 Void ratio determination in fiber-reinforced sands

There are two main definitions of the void ratio of composite materials: global void ratio and skeleton void ratio. Let us consider both approaches to understand the principals to choose any of them.

The skeleton-void-ratio is mainly used to compare the effect of fines content on the void ratio values of sandy soil through the following equation (Kuerbis et al., 1988; Pitman et al., 1994; Thevanayagam, 1998; Yang et al., 2015):

$$e_s = \frac{e_0 + \mathrm{FC}/100}{1 - \mathrm{FC}/100} = \frac{V_v/V_s + FC}{1 - \mathrm{FC}} \tag{A1}$$

where FC is the percentage of fines content, V_v is the volume of voids (air), and V_s is the volume of solids (sand).

In the literature related to fiber-reinforced sand, there is no standardized method of calculating the void ratio of fiber-reinforced soil, and different methods were used in different studies.

The global void ratio, counting fibers as a part of solids (Michalowski and Ĉermak, 2003; Heineck et al., 2005; Dos Santos et al., 2010):

$$e_r = \frac{V_v}{V_s} = \frac{V_a}{V_{sp} + V_f} \tag{A2}$$

where V_a is the volume of air, V_f is the volume of the fibers and V_{sp} is the volume of soil particles; V_v is the volume of the voids and V_s is the volume of solids.

The global void ratio, counting fibers as a part of voids (Diambra et al., 2010; Ibraim et al., 2012; Muir Wood et al., 2016)

$$e_r = \frac{V_v}{V_s} = \frac{V_a + V_f}{V_{sp}} \tag{A3}$$

Eq. (A2) is used in this study. If concept of skeleton-void-ratio in Eq.(A1) is applied to the fiber-reinforced sand, the following equation can be derived by FC replacing with w_f:

$$e_s = \frac{e_0 + w_f/100}{1 - w_f/100} = \frac{V_a/V_{sp} + w_f/100}{1 - w_f/100} \tag{A4}$$

where w_f is a percentage of fiber inclusions. For unreinforced sand, the values of void ratio calculated through the skeleton-void-ratio is exactly the same as the global void ratio. Consequently, there is no difference in the dilatancy behavior of unreinforced sand.

Using the skeleton-void-ratio for fiber-reinforced sand brings a small difference in the values of void ratios (the following table):

Table A1.1 Void ratios calculated by different approaches

Test	w_f, (%)	$e_{global,}$ fiber as solids (this study)	$e_{global,}$ fiber as voids	$e_{skeleton}$	$D_{r,}$ (%)	p'_0, (kPa)
L100-00	0.0	0.823	0.823	0.823	30	100
M100-00-a	0.0	0.771	0.771	0.771	60	100
M100-00-b	0.0	0.772	0.772	0.772	60	100
D-050-00	0.0	0.721	0.721	0.721	80	50
D-100-00	0.0	0.719	0.719	0.719	80	100
D-200-00	0.0	0.717	0.717	0.717	80	200
L100-02	0.2	0.829	0.839	0.839	30	100
M100-02-a	0.2	0.77	0.781	0.781	60	100
M100-02-b	0.2	0.773	0.784	0.783	60	100
D-050-02	0.2	0.715	0.725	0.724	80	50
D-100-02	0.2	0.713	0.723	0.723	80	100
D-200-02	0.2	0.709	0.722	0.721	80	200
D-400-02	0.2	0.699	0.711	0.710	80	400
L100-04	0.4	0.821	0.834	0.834	30	100
M100-04-a	0.4	0.772	0.786	0.785	60	100
M100-04-b	0.4	0.774	0.787	0.786	60	100
D-050-04	0.4	0.712	0.725	0.724	80	50
D-100-04	0.4	0.712	0.726	0.725	80	100
D-200-04	0.4	0.705	0.718	0.717	80	200
M100-10-a	1.0	0.775	0.796	0.794	60	100
M100-10-b	1.0	0.772	0.792	0.791	60	100
D-050-10	1.0	0.711	0.730	0.727	80	50
D-100-10	1.0	0.708	0.728	0.725	80	100
D-200-10	1.0	0.705	0.726	0.723	80	200

L - loose; M - medium dense; D - dense

The difference between two values of void ratios calculated through the global-void-ratio (this study) and skeleton-void-ratio increase with the increase in the fiber contents. However, the difference is less than 0.02 even for 1.0% fiber-reinforced sand. Overall, the use of skeleton-void-ratio concept will not bring significant difference in the mechanical properties, and the trend of

dilatancy will not change, because the percentage of fiber inclusions is low. The following figures are examples (Fig. A1.1):

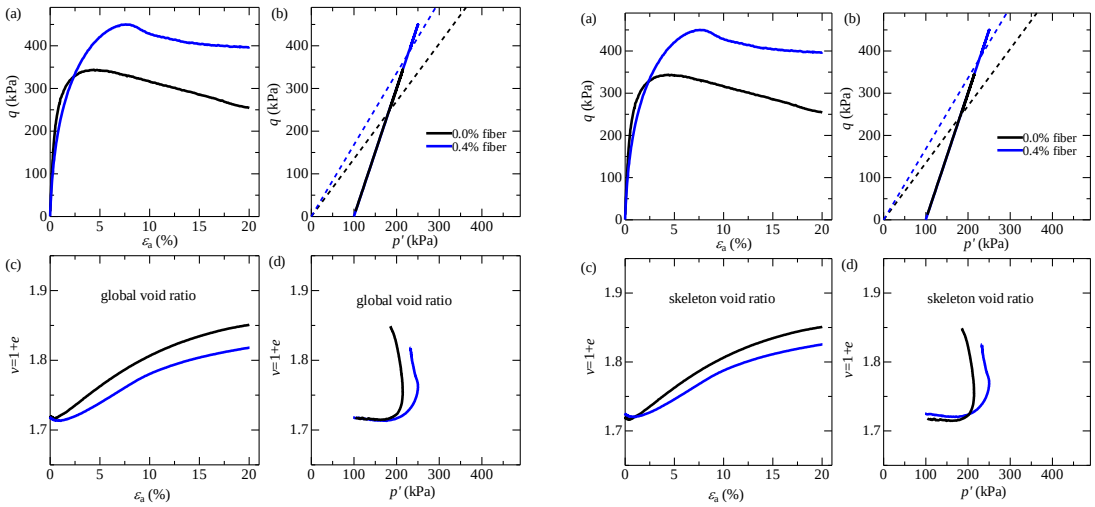

Fig. A1.1 Example of pure sand and 0.4% fiber-reinforced sand sheared under the same confining pressure and prepared with the relative density of 80%: a) specific volume represented through global void ratio and b) specific volume represented through skeleton void ratio

Initial void ratio of fiber-reinforced sand represented through the skeleton-void-ratio concept is higher, however, final void ratio of fiber-reinforced sand is less than that of unreinforced sand. Moreover, the values of void ratios calculated through the skeleton-void-ratio concept is very close to the values calculated through the global-void-ratio counting fibers as a part of voids. However, fibers cannot be considered as a voids due to a significant impact of fibers' volume on the soil. Therefore, global void ratio counting fibers as a part of solids has been used in this study.

A2 Sensitivity analysis of individual parameters on the drained/undrained behavior and determination of evolution rule parameters

The evolution rule parameters are determined according to the formulation of the SYS Cam-clay model and the reproduction of the experimental results through sensitivity analysis. The formulation of the SYS Cam-clay model says that both sandy and clayey materials are initially in overconsolidated and structured state. During the deformation processes the decay of structure in sandy soils occurs relatively fast, while maintaining overconsolidation. In contrast, the clayey materials reach normally consolidated state comparatively fast (loss of overconsolidation), but with a certain amount of structure. When relatively high strain rates are applied to the soils, both sand and clay finally reach a fully remolded and normally consolidated state. Fig. A2.1 represents the sensitivity analysis of the four parameters governing the degradation of soil skeleton structure and the following dependency of the parameters' variations was obtained.

- Degradation index of overconsolidation m: the larger the m – the larger the peak intensity (Fig. A2.1a), i.e. the degree of hardening increases; compressibility is larger when m is smaller. The value of m controls the speed of the overconsolidation loss, where, generally, m is smaller for sandy material compared to clayey soils. The smaller m value means the slower the process of overconsolidation loss or the slower rate of the soil reaching the normally consolidated state.
- Degradation index of structure a: the larger the a – the smaller the peak intensity (Fig. A2.1b), i.e. the degree of softening increases; the degradation rate of structure does not particularly affect the compressibility. The value of a affects the speed of de-structuring of soils, where the value of a is higher for sandy materials.
- Rotational hardening index b_r: this parameter mainly controls the development of the anisotropy. The larger the b_r – the larger the peak and post-peak strength, i.e. the degree of hardening increases and degree of softening decreases; expansion is larger when the b_r is larger especially in the intermediate strain (Fig. A2.1c).
- Limitation of rotational hardening m_b: this parameter defines the limitation of the degree of anisotropy and affects the border of hardening and softening (M_a). The larger the m_b – the larger the peak and post-peak stresses; the compressibility is similarly affected as in the case of b_r (Fig. A2.1d).

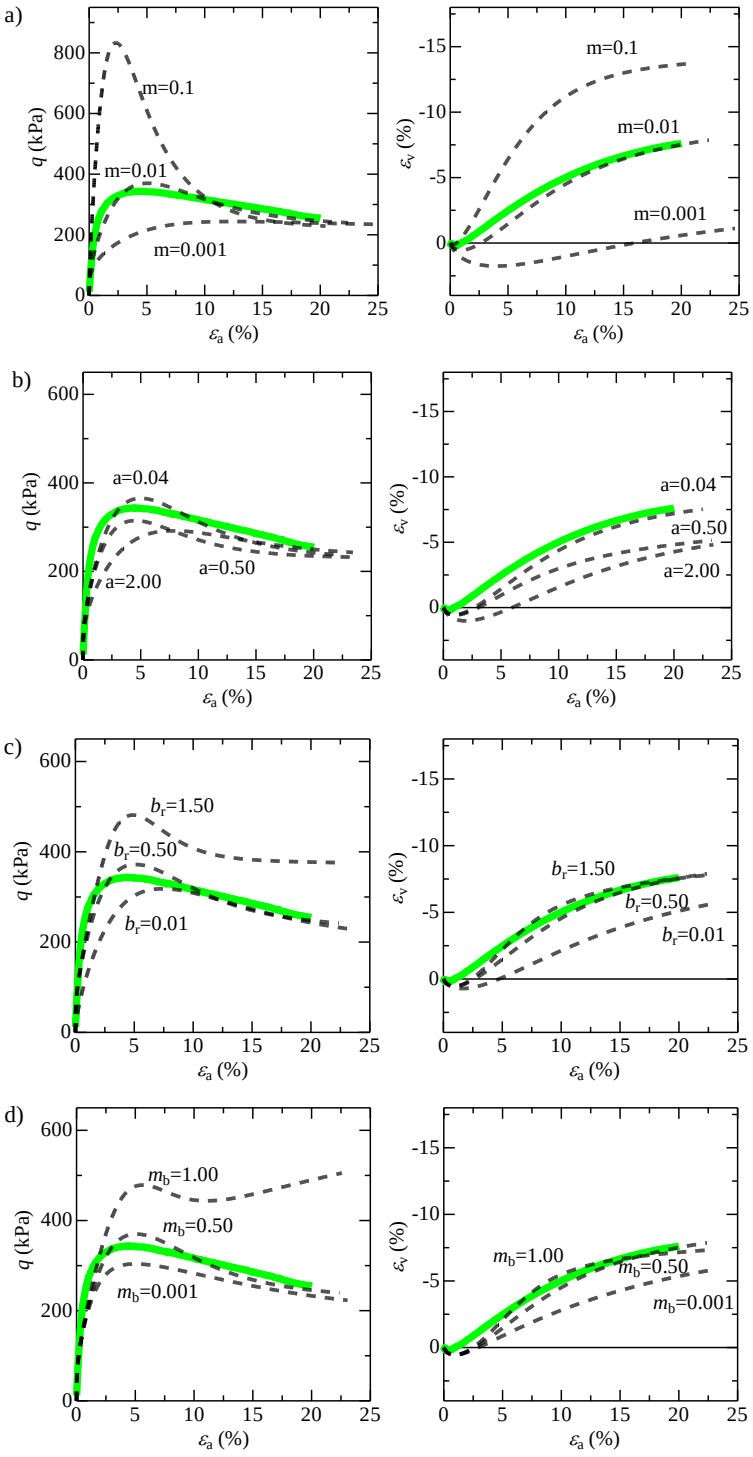

Fig. A2.1 Sensitivity analysis of evolution rule parameters (solid line – experimental results, dashed lines – model response)

The parameter c_s that represents the ratio of plastic shear deformation to plastic compression deformation varies in the interval from 0 to 1. $c_s \rightarrow 1$ for sandy materials which means the decay of structure is mainly due to the shear deformation, while $c_s \rightarrow 0$ for clay where the decay of structure is mainly due to the compression.